JAERI-M
7947

AN ANALYSIS OF LOFT L1-2 EXPERIMENT BY ALARM-P1 COMPUTER CODE

October 1978

Shinobu SASAKI

日本原子力研究所
Japan Atomic Energy Research Institute

JAERI-M 7947

— An Analysis of Loft L1-2 Experiment by ALARM-P1 Computer Code —

Shinobu SASAKI
Division of Reactor Safety Evaluation,
Tokai Research Establishment, JAERI

(Received October 6, 1978)

This report concerns analysis by the domestic evaluation code ALARM-P1 of LOFT nonnuclear test series L1 experiment 2 which was conducted at the Idaho National Engineering Laboratory (INEL) as system level tests.

This L1 experiment was attempted with the aim of providing the basic and valuable data for nuclear tests with active core scheduled in the forthcoming future. As preliminary prior to nuclear tests, a simple blowdown experiment (L1-2) was performed in which the core is only composed of a configuration simulating frictional resistance and overall experimental facility is maintained isothermally without ECC water injection.

At the beginning of computation, input data were chosen from RELAP-4J data used by the LOFT analysis group of Reactor Safety Laboratory 1 and then converted as relevant to the ALARM-P1 input specifications.

The purpose of analysis performed is not only to obtain a better understanding of blowdown phenomenon, but also to clarify validity or system performance characteristics of ALARM-P1 code (version 3).

By the large, good agreements were obtained between calculational results and experimental data.

Keywords : LOCA, Blowdown Simulation, ALARM-P1 Code, LOFT, Code Validity

JAERI−M 7947

ALARM−P1 コードによるLOFT・L1−2 の解析

日本原子力研究所東海研究所安全解析部

佐々木　　忍

（1978 年 10 月 6 日受理）

本報告書は，米国アイダホの国立研究所で行われたLOFT 炉によるL1 シリーズ実験(非核実験）の内，特にL1−2 に関しての実験をALARM−P1 コードを用いて解析したものである。

本実験は，将来の核実験への基礎となるもので，その手はじめとして，炉心は単なる抵抗体とみなし，ECCS を考慮せず，系全体を等温としたブローダウン実験である。計算に際して，そのインプットデータは，安全工学第一研究室で行われたRELAP−4 J コードによる本実験解析のデータを参考とし，ALARM−P1 コード用に移しかえて使用した。

解析の主たる目的は，ブローダウン現象の把握とあわせて，本コードに関しての妥当性，特徴等を明確にすることにあり，本実験結果との照合では，比較的満足な予測を示した。

CONTENTS

目　　次

List of Figures

List of Tables

1. Introduction

From the viewpoint of the safety analyses of a water-cooled power reactor, one of the unlikely events considered is a hypothetical sudden break of the primary coolant piping leading to a loss of the coolant and a rapid decompression. To date, the LOCA (Loss-of-Coolant-Accident) analytical techniques have been highly developed and improved especially in the U.S. as well as some other countries. Nowadays, these developments are steadily proceeding in pursuit of more advanced models and an amazing amount of reliable information on the coolant behavior by means of experiments or analyses has been acquired. In particular, much recent effort has been directed toward developing the capability of assessing the performance of engineered safety features which are supposed to have been designed to function adequately over a wide range of loss of coolant accident conditions such as the variety of rupture sizes, rupture locations and rupture types i.e., guillotine or split break. Such systems are intended to mitigate substantial consequences of accidents, with sufficient redundancy. ECCS (Emergency Core Cooling System) is one of such engineered safety systems and is equipped to arrest a serious damage (especially core meltdown) in the reactor. Since ECCS is such an important system for LWR's, its performance must carefully be evaluated.

Consequently, the development of computer code serves quantitatively to assure effectiveness of ECCS as well as to predict the course of a LOCA.

In Japan, this kind of blowdown code for PWR's developed in Japan Atomic Energy Research Institute (JAERI) originates with ALARM-P1.

This is a digital computer program which calculates pressures, mass and/or energy inventories, flows and others in the reactor plant, and

thereby provides a better understanding for complicated blowdown phenomena.

For the present, this code is one of the basic tools of JAERI's blowdown calculation for a PWR. In rigorous mathematical treatments of physical phenomena such as a LOCA, it is generally so difficult to present a realistic prediction of process because of various uncertainties involved.

Therefore, in a LOCA analysis, evaluation models presupposing less favorable conditions than reality are conservatively applied for safety margins. Above models are fundamental calculational framework in the current reactor system accident analyses. Because such conservatism postulates events as highly unlikely as to be beyond the bound of reality, it tends to present severer oriteria against uncertainty factors than realistic results, as the case may be. Prime concerns are how margins for safety are defined and estimated.

These technical considerations and guidelines are specified in the Acceptance Criteria[4]* established by the Japan Atomic Energy Commission.

As above mentioned, the ALARM-P1, which is considered to be a part of ECCS evaluation code system, treats primarily the system decompression process — blowdown phase — in accordance with Acceptance Criteria, and in the future will be used as licensing calculations to implement conservative assessments of ECCS performance by the regulatory staff. As a concrete investigation in order to assess ECCS performance successfully, it is evaluated by transitions of the reflooding rate through the reactor core under the influence of steam binding. Although the conservative predictions of ALARM-P1 intend to approach a best estimate, they are far from satisfactory at the present stage.

---

* Numbers in brackets designate References.

In the present analysis, LOFT (L1-2) test was selected as a sample problem in order to understand the characteristics of the ALARM-P1 code. The results of analysis are described in section III, including the comparisons with integral test data.[3] In general, experimental data and calculational results were in excellent agreements except for some outputs such as the pressurizer pressure or mixture level. From these results, crude estimates can be obtained of unknown quantities at the locations in the reactor system where access for measurement is impossible. Further, a few open problems were pointed out from code verification purposes. In this way, the ALARM-P1 code is found to be an useful tool for qualitative evidence of the reactor safety, but of course much is still left to be done before we conclude the validity of this code.

II. General Résumé of Calculation Performed by ALARM-P1

II-1 Outline of Experiment

The objective of the LOFT (Loss-of-Fluid-Test) nonnuclear experiments — TEST SERIES L1 — is to make available large scale isothermal blowdown and in particular (in case of L1-2 experiment)[1][2] to provide fundamental thermal-hydraulic data for a cold leg large break as preliminary prior to nuclear blowdown tests. These data are indispensable to modify or extend the analytical methods currently used to predict the LOCA behavior as well as to evaluate the performance characteristics of computer codes.

Though the experiment L1-2 was conducted without ECC water injections, the performance of engineered safety features with particular emphasis on ECCS is to be obtained through another experiment of TEST SERIES L1 (i.e., L1-4)[14] and future advanced tests. Selected experiment L1-2 simulates a 200 % (100 % of the break area in each leg) double-ended offset shear of the cold leg pipe in a large PWR (Pressurized Water Reactor) with a typical four-loop system.

Usually such break conditions are regarded to be severest for the core hot region temperature. A core simulator installed in place of a active core, provides a representative reactor vessel pressure drop across a nuclear core. The LOFT reactor (55 MWt) is a small PWR designed to carry out LOCA experiments on a scale between research reactor and typical commercial PWR (3300 MWt). The configuration of experimental facility is shown schematically in Figure 1.

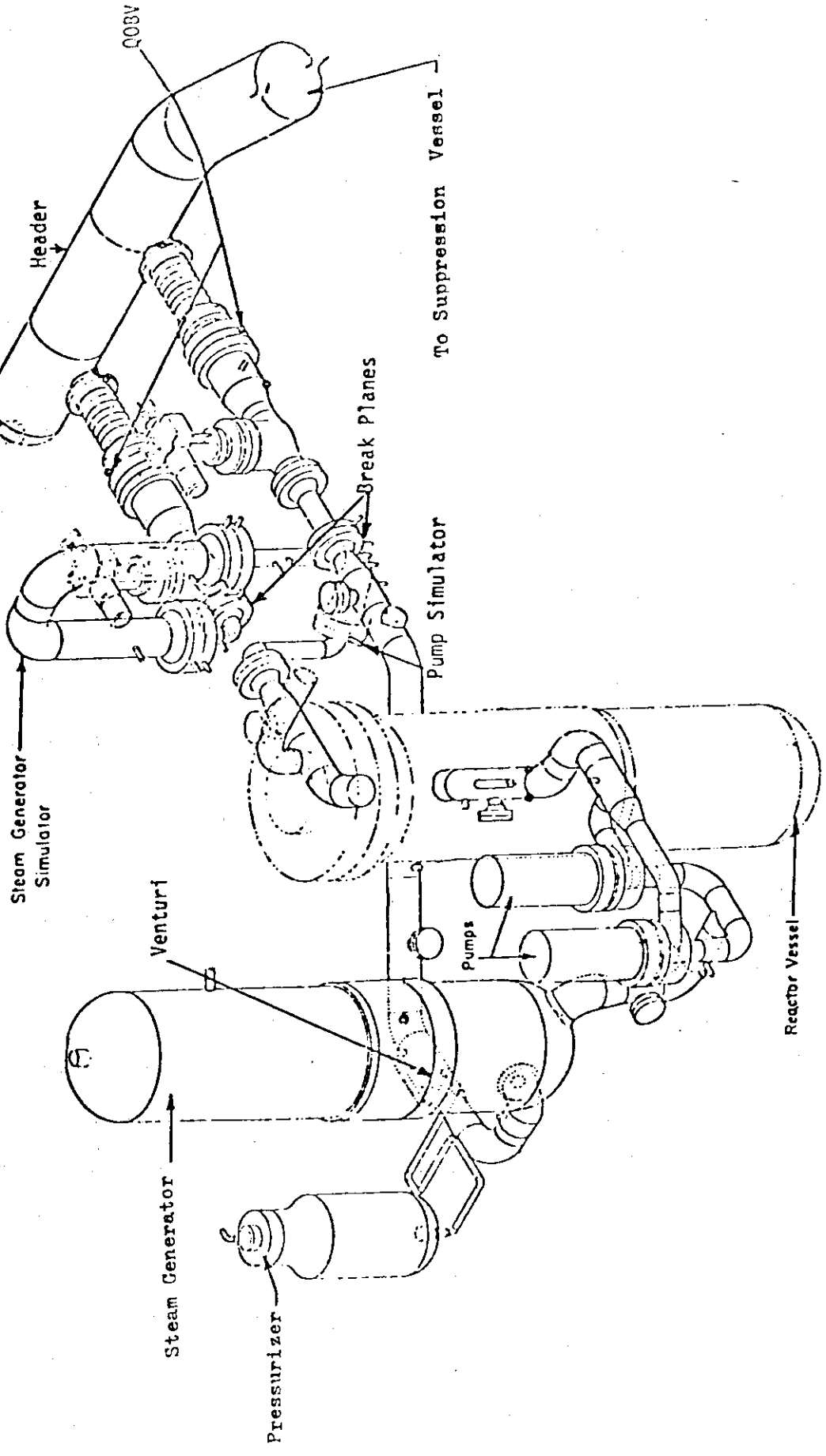

FIGURE 1: LOFT System Isometric

II-2 Features of ALARM-PI Evaluation Code

Given in this section is a brief description of the ALARM-PI employed to solve this sample problem. However, the introductions of heat transfer, nuclear kinetics and numerical techniques, etc. are not described herein, because they are not required for isothermal calculation. The details will be treated in the ALARM-PI code manual.(5)

The ALARM-PI code predicting transient pressure, flow rate, temperature and others during the blowdown was developed as a one-dimensional multinode and multi junction type loop code. In particular, it was programmed in order to investigate time-varying physical phenomenon expected in PWR accidents with large breaks. The program user has flexibility in describing the system geometry, furthermore the number of control volumes and junctions can be specified arbitrarily by the introduction of variable dimension technique. ALARM-PI source decks for the FACOM-230 series use double precision (72 bits words) as the computer word length.

The basic conservation equations of mass and energy integrated over control volume are solved for the volume node at each time step on the assumption of thermo-dynamical equilibrium during any given time mesh. Also, either the homogeneous flow or simple bubble rise model is applied for the two phase coolant behavior. Then, the nodal pressure which provides the mean value within a control volume is determined implicitly by using an equation of state and steam tables. The governing equations are in the form of time dependent ordinary differential equations, and currently kinetic and frictional energy term in energy equation are neglected in this program.

The junctions or flow paths connect directly the control volumes at specified elevations. The conservation of momentum equation is solved for each junction. Thus, mass and energy transfer through junctions to and from the connected control volumes are determined. Although the numerical solutions obtained by the forward finite difference approximation tend to be unstable, special considerations for this problem are not yet prepared in the present version except for some selections of smaller time step sizes empirically learned in order to maintain the stability of solutions for every control volume and junction. In solving these equations, however, the ALARM-PI code employs a junction enthalpy smoothing technique for each junction. If the junction is treated as a horizontal opening and it is not connected with the top or the bottom of a volume, the following problem appears; the state-quantity such as the enthalpy or quality at the junction, changes discontinuously whenever the mixture level passes such a junction, which leads to instability. Therefore, the junction should be considered to have some reasonable vertical-dimension; that is, it should be regarded as common flow area of a connected volume. As long as a interface between the two-phase mixture and the steam phase remains within a junction width or junction diameter, modified enthalpy through the junction with significant cross section area is assumed to be composed of a combination of mixture enthalpy and saturated steam enthalpy. In this case, a distribution of steam and mixture is weighed according to proportional relations between the junction diameter and the mixture level, respectively. Thus, a rapid change of the enthalpy or the quality is smoothfied to some extent as compared with a point-wise junction geometry. In the fluid flow equation, the momentum flux term which accounts for the pressure drop resulting from the spatial change in velocity and density, is incorporated explicitly.

In addition, the momentum mixing model is available when different streams with angle $\theta(\theta \neq 90°)$ mingle with each other at a junction.

The hydraulics in the control volume is assumed to be either homogeneous or non-homogeneous. In the former model, steam and liquid mixture within a control volume during the blowdown is treated as being completely uniform. On the other hand, a phase separation model with bubble distribution is one in which partial density of bubbles within the two-phase mixture is represented as a linear function of height above the bottom of the volume. Steam bubbles are created by bulk flashing of the liquid and then move upwards. A bubble density is naturally minimum at the bottom. A calculation with bubble rise requires bubble density gradient and bubble rise velocity as input data. In this case, if the former is zero, bubbles distribute homogeneously, while if the latter is set to zero, no steam dome will be formed in the volume.

During the blowdown transients, the discharge model of flow through the break plane to the suppression tank, in general, applies principally the Moody's maximum mass flow rate[9] consistent with the assumption of equilibrium throat condition.

It is considered that the Moody's choked flow model determined from an interpolation of tabular values of mass flux vs. stagnant pressure and enthalpy, is pertinent for use through break spectrum analyses of reactor plant transients. However, in general, the calculated discharge flow rate overpredicts experimental data when the break exit plane quality exceeds about two percent.

On the other hand, for the blowdown period which the subcooled liquid or saturation fluid with quality of less than two percent exists at the break exit plane, the Moody's computation model may underpredict

experimental data.

From this point, the effluent flow out of the break plane is modified empirically by multiplying the discharge coefficient C_D, which is constant through the transient. Usually the value of C_D is 0.6, at which calculated discharge flow seems to agree with the test data. During the early period of blowdown before quality reaches 0.02, if C_D mentioned above is set at more than 1.0, the underpredicted discharge flow rate may be improved to some extent.

For such region of less than two percent quality, ALARM-P1 employs the Zaloudek's correlation,[12] which is modified so as to have continuity with the Moody's at zero quality. In addition, for the superheated steam region the Mardock-Bauman's choked flow model[13] is available. The Moody's model also presents the throat pressure as a function of stagnant pressure and enthalpy, and thereby, when the back pressure is above the critical throat pressure, choked flow no longer exists and flow is derived from an orifice flow equation. At the present version of ALARM-P1, it is considered that blowdown has come to an end at this time together with nearly zero flow.

At all times during the blowdown, the ALARM-P1 code checks whether an effluent flow is critical or non-critical, viz., inertial, and the smaller value of two is always selected. This is also true of any junction flow except fill junctions.

In ALARM-P1 fluid flow equation, the Fanning frictional factor for laminar flow is calculated from f=64/Re(Re : Reynolds number), while for turbulent flow from the Karmann-Nikuradse equation. At the two-phase fluid flow region, the increasing effect of the wall frictional losses is determined from a two-phase frictional multiplier, which is represented by a combination of the Thom[10] and Martinelli-Nelson's correlation.[11]

Above correlation is incorporated in the form of data table.

The primary coolant pumps in a water-cooled nuclear reactor influence the thermal-hydraulic behavior of the reactor system during a LOCA. The pump in the broken loop affects only the effluent flow rate. Usually this is treated as an equivalent flow resistance. On the other hand, the pump in the intact loop influences the circulation of fluid in the intact portion of the primary system including the reactor core. In the ALARM-P1 pump model, the value of head and torque are uniquely determined from the relations between pump impeller speed and volumetric flow, i.e., known pump performance characteristics curves and the "Homologous Law."[8] These curves, however, are based on single phase fluid conditions and given as input data table.

Two-phase effects are neglected in the present analysis because of the lack of appropriate data to simulate them. The pump model in the two-phase region will in the future be verified by applicable two-phase pump performance data. When cavitation has occurred, the function of pump becomes ineffective by degrees. In this code, the pump head or the hydraulic torque is treated as a function of cavitation. This cavitation model is not used in the present analysis because time dependent cavitation effects are unknown. Further, the frictional torque is neglected during pump coast-down.

With respect to choice of the time step sizes, although it is not now possible to give a rigorous formulation of limits on acceptable time step in ALARM-P1, it is generally required, for the purpose of verifying solution accuracy or preventing numerical instability, to select sufficiently small time steps (especially for the rapid change during the initial subcooled decompression) because of fully explicit technique.

II-3 General Remarks about Computation

Figure 2 shows the volume node and flowpath setup used to represent the system. The LOFT experimental system was simulated by 28 control volumes with 30 junctions for ALARM-P1 in the same manner as for RELAP-4J,[6][7] on the understanding that the number of loops modeled is usually suppressed to two, i.e., intact loop and broken loop. In four-loop system, three intact loops can be treated as a single loop with appropriate scaling factors.

The broken loop cold leg line was divided into three control volume, connected with the suppression tank through junction 29. On the other hand, the broken loop hot leg line is composed of seven control volumes including the steam generator, the pump simulator and others.

The pressure vessel is made up of four control volumes; downcomer, lower-plenum, reactor core (simulator with no heat addition), and upper-plenum. A bubble rise model with phase separation is adopted to the downcomer and the upper-planum. In addition, heat from structures is taken into consideration in the downcomer.

The pressurizer system, which is shown in Fig.2 to be on the intact loop, consists of the pressurizer and the surge line. The former is modeled with one volume and the latter with two volumes. Because the surge line is of a very long and narrow pipe, it was divided into two volumes. Similarly, a phase separation model is applied to the pressurizer, which is assumed to be saturated uniformly prior to break.

The operating loop hot leg is represented by six control volumes; one volume as the hot leg fluid path, two volumes as the steam generator and one volume between the steam generator outlet and the pump inlet. The steam generator inlet volume also uses a bubble rise model and takes no account of heat exchange.

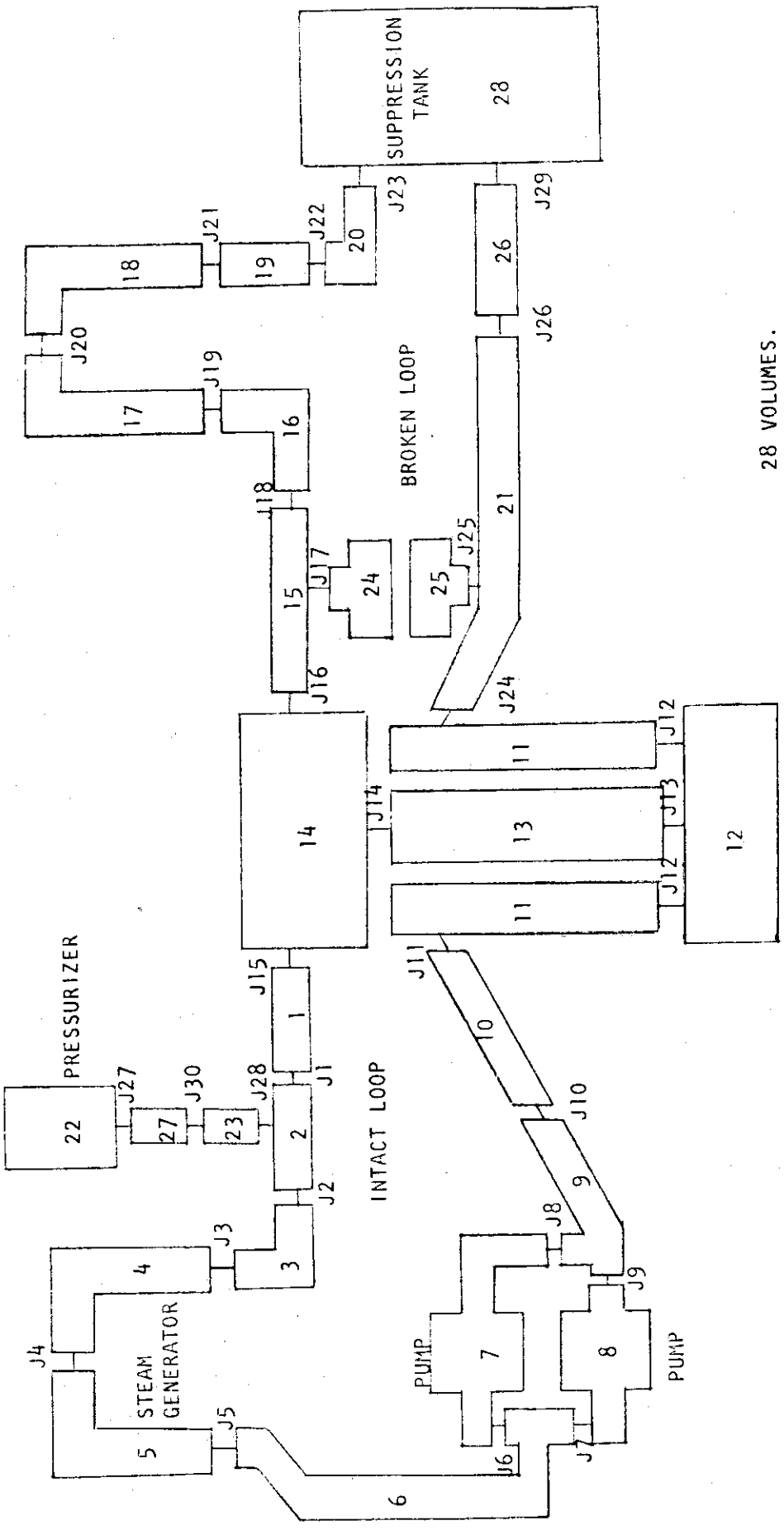

Fig. 2 NODING FOR LOFT L1-2 EXPERIMENT

On the other hand, two control volumes are assigned for simulation of a intact loop cold leg. A pump is treated as one control volume.

The suppression tank which stores effluent flow through the break plane is represented by Volume 28 and simulates the containment back pressure of reactor. Also, the principal initial conditions and parameters used in this calculation are as follows:

(1) Initial mass flow rate in the primary cooling system

265.85 (kg/s)

(2) Initial temperature in the primary cooling system

281.65 ± 0.56 (°C)

(3) Pressurizer pressure 159.61 (kg/cm^2)

(4) Pressurizer temperature 345.56 (°C) saturated

(5) Water level in pressurizer 1.053 (m)

(6) Pump head 100.58 (m)

(7) Pump volumetric flow 0.3154 (m^3/s)

(8) Moment of inertia 0.412 (kg/m^2)

(9) Rated torque and speed 9.748 (kg/m), 367.7 (rad/s)

(10) Option employed in ALARM-P1

(A) VOLUME DATA

(i) Bubble rise model (Volume 4, 11, 14 and 28)

bubble density gradient 0.8

bubble rise velocity 0.9144 (m/s)

(ii) Heat slab (Volume 11)

material stainless steel SUS 304

(iii) Pump (Volume 7 and 8)

Calculation uses only single phase pump data.

Cavitation constant is 10^{-5} on the assumption that no cavitation occurs.

(B) JUNCTION DATA

(i) Discharge coefficient of critical flow

Input constant C_2 was chosen as 0.85 for the Zaloudek's correlation while for the Moody's two-phase critical flow model, a contraction coefficient of 0.6 was applied to the break exit planes and the pressurizer surge line.

(ii) Momentum flux and junction flow smoothing

These two options were used at each junction in the present calculation.

(iii) Break simulation (Junction 23 and 29)

Break is simulated by check valve opening.

Break area is 0.00836 (m^2).

(C) TIME STEP DATA

Time meshes selected in this calculation were:

$0 \leq t \leq 0.05$	$t = 0.00001$ (sec)
$0.05 \leq t \leq 0.30$	$t = 0.00005$ (sec)
$0.30 \leq t \leq 1.0$	$t = 0.0001$ (sec)
$1.0 \leq t \leq 5.0$	$t = 0.0005$ (sec)
$5.0 \leq t \leq 50.0$	$t = 0.001$ (sec)

In addition, break initiation time and pump trip time were assumed to be 0.0 second.

TABLE 1. SATURATION INITIATION TIMES

DESCRIPTION		VOL. NO	TIME (SEC)
INTACT LOOP	HOT LEG	1	0.88
		2	0.17
		3	0.31
	STEAM GENERATOR	4	0.67
		5	0.35
		6	0.21
	PUMP #1	7	1.60
	PUMP #2	8	1.50
	COLD LEG	9	2.40
		10	2.40
PRESSURIZER SYSTEM	PRESSURIZER	22	SATURATED PRIOR TO BREAK
	SURGE LINE	23	0.16
		27	0.41
PRESSURE VESSEL	DOWNCOMER	11	1.25
	LOWER-PLENUM	12	4.65
	SIMULATED CORE	13	4.00
	UPPER-PLENUM	14	2.15
BROKEN LOOP	HOT LEG	15	3.25
		16	1.20
	SIMULATED SG	17	4.30
		18	6.20
	SIMULATED PUMP	19	5.35
		20	0.11
	COLD LEG	21	1.45
		26	0.15
	REFLOOD ASSIST LINE	24	11.90
	REFLOOD ASSIST LINE	25	11.85
CONTAINMENT	SUPPRESSION TANK	28	SATURATED PRIOR TO BREAK

TABLE 2. SPECIFIC ENTROPY AT AN EARLY TIME OF BLOWDOWN

TIME (sec)	AH21	AT21	SPECIFIC ENTROPY	AH15	AT15	SPECIFIC ENTROPY
0.0	295.12	280.56	1.052	293.78	279.44	1.051
0.05	294.18	279.52	1.052	292.68	278.28	1.052
0.15	292.94	278.03	1.054	291.05	276.49	1.053
0.25	292.94	278.01	1.054	291.33	276.74	1.053
0.30	293.03	278.10	1.054	291.43	276.82	1.054

TIME (sec)	AH10	AT10	SPECIFIC ENTROPY	AH1	AT1	SPECIFIC ENTROPY
0.0	297.15	282.22	1.053	296.48	281.67	1.053
0.05	295.67	280.63	1.054	295.24	280.33	1.053
0.15	294.25	279.06	1.054	293.67	278.59	1.054
0.25	294.17	278.98	1.054	293.72	278.64	1.054
0.30	294.16	278.97	1.054	293.68	278.58	1.054

III. Discussion of Results

The calculational results of isothermal decompression process are presented here in conformity with the LI-2 experimental conditions described in the previous section. In addition, some comparisons of calculational outputs and experimental data[3] are discussed in III-2. In Appendix 1 to 3, an input listing for this sample problem and corresponding printed output at the steady and final state are presented to serve as an input preparation guide. Detailed definitions of the input variables and their card formats are given in the reference.[5]

III-1 Interpretations of Calculational Results

Presented herein is a summary of description of the principal blowdown results obtaind using the ALARM-P1 program and their qualitative interpretations. Calculated results are indicated in Figs.3 through 58.

(1) Broken Loop Cold Leg

By an instantaneous cold leg break, the fluid in the experimental facility is confronted with extremely different boundary conditions. The blowdown then starts with a rapid depressurization. Figures 3 to 5 show the behaviors of the coolant inflow to the cold leg piping (flow at junction 24), discharge flow at the break exit plane (flow at junction 29), and the flow at the reflood assist line outlet (flow at junction 25), respectively. In Fig.3, this flow proceeding positively throughout the blowdown, receives the oscillatory influence of the reflood assist line outlet at an early time of the blowdown transient. As the fluid in the downcomer reaches the saturation condition at 1.25 seconds after break (see Table 1), the inflow rate to the cold leg decreases. Up to about six seconds, the cold leg inlet flow oscillates on account of the combined

factors of the frictional pressure loss, acceleration loss, gravitational head loss and others, but the flow is almost stable at 150 kg/sec for the following reasons; because the inflow rate from the intact loop cold leg to the downcomer is considerably large as can be seen in Fig.30, and the downcomer fluid volume is large, the mixture level in the downcomer has not yet reached the top of the cold leg piping connected to the pressure vessel. (see Fig.26) Thus, the average quality of the downcomer is suppressed down to an extremely small degree, with the consequence that the cold leg inlet flow remains stable for a while. (see Fig.35) At 5.94 seconds, when the mixture level reaches the top of the cold leg piping, junction flow to the cold leg shrinks drastically. Subsequently, it brings in its train sudden augmentation because of the increase in the reverse flow from the lower-plenum. A negative flow from the lower-plenum results in temporal increase of the downcomer inlet flow caused by a slight reduction of the downcomer quality at 6.75 seconds. (see Figs.30 and 31) As can be seen in this junction (Junction 24), a pulse-shaped variation with large amplitude has a direct effect on the discharge flow, producing a V-typed change temporarily. Comparison of the two shows that the former has, in general, a slightly smaller trend than the latter.

Both flows, however, are comparatively well-balanced up to about 6.0 seconds from time of rupture, though the junction flow (Junction 24) is oscillating partly. Immediately after the break, the discharge flow becomes critical; this choked flow by approximately 0.55 seconds was determined from the Zaloudek's correlation, while the Moody's two phase flow model was applied later. After 11.85 seconds, the break flow rate is bigger than the amount of coolant inflowing to the cold leg, because the fluid in the reflood assist line joined with the cold leg piping initiates boiling at this time and goes into the cold leg. Then, this difference

between the break flow and the cold leg inlet flow becomes smaller with time and thirty seconds later the two is well-balanced again. The fluid in the reflood assist line (Volume 25) is considered as dead water existing at the subcooled state up to 11.85 seconds.

For the initial 1.25 seconds after break, occur small oscillations with rapid stabilization, as can be seen in Fig.5. After the initiation of coolant inflow, the flow at the reflood assist line outlet decreases slowly as time goes on.

As shown in Figs.6 through 7, the flow quality to the cold leg from the downcomer rises at 5.94 seconds under an influence of the liquid level variation in the downcomer mentioned above, and reaches a peak in the neighborhood of 6.28 seconds. The ascension of this flow quality leads to that of the effluent flow quality at the break exit plane at the almost same time.

Afterwards, the water level recovers as far as the vicinity of the top of the cold leg piping for a while, hence the flow quality declines, after which it has a rising tendency because of a slow reduction in the liquid level. (see Fig.26) The rising rate of these qualities, however, is greatly restrained because the mixture level in the downcomer remains only slightly above the center line of the cold leg piping and the fluid in the downcomer is of low quality. (see Fig.35) Between the downcomer outlet and break node (i.e., in the broken loop cold leg), there exists no large frictional loss which causes a remarkable pressure differential, therefore, the discharge flow quality at the break plane is similar to the junction quality to the cold leg ; the similarity is marked after approximately 16.0 seconds. At 1.45 seconds, the fluid in the cold leg reaches saturation and its density decreases together with bulk-flashing in the downcomer liquid as indicated in Fig.8. In succession, it begins

to decrease abruptly at 5.94 seconds, when the liquid level reaches the top of the cold leg piping. Thereafter, the density increases because of the temporary rise in water level, but tapers off again with the reduction of the water level, i.e., of the inflow rate from the unbroken loop cold leg.

Although each trend of transient densities is similar as shown in Figs.8 to 9, the density of a break node has a faster decline than the cold leg density, because the pressure in the former drops faster than that in the latter.

Shown in Figs.10 and 11 is both pressure histories.

(2) Broken Loop Hot Leg

If the two discharge flow rates are compared in this calculation on the assumption of a 200 % cold leg break, the flow rate expelled through the cold leg is evidently larger than that through the hot leg.

This is due to the fact that the hot leg side, as compared with the cold leg side, contains a steam generator simulator or a pump simulator, either of which causes larger frictional loss. (see Figs.4 and 12) Particularly, the pump simulator resistance is very high. Fig.27 depicts the behavior of the mixture level in the upper-plenum. The inflow rate through the upper-plenum to the hot leg, as indicated in Fig.13, decreases gradually after 2.15 seconds, when the fluid in the upper-plenum reaches saturation state. Then, the hot leg inlet flow decreases drastically when the mixture level in the upper-plenum reaches the top of the hot leg at 6.75 seconds.

Afterwards, the mixture level continues to decrease down approximately to 0.13 m above the bottom of the upper-plenum at 10.94 seconds.

The reduction of the water level results from negative core outlet

flow. After showing almost a constant flow rate for a while, the inflow rate to the hot leg also increases together with the recovery of the water level.

This is due to return to the normal direction of the core outlet flow. Around 16.5 seconds, junction flow (at junction 16) decreases receiving the influence of reverse flow reduction at the steam generator inlet. (see Fig.47) Also, this effect leads to the reduction of the core outlet flow after 16.5 seconds. (see Fig.28) In respect to the steam generator simulator inlet flow (at junction 19) and to the pump simulator outlet flow (at junction 22), the hot leg inlet flow is similar to the former in its behavior and the break flow (at junction 23) to the latter, as given in Figs.12 through 15. This tendency is common to the quality as shown in Figs.16 to 19. But the fluid in the reflood assist line (Volume 24) connected to the hot leg piping begins to boil at 11.9 seconds and goes into the hot leg, with the consequence that a slight difference appears between the flow at junction 16 and at junction 19 as long as the coolant inflow appears significantly in Fig.20. This is also analogous to the quality. In view of above facts, the change of the liquid level in the upper-plenum has a direct influence on the inlet flow rate to the hot leg in case of the cold leg break, but it produces little effect on the discharge flow rate at the exit plane because of large frictional resistance of simulators. In Figs.7 and 19, comparison of the discharge flow quality at each exit plane, shows that the outlet flow quality from the hot leg side increases to about 8 % immediately and reaches a peak value of 41 % at about seventeen seconds after the break. This quality is larger than the one from the cold leg side up to seventeen seconds, then the later becomes larger. This can be explained by the fact that the water level in the upper-plenum recovers in time before

reaching slightly below the top of the hot leg piping at 16.5 seconds, the fluid with low quality consequently flowing into the hot leg from the upper-plenum. After that, second reversal is due to a sudden increase of the flow quality at junction 23. When the mixture level in the upper-plenum goes down as far as to the top of the hot leg piping at 6.75 seconds after the break, a sudden ascent of the flow quality at junction 16 occurs and there exists saturated vapor at the interval between 7.35 and 15.0 seconds; during this interval the water level remains below the hot leg piping.

With the recovery of the liquid level as far as to the bottom of the hot leg piping, the flow quality at junction 16 shrinks drastically from 1.0 to 0.1 as shown in Fig.16. Afterwards, temporal increase of this junction quality results from a small amount of liquid level variations in the upper-plenum.

On the other hand, the average quality of the intact hog leg grows together with boiling at 3.25 seconds and rises suddenly under the influence of the hot leg inlet flow. Then, the average quality decreases for the duration, where the coolant inflow from the reflood assist line is observed clearly. (see Figs.20 and 23) It almost follows the flow quality at junction 16 which decreases significantly, when the liquid level in the upper-plenum rises from the bottom of the hot leg piping at about 15 seconds as can be seen in Figs.16, 23, and 27. Since the flow to the hot leg is always in the normal direction, the density of the hot leg decreases with saturation of the upper-plenum at 2.15 seconds. (see Fig.21) Its density continues to decrease further beyond 6.75 seconds caused by a portion of the hot leg piping being exposed to vapor atmosphere, and the steam flow going into the hot leg.

At 11.90 seconds, the hot leg density fluctuates slightly because

of the coolant inflow effect from the reflood assist line.

With the recovery of the mixture level at about 15 seconds, the density of the hot leg has an increasing trend, but before long it decreases and accelerates the reduction because of the mixture level change around 31 seconds.

The increase of the mixture level in the upper-plenum results from a considerable amount of negative flow through the steam generator in place of dominant pressurizing effect.

Outlet fluid characteristics through the hot leg fluid path are not only of high enthalpy at a very early stage of blowdown, but also successively of high quality. This is due to the fact that steam accumulated in the upper-plenum runs towards the break plane; high effluent energy contributes to accelerate a depressurization. Therefore, the density of the break node is maintained at a very low level as given in Fig.22. Likewise, the pressure in the break node shows the lower value in comparison with that of other nodes. (see Figs.24, 25, 10 and 11) In these figures, the system pressure drops almost instantaneously from the initial pressure to the saturation pressure corresponding to the initial temperature of the compressed coolant.

Particularly, in a transition region from subcooled decompression to saturated decompression, an undershoot phenomenon is temporarily observed in a pressure behavior. In general, such a sudden change in the fluid velocity causes a large pressure change and resulting pressure waves propagate through the system at sonic velocity relative to the flow. After the saturation pressure of the coolant being reached, pressure waves are damped and the choked flow occurs with rapid reduction of sonic velocity. When rupture occurred, Volume 20 reaches saturation first.

A calculation predicts that the critical flow appears immediately. The flow at the reflood assist line outlet has a little influence on the discharge flow because of large frictional resistance of simulators as already noted. It can be seen in Fig.14 that the mass flow rate at junction 19 only slightly increases during the coolant inflow from the reflood assist line.

The hot leg inlet flow oscillates under above influences during the first three seconds prior to the initiation of the coolant inflow, as observed in the cold leg inlet flow.

(3) Pressure Vessel

The mixture level in the downcomer remains fixed in subcooled conditions and decreases after saturation at 1.25 seconds as depicted in Fig.26. At 5.94 seconds after rupture, it arrives at the top of the cold leg piping connected to the pressure vessel and shows the lowest position at 6.28 seconds. Afterward, the liquid level does not show marked variations, remaining stable above the center line of the cold leg.

Meanwhile, the water level in the upper-plenum begins to fall off at 2.15 seconds and reaches the top of the hot leg piping at 6.75 seconds as can be seen in Fig.27. Moreover, it continues to decrease up to approximately 10.94 seconds because the flow through the core to the upper-plenum reverses at 5.8 seconds under the influence of stream from the pressurizer and of pump capability reduction. For 2.2 seconds, the liquid level in the upper-plenum keeps a constant level (0.13 m above the bottom of the upper-plenum), however the water level rises again at 13.14 seconds when the core outlet flow returns to the normal direction. This is due to a significant decrease of coolant flow from the pressurizer.

At 16.5 seconds, the mixture level in the upper-plenum settles slightly below the top of the hot leg piping. At 31.25 seconds after the break, the coolant flows down through the upper-plenum to the core again, causing the decrease in the liquid level. (see Fig.28) After the liquid level recovers within 5.0 seconds, it is held almost constant as the flow rate approaches zero. The level is to some extent above the center line of the hot leg piping when the problem was terminated at 50.0 seconds. As indicated in Fig.29, the flow from the upper-plenum to the intact loop hot leg proceeds positively for a short time after break due to a large amount of inflowing fluid through the core from the intact loop cold leg. In this figure, fluctuations observed up to 2.2 seconds are attributable to changes of frictional pressure losses between nodes. Then, it reverses at 2.2 seconds after the break owing to decrease of the coolant inflow through the downcomer from the unbroken loop cold leg as well as to influence of the pressurizer. The flow at junction 15 is in this direction all the time beyond 2.2 seconds.

In four flow paths joined with the pressure vessel, two flows of intact loop side go into the pressure vessel and two of broken loop side outflow through the pressure vessel exclusively. In this case, as the inflow rate is smaller than the outflow rate, the liquid inventory in the pressure vessel decreases gradually. In Fig.28, the reactor core outlet flow at junction 14 runs in the normal up to 5.8 seconds after the break, then being kept negative by 13.14 seconds. The reverse flow during this period corresponds to the reduction of mixture level in the upper-plenum, as can be seen in Fig.10. In particular, the drop of the pump head caused by steam-voids generated in the primary system results in the decrease of flow after three seconds. As shown in Figs.27 and 28, the interval between 5.8 and 6.75 seconds — where the core outlet

flow begins to run in reverse and increases rapidly in that direction because the influence of pressurizer to the primary coolant system became strong temporarily — shows that the trend of water level reduction in the upper-plenum and of the negative flow increase are well corresponding. This shows that the pressurizer operates sufficiently. When a portion of the surge line nozzle is uncovered at 9.56 seconds and its influence appeares strongly at 10.94 seconds, the core outlet flow (at junction 14) approaches zero rapidly. Therefore, the water level remains fixed without decreasing for 2.2 seconds from this time. As the core outlet flow returns positive after 13.14 seconds and increases gradually, the mixture level in the upper-plenum has a rising tendency until 16.5 seconds.

Then, the core outlet flow begins to decrease under the influence of reverse flow from the steam generator inlet volume instead of decreasing capability of the pressurizer.

Thereafter, since the flow rate at three junctions coupled with the upper-plenum maintains equilibrium between incoming and outgoing flows, the mixture level remains constant. The flow quality through the intact loop hot leg rises rapidly because of a steam flow from the pressurizer, while negative flow quality at the core outlet is kept low. (see Figs.33 and 34) The reason for the low quality is that the core outlet is connected with the bottom of the upper-plenum and submerged below the water. It can be seen in Figs.28 and 29 that the influence of reversal flow from the steam generator appears more conspicuously in the flow through the core than that through the unbroken loop hot leg. In Figs.28, 31, and 32, the core outlet flow, the core inlet flow and flow through the downcomer to the lower-plenum have similar tendencies one another. An individual flow rate indeed decreases suddenly under the predominant

influence of steam efflux through the pressurizer surge line about ten seconds, and especially this situation is clearly observed in the flow at the core outlet nearest to the pressurizer. The tendency which pressurizing effect to the primary system grows strong is also observed commonly among these three flows. The reactor core outlet flow runs as a positive current after 13.14 seconds, but the other two decrease while continuing to run in reverse. When the amount of coolant inflowing through the intact loop cold leg becomes smaller than that through the broken loop cold leg, a flow through the downcomer to the lower-plenum decreases and soon reverses. A density history in the upper-plenum is similar to the mixture level curve, as already noted. Qualities in the pressure vessel are, in general, very low. The average quality in the upper-plenum using a bubble rise model is somewhat high in comparison with others as long as the mixture level remains below the hot leg piping. With respect to each pressure curve, individual behaviors are similar to the primary system pressure.

In the present analysis, the heat slab was considered only in the downcomer with a small cross section and large heat transfer area.

With the lapse of blowdown, the fluid temperature in the downcomer falls along saturation curve as the pressure drops. Therefore, even if no temperature difference is observed between the slab and the coolant at the initial stage of experiment, transient heat transfer through the slab to the coolant deserves much attention. In the final state, the average coolant temperature in the downcomer was 145.35 °C, while the surface temperature of heat slab was 183.90 °C.

(4) Pressurizer

The pressurizer using the bubble rise model is already assumed to be saturated prior to break, therefore its mixture level decreases with rupture as indicated in Fig.36. At 9.56 seconds the liquid level reaches the top of the surge line nozzle, and falls very slowly from that time on. After thirteen seconds from the initiation of blowdown, the level change is extremely small. The liquid level reaches the lowest position of nozzle hole around 29 seconds after the break. The terminal level in the pressurizer remains 0.053 m above the bottom. The pressurizer pressure drops linearly at a slow pace before the mixture level arrives at the top of surge line nozzle, however after 9.56 seconds from break a decompression rate speeds up in consequence of steam efflux into the pressurizer surge line. Thus, the pressure approaches to the primary system pressure by degrees as can be seen in Fig.37.

Mass flow rate through the surge line can be regarded almost as settled after the two-phase critical flow occurs at 0.11 seconds. (see Fig.38)

It decreases drastically when the mixture level in the pressurizer reaches the top of surge line nozzle hole. In Fig.38, there remains a doubt in the result showing that the flow rate at the surge line outlet remains constant as vapor flow without approaching zero after 25 seconds. When the influence of the pressurizer disappears, effluent flow rate from the pressurizer naturally must nearly be zero with the lapse of time. Flow rate changes occurred in the neighbourhood of 3 and 25 seconds, respectively draw much attention. The former results from a change into a inertial flow from the critical flow. The latter might be caused by a discontinuity between a single phase friction factor of

saturated vapor and Thom and Martinelli-Nelson's two phase multiplier.

This influence is also observed in the pressure of Volume 23 (surge line). The fluid in this volume reaches saturation at 0.16 seconds through a decompression caused by break. The average quality in Volume 23 rises after the break, with a slow decrease due to the liquid coming from node 27. (see Fig.39)

Then, it rapidly approaches 1.0 by steam efflux after 9.56 seconds. The flow quality at the surge line exit is similar to the average quality of Volume 23 as indicated in Fig.40.

The average quality of the pressurizer, which represents the liquid quality below the mixture level, reaches a peak at approximately 11 seconds and then decreases gradually, because the steam flow, entering the primary system through the surge line when a portion of surge line hole is uncoverd, amounts to more than vapor quantity generated by decompression boiling. (see Fig.41)

The flow quality at the nozzle inlet (junction 27) also approaches one, i.e., saturated vapor, rapidly owing to the steam discharge at 9.56 seconds as can be seen in Fig.42.

(5) Intact Loop Hot Leg

The primary system pressures of intact loop hot leg side show similar behaviors as indicated in Figs.43 and 45. Through the drastic change after the break, individual pressures settle in saturation condition. For about ten seconds, the decreasing rate of pressure is small on account of the pressurizer effect. Thereafter, the pressure dwindles by degrees according as the pressurizer pressure drops. When the fluid in the hot leg initiates bulk-boiling at 0.88 seconds, that density begins to drop as can be seen in Fig.46. Some time after the

break, in addition to the pressurizer's effect, a decline of pump suction capability causes the reversal of the flow to the hot leg (junction 15) at 2.2 seconds, inviting the rapid decrease of hot leg density. (see Fig.29)

The reduction of pump head results in that of the inflow rate to the downcomer. Since the negative flow through junction 15 remains fixed at the interval between 7.35 and 9.56 seconds, so does the change of the density.

When the mixture level in the pressurizer falls as far as to the top of the surge line nozzle, the steam flow goes into the hot leg through the nozzle, with the consequence that the density of the hot leg drops more and more.

Afterwards, a temporal rise in the density is due to the fact that the reverse flow with low quality occurs towards the hot leg from the steam generator inlet as the pressurizer pressure goes down. (see Fig.47)

Figure 29 shows that the coolant trapped in the steam generator runs to the hot leg and affects the hot leg inlet flow in the neighborhood of 15 seconds. As the fluid in the steam generator inlet volume begins to boil at 0.67 seconds, inlet flow rate (at junction 3) decreases suddenly and the mixture level of volume also falls off, as shown in Fig.48. From about 2.34 to 12.8 seconds, each flow rate at the inlet and outlet of Volume 4 is well-balanced, hence there exists little variation in the mixture level.

Beyond 12.8 seconds, the steam generator inlet flow reverses because the pressurizer pressure is reduced to a large extent. Accordingly, a reduction of the mixture level in the steam generator is promoted.

After the mixture level arrives at the junction 3, connected to the hot leg pipe line, the negative flow rate at the inlet shrinks suddenly and comes near zero. It is shown at about 31 seconds in Fig.47. The outlet

flow (at the junction 4) shown in Fig.49 usually runs in the normal direction, but it changes that direction for some time as depicted in Fig.50. This change of flow is too small to identify it apparently.

The fluid in the steam generator outlet volume (Volume 5) initiates boiling at 0.35 seconds, and that density drops somewhat rapidly because the flow at junction 4 decreases in the positive direction. (see Fig.51) Similarly, the steam generator outlet flow (at junction 5) is positive during the blowdown.

The average quality of the hot leg given in Fig.52 has a rising tendency after bulk-flashing at 0.88 seconds. At 9.56 seconds it increases rapidly because a portion of the surge line nozzle is uncovered and the steam flow enters the hot leg.

After 13 seconds, it decreases all of a sudden under the influence of the negative flow from the steam generator. Afterwards, this quality rises quite drastically together with the reduction of the steam generator's effect.

(6) Intact Loop Cold Leg

The compressed coolant from the intact loop cold leg to the downcomer, initially runs as a positive current because the discharge flow through the break plane promotes a depressurization and a pump operates so as to circulate the coolant in the primary system. However, as the steam-voids developing in the loop with the lapse of time gradually render the pump ineffective, the amount of inflowing fluid to the downcomer decreases rapidly as demonstrated in Fig.30.

On the other hand, the inflow rate to the broken loop cold leg from the downcomer increases beyond 3.75 seconds against the reduction of the downcomer inlet flow, as can be seen in Figs.2 and 30.

Therefore, the flow through the downcomer to the lower-plenum changes that direction at 4.4 seconds. (see Fig.31)

After the reversal flow appeared, the rising rate of this flow is small because of flashing in the lower-plenum.

The negative flow from the lower-plenum invites the descent of the downcomer quality. Consequently, the inflow rate to the downcomer increases temporarily at 6.75 seconds as shown in Fig.30. The flow quality through the cold leg rises smoothly with the ascent of the average quality in the cold leg. (see Fig.53)

After saturation at 2.4 seconds, the cold leg density falls smoothly with the pressure reduction. (see Fig.54) A pressure history in the cold leg is shown in Fig.44, which is nearly identical with the hot leg pressure.

From the observation of the coolant behavior through the recirculating pump, it can be seen that the closer to the cold leg pipe, the larger the flow rate becomes, and the lower the quality; inversely, the density becomes greater in contrast with change of the quality.

(7) Pump

The mass flow rate at the pump inlet and outlet are well-balanced up to 2.18 seconds, but the amount of flowing coolant at the pump exit increases temporarily because the pump head has changed as can be seen in Fig.56.

This flow increment has a influence on the inlet flow to the downcomer. Afterwards, the pump becomes ineffective due to generation of steam-voids, that is, to a reduction in the suction pressure.

Thirty seconds later, both flows approaches zero. As the two pumps are tripped immediately after the break in this calculation, pump

capability to circulate the primary coolant is not to be seen clearly. Therefore, it cannot be considered that the pump is a potent factor on fluid characteristics in this test. (isothermal test)

(8) Suppression Tank

The coolant discharged from the break planes accummulates in the suppression tank. In Fig.58, the pressure in the suppression tank rises smoothly up to 30 seconds, then the rising rate becomes smaller because the effluent fluid is depleted. The terminal suppression pressure is only 1.64 kg/cm^2. This is due to extremely volumious tank capacity, hence the pressure variation is so small as to be 0.60 kg/cm^2 over the long term (50 seconds after the blowdown). The mixture level changed from 2.87 m into 3.17 m as shown in Fig.57. The rising of quality is also very small, and it was 0.025 % at the final state.

Probably, the calculated suppression tank pressure may be lower than the measured. Because air in the tank affects increase of pressure, while the current computation model allows the pressure of air in the volume, but not air flow through the junction to and from the control volumes.

In respect to the initial pressure in the suppression tank, it is slightly higher than 14.7 psia, which is lower-limit of built-in pressure data in the calculation of the two phase multiplier.

Therefore, the pressure less than 14.7 psia is not permitted in ALARM-P1.

III-2 Comparisons with Experiment

The analytical results are herein compared with the experimental data[3] as shown in Fig.59 through 76. In these figures, "A" indicates the calculational results by ALARM-P1 and others the measurement data.

(1) Pressure

Comparison with the calculational results of the experimental data is shown in Figs.59 to 64 and 76. Here, pressures in the broken loop both cold leg and hot leg, in the broken loop pump simulator inlet volume, in the pressurizer and in the intact loop both hot leg and cold leg, are compared, respectively. In regard to system of units, it should be noticed that experimental data are represented by gauge pressure, whereas the calculated by absolute pressure. Except for the pressurizer pressure, each is in good agreement, however, the results obtained from the ALARM-P1 show somewhat larger values than measured experimental data in the neighborhood of 20 to 45 seconds because of a slower decompression of the pressurizer.

As discussed in the section III-1 (4) in respect to the inconsistency of the pressurizer model, a marked difference from experimental data really appeared because of the slow depressurization pace, although the pressure must have been reduced further through steam discharge after about twenty seconds.

This is due to the fact that steam efflux through the surge line did not approach zero. In addition, test datum of the pressurizer pressure does not accord with the calculated at a very early stage of blowdown, because, though the pressurizer is assumed to be uniformly saturated in ALARM-P1 computation model, the region below the electric heater installed in the pressurizer of experimental facility is subcooled

locally prior to rupture, and the very subcooled water mingles with the saturated above the heater at the same time after the break, causing the subcooled decompression. In the present calculation, after approximately ten seconds, the mixture in the pressurizer reaches the top of the surge line nozzle, while there was a delay of about two seconds in the experimental results. The overprediction in the amount of outflowing coolant through the surge line is presumably due to small friction factor.

These two pressure histories agree well for some time after the beginning of steam discharge.

Further examinations await the unexpected, and still unexplained calculated behavior of the pressurizer. The compartment pressure of Volume 26 is also identical with the experimental result. (see Fig.76)

(2) Temperature

Shown in Figs.65 to 69 is the fluid temperatures; the broken loop both cold leg and the hot leg, the pressurizer, and the unbroken loop both hot leg and cold leg. The average temperature in each volume, both measured and calculated, except in the pressurizer falls about 3 ~ 4 degrees immediately after the break. This is due to decompression through isentropic condition.

As described in Table 2, specific entropy equals to 1.052 ~ 1.054. Respective nodes reach saturation within four seconds, and their temperatures fall at saturation temperature corresponding to the system pressure.

At the last stage of blowdown, each temperature measured has a rising tendency because of heat transfer from the structures.

Measurement data in the pressurizer vary with the instrument locations. Although the pressurizer was assumed to be saturated in this

calculation, experimental data suggests that superheated vapor existed in the pressurizer. (e.g., pressure=25 kg/m^2, temperature=290 degrees at 30 seconds).

In Fig.67, the TEFTD204 measurement indicates a constant value after about 23 seconds. This thermo-couple may possibly have been out of order.

(3) Mixture level

On the first inspection of Fig.70, experimental data in the pressurizer which were measured at three peripheral points, agreed well one another, but disagreed with the calculated with respect to the initial water level and the successive reducing speed of the water level.

(4) Density

The broken loop both cold leg and hot leg, the intact loop both hot leg and cold leg and the pump inlet volume — these density calculations are compared with the test data as indicated in Figs.71 to 75.

Density measurements are made using gamma densitometers with a cesium 137 gamma ray source and determined from the attenuation of gamma ray through the pipe wall and fluid. Gamma ray is applied from three directions. The density in the broken loop cold leg, in the intact loop cold leg and in the pump inlet volume are in excellent agreement with the experimental data. Measurement results of the hot leg vary with the irradiated direction. This is probably due to complicated flow regime arising within the pipe. Since in ALARM-P1, fluid equations are dealt with a homogeneous flow, measured data at the region where the homogeneous flow exists comparatively such as at the broken loop cold leg, at the intact loop cold leg, and at the pump inlet, agree well with the calculated. In particular, when a large amount of flow runs through the

broken loop cold leg during the entire blowdown transients, "Homogeneous Flow" assumption is reasonable. Hence, each cold leg density given in terms of calculation and experimental datum is in a good agreement.

Meanwhile, the flow through the hot leg decreases drastically about three seconds later, so that homogeneous flow assumption is invalid, and a marked difference appears between calculational result and experimental data.

There existed significant differences among the three measurement data in the broken loop hot leg. In particular, from a measurement instrument DEBTD006 it suggests that the flow pattern is composed of a stratified flow. It can be concluded from these figures that the analytical solutions are in reasonable agreement with experimental data on the whole, and are sufficient to give qualitative explanations of blowdown phenomena.

IV. Conclusions

The ensuing conclusions can be drawn in the light of the results obtained in this run.

1. The ALARM-PI computational model used to simulate LOFT LI-2 experiment related to the blowdown phenomenon has presented satisfactory results about the pressure, the temperature, the density, and others in the reactor system as compared with experimental data. Thus, the adequacy of the analytical techniques was established for the present trial.
2. Inconsistency of the pressurizer model in ALARM-PI decelerated the decompression in the pressurizer. Therefore, the calculated in the pressurizer had a notable discrepancy with experimental results. In particular, it should be kept in mind that there existed discontinuous changes of flow through the surge line.
3. "Homogeneous assumption" as the fluid properties is reasonable at the places where the amount of flowing coolant is large and that direction is fixed such as the flow through the broken loop cold leg. In the very early portion of blowdown, a homogeneous model is pertinent for use because flow velocity is very high for large breaks.

   On the other hand, when the flow rate, as shown in the hot leg flow, varies to a large extent including the direction of the flow, stratified flow or other patterns may be appropriate in view of experimental results presented in density histories.
4. As the current analysis was performed on the basis of isothermal condition, heat slab considered in the downcomer had little conspicuous influence on fluid in the reactor system.

5. The pump effect appeared little at each part of the primary cooling system because pump power was cut-off simultaneously after the break initiation. Also, the present analysis in terms of insufficient pump data and crude assumptions i.e., ignorance of two phase pump characteristics did not show significant features in the fluid behaviors.
6. Throughout this test run, time step sizes used were appropriate without numerical instability.
   Though economizing in computation time (CPU time is about 1.4 hours in this run) is desired, it will be impossible to further increase these time step widths given in input list. Possibly, present time step sizes for LI-2 experimental analysis are a limit of the ALARM-PI code solved in terms of fully explicit method.

As concluded above, the validity of computer code ALARM-PI was indeed to some extent verified from this analysis, but modifications and refinements are expected to be incorporated into the fundamental system representation of this code in order to complement the insufficient analysis techniques intrinsic in the code, and to obtain further improved representations of blowdown phenomena. In addition, it is hoped that problems inherent in extrapolating as responses of commercial nuclear power reactors from either analytical or experimental results will be solved through further scale effect tests and development of codes with elaborate models.

Acknowledgment

The author would like to express his gratitude to LOFT analysis group of Reactor Safety Laboratory 1, who presented reference data and to Mr. K. Sato, chief of Reactor Safety Code Development Laboratory, who critically read a draft of the paper and made useful suggestions.

REFERENCES

1. H.C. Robinson, "LOFT SYSTEM AND TEST DESCRIPTION (Loss-of-Coolant Experiments using a core simulator)", TREE-NUREG-1019, Nov. 1976.
2. H.C. Robinson, "LOFT SYSTEM AND TEST DESCRIPTION (Loss-of-Coolant Experiments using a core simulator)", LTR-20-57, Mar. 1976.
3. H.C. Robinson, "EXPERIMENTAL DATA REPORT FOR LOFT NONNUCLEAR TEST L1-2", TREE, NUREG-1026, Jan. 1977.
4. Committee on Reactor Safety Examinations, Japanese Atomic Energy Commission Monthly Report, 20(6), 1975.
5. M. AKIMOTO, et al., "ALARM-P1 —— A COMPUTER PROGRAM FOR PWR BLOWDOWN ANALYSIS", to be published.
6. K.V. Moore, W.H. Rettig, "RELAP-4 —— A COMPUTER PROGRAM FOR TRANSIENT THERMAL HYDRAULIC ANALYSIS", ANCR-1127, Dec. 1973.
7. K. Tasaka, et al., "ANALYSIS OF LOFT (L1-2) EXPERIMENT BY CODE RELAR-4J", JAERI-M 7037.
8. D.J. Olson, "SINGLE AND TWO-PHASE PERFORMANCE CHARACTERISTICS OF THE NŌD-1 SEMISCALE PUMP UNDER STEADY STATE AND TRANSIENT FLUID CONDITIONS", ANCR-1165, 1974.
9. Moody, "MAXIMUM FLOW RATE OF A SINGLE COMPONENT, TWO-PHASE MIXTURE", J. of Heat Transfer, Trans. ASME, 87, No.1, 1965.
10. J.R.S. Thom, "PREDICTION OF PRESSURE DROP DURING FORCED CIRCULATION BOILING OF WATER", Int. J. of Heat & Mass Transfer, 7, 1964.
11. R.C. Martinelli, D.B. Nelson, "PREDICTION OF PRESSURE DROP DURING FORCED CIRCULATION BOILING OF WATER", Trans. ASME, 70, 1948.
12. F.R. Zaloudek, "THE CRITICAL FLOW OF HOT WATER THROUGH SHORT TUBES", HW-77594 UC-38, 1966.

13. J.W. Murdock and J.M. Bauman, "THE CRITICAL FLOW FRICTION FOR SUPERHEATED STEAM", Trans. ASME, PP507-518, Sep. 1964.

14. K. SODA, et al., "PREDICTION OF LOFT L1-4 EXPERIMENT —— CSNI STANDARD PROBLEM NO.5 ——", JAERI-M 7329.

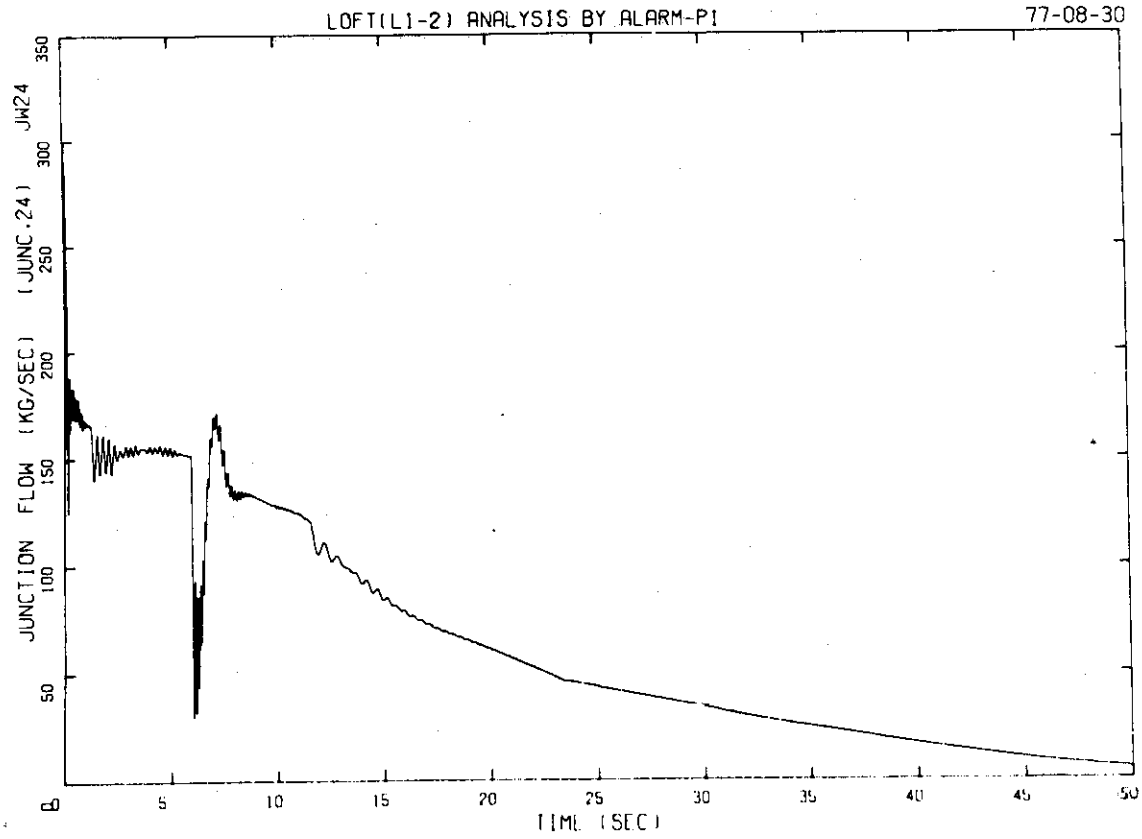

Fig. 3 Mass Flow Rate from Downcomer to Broken Loop Cold Leg

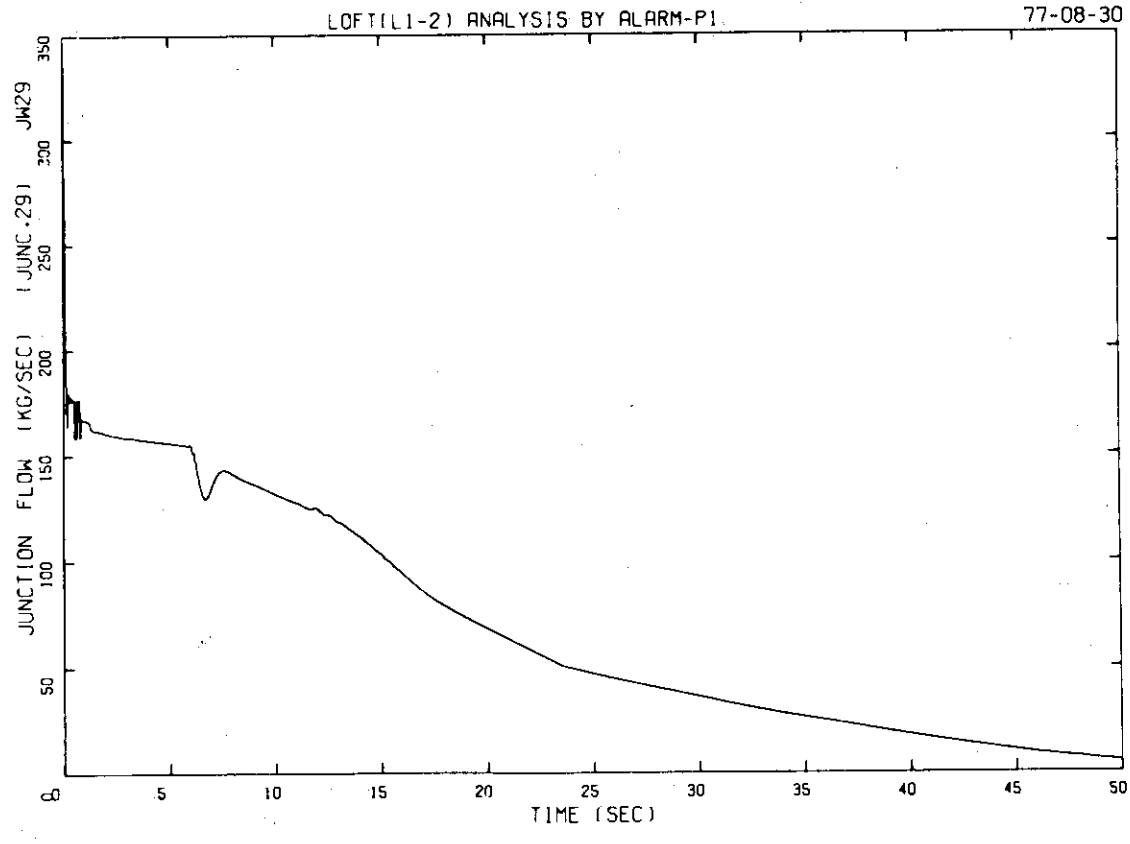

Fig. 4 Discharge Flow Rate at Broken Loop Cold Leg Break Plane

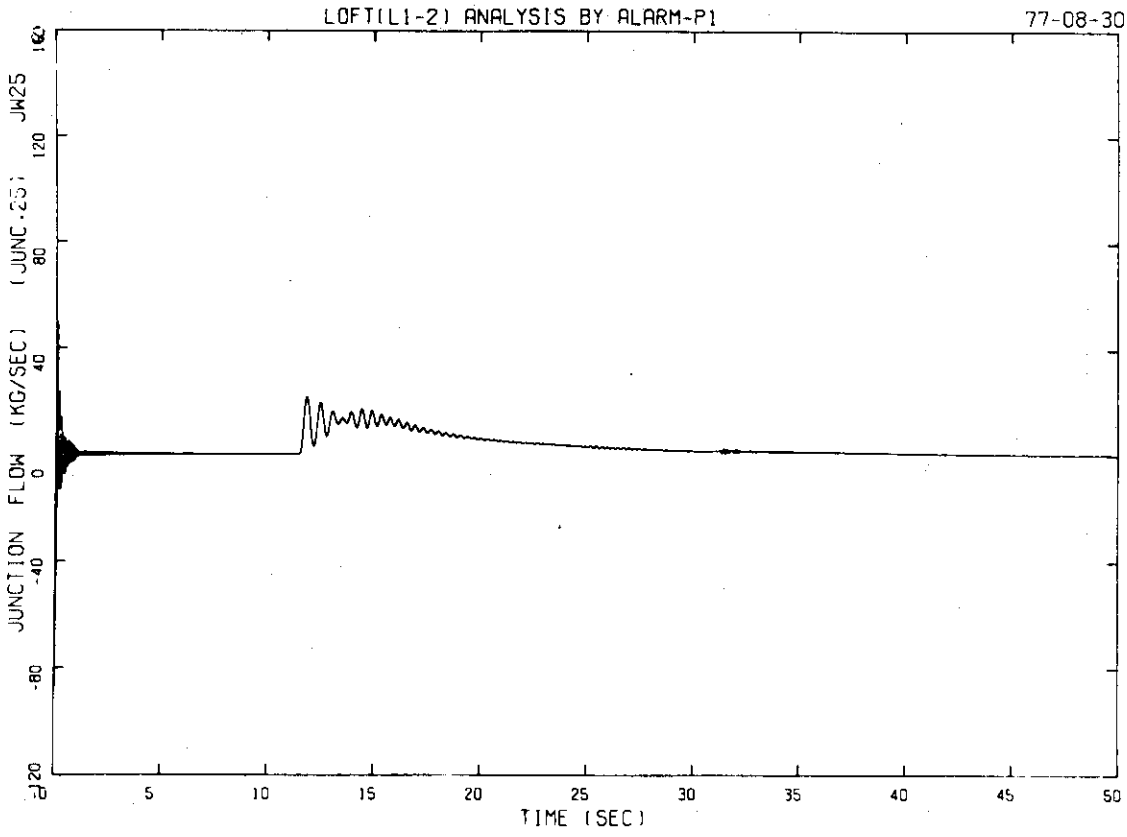

Fig. 5 Mass Flow Rate at Reflood Assist Line Outlet Connected to Broken Loop Cold Leg

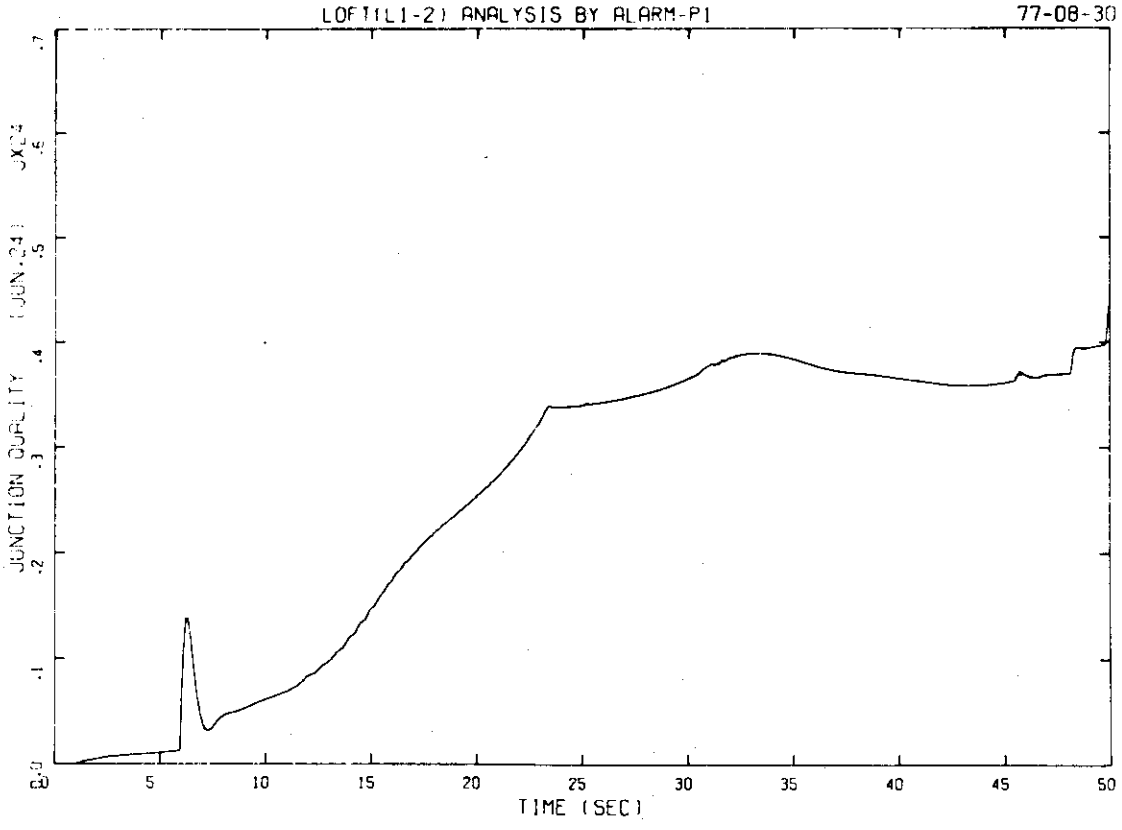

Fig. 6 Junction Quality between Downcomer and Broken Loop Cold Leg

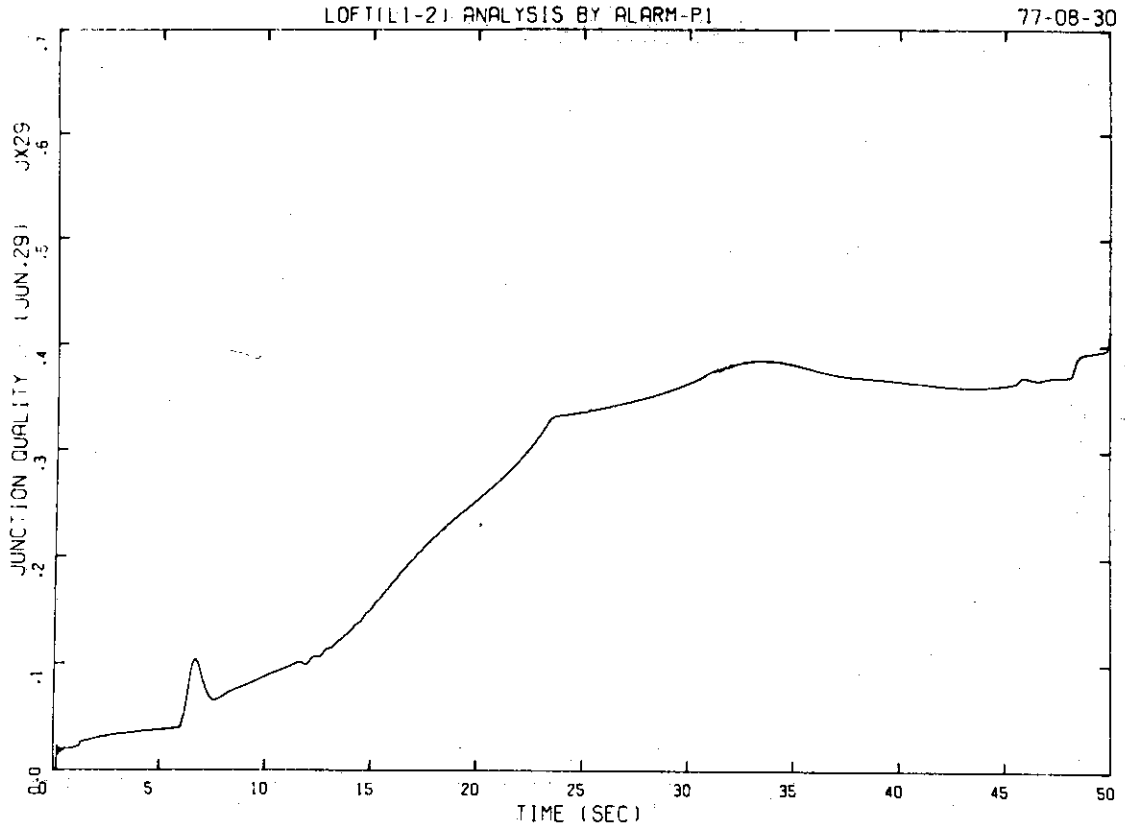

Fig. 7 Discharge Flow Quality at Cold Leg Break Plane

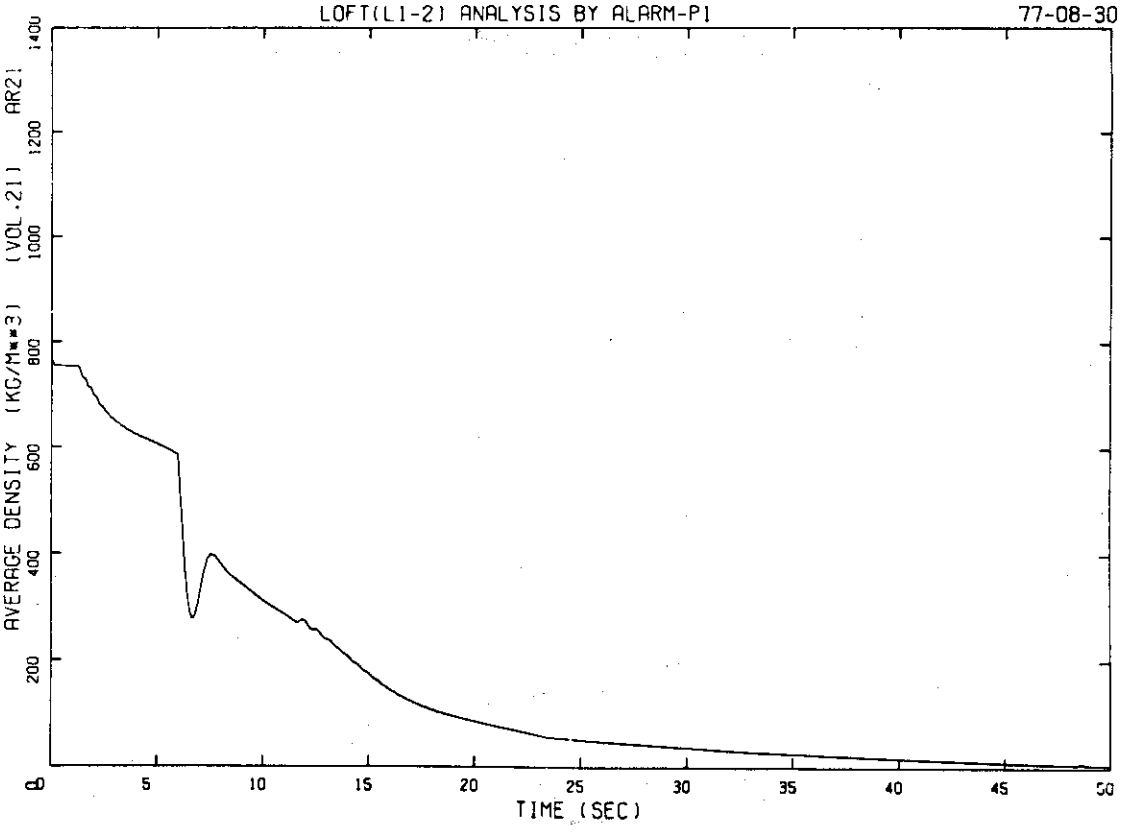

Fig. 8 Average Density in Broken Loop Cold Leg

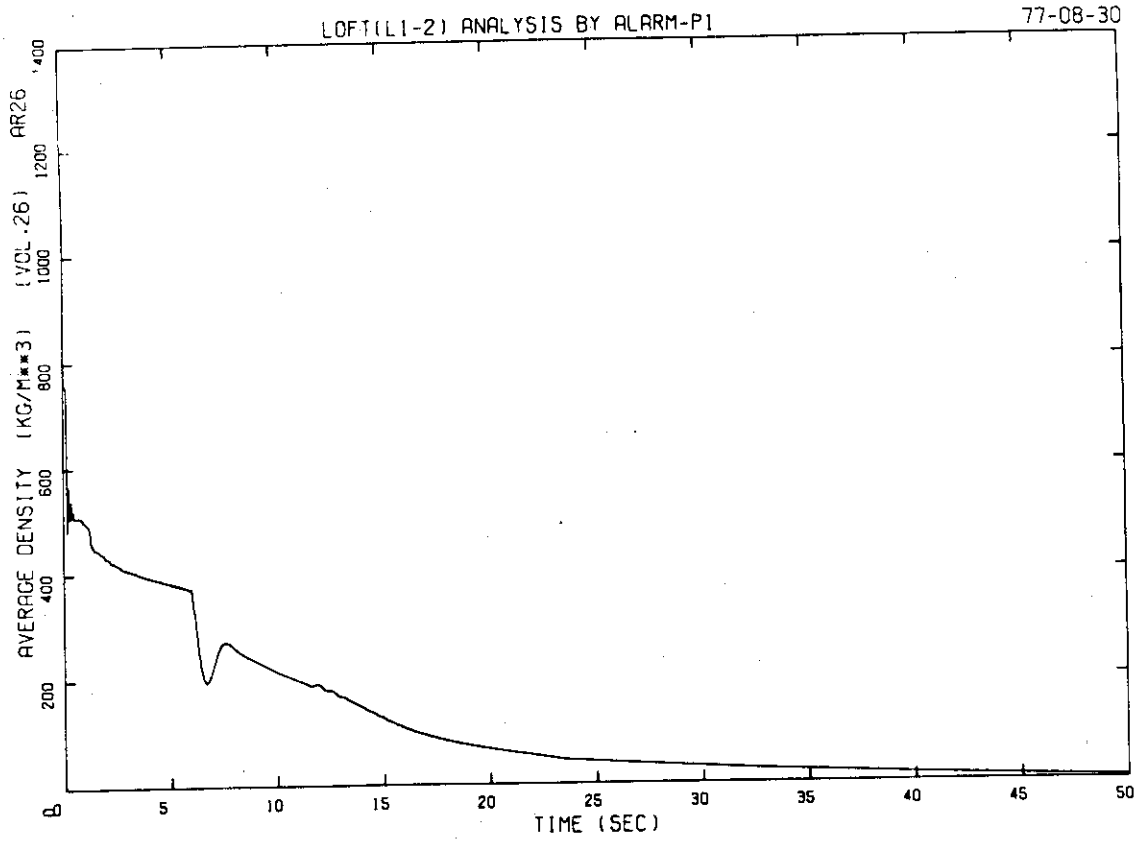

Fig. 9 Average Density in Break Node

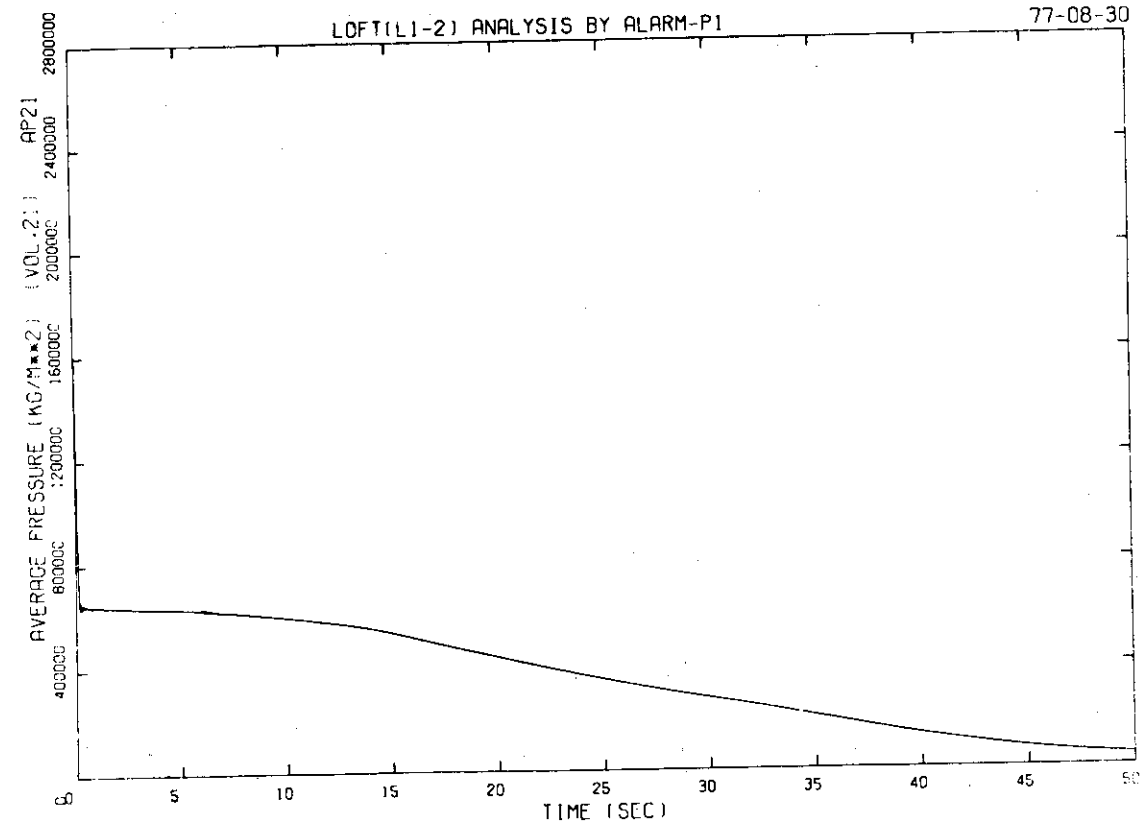

Fig. 10 Average Pressure in Broken Loop Cold Leg

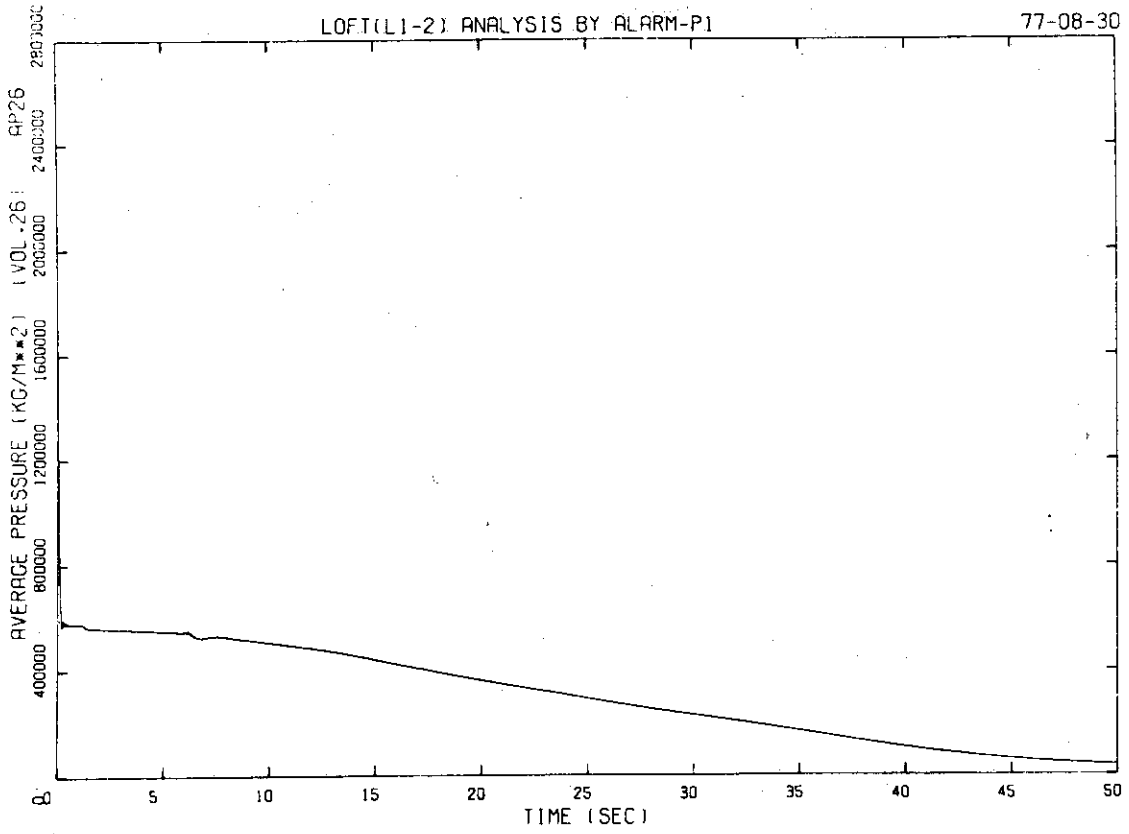

Fig. 11 Average Pressure in Break Node

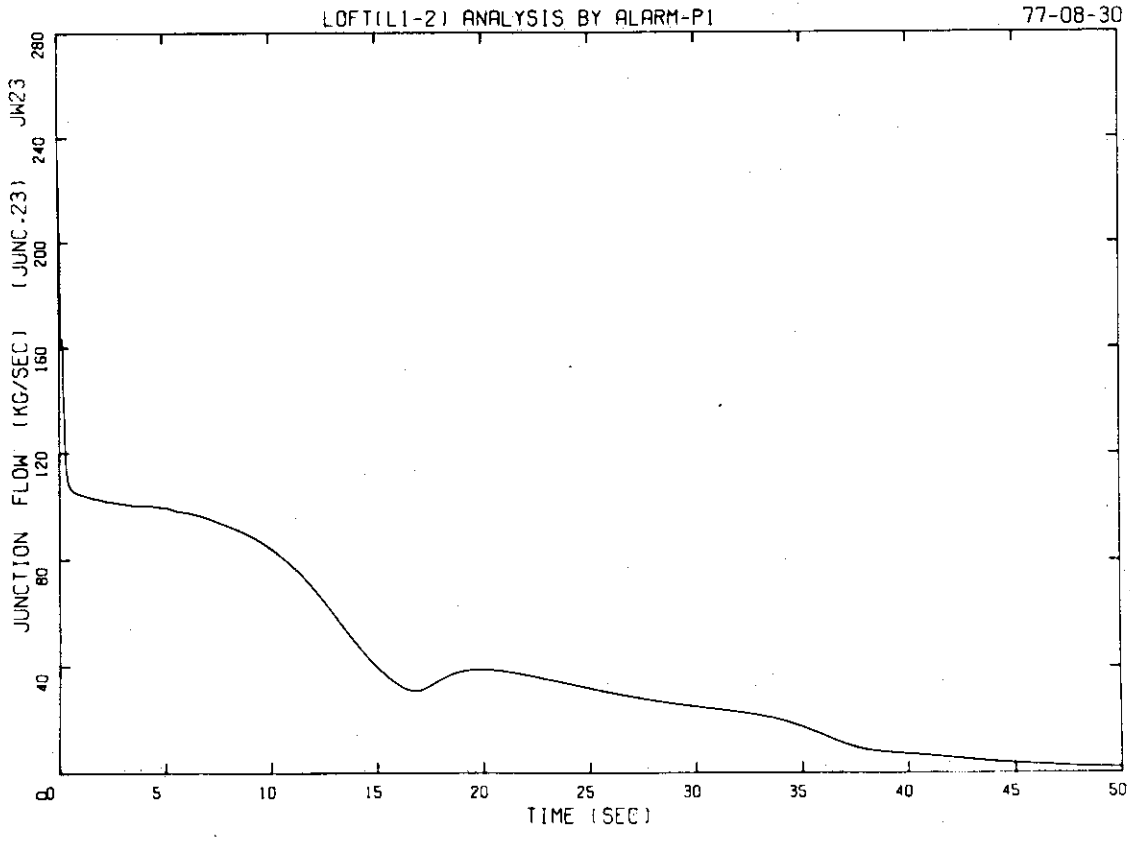

Fig. 12 Discharge Flow Rate at Broken Loop Hot Leg Break Plane

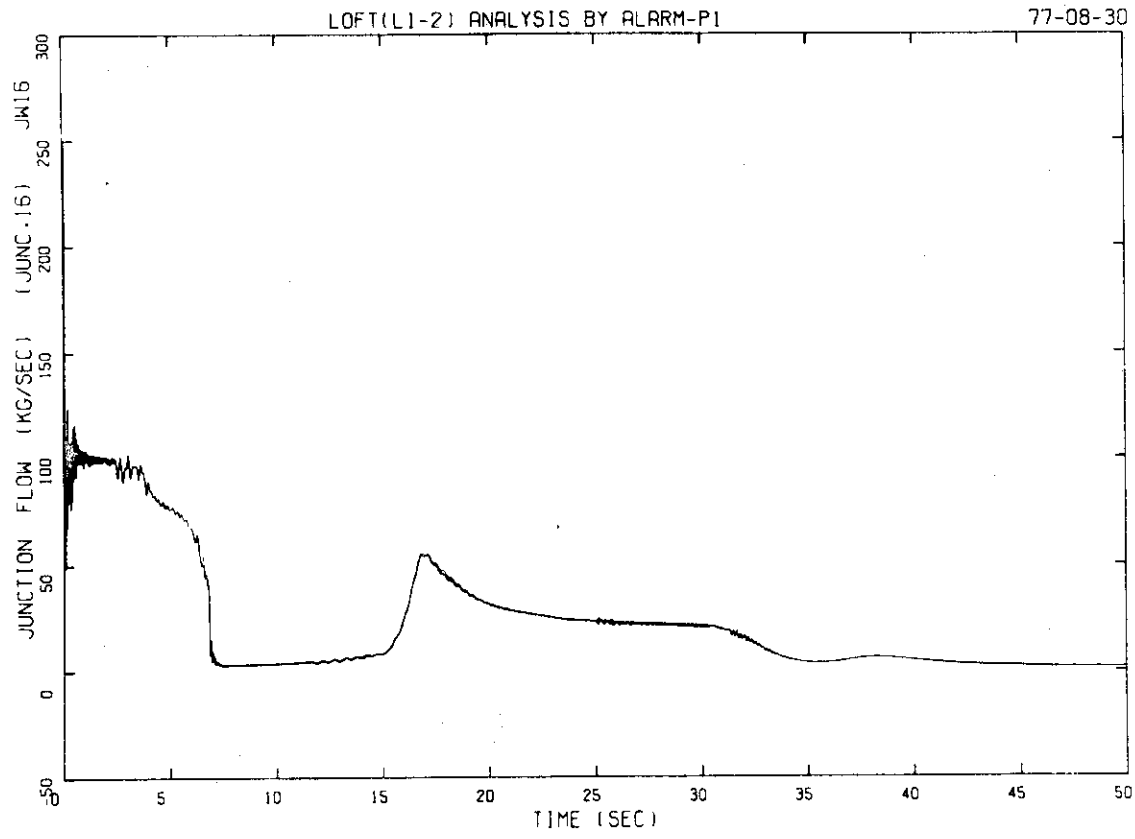

Fig. 13 Mass Flow Rate from Upper-Plenum to Broken Loop Hot Leg

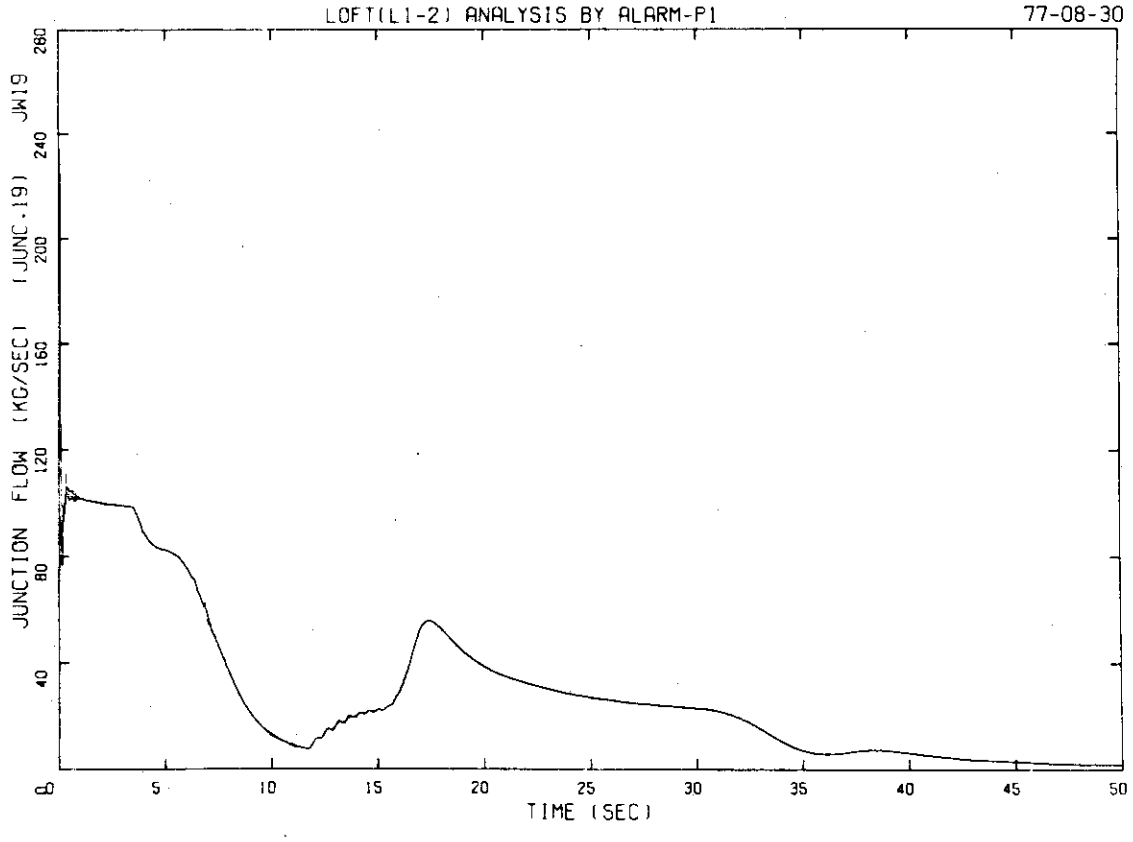

Fig. 14 Mass Flow Rate at Steam Generator Simulator Inlet

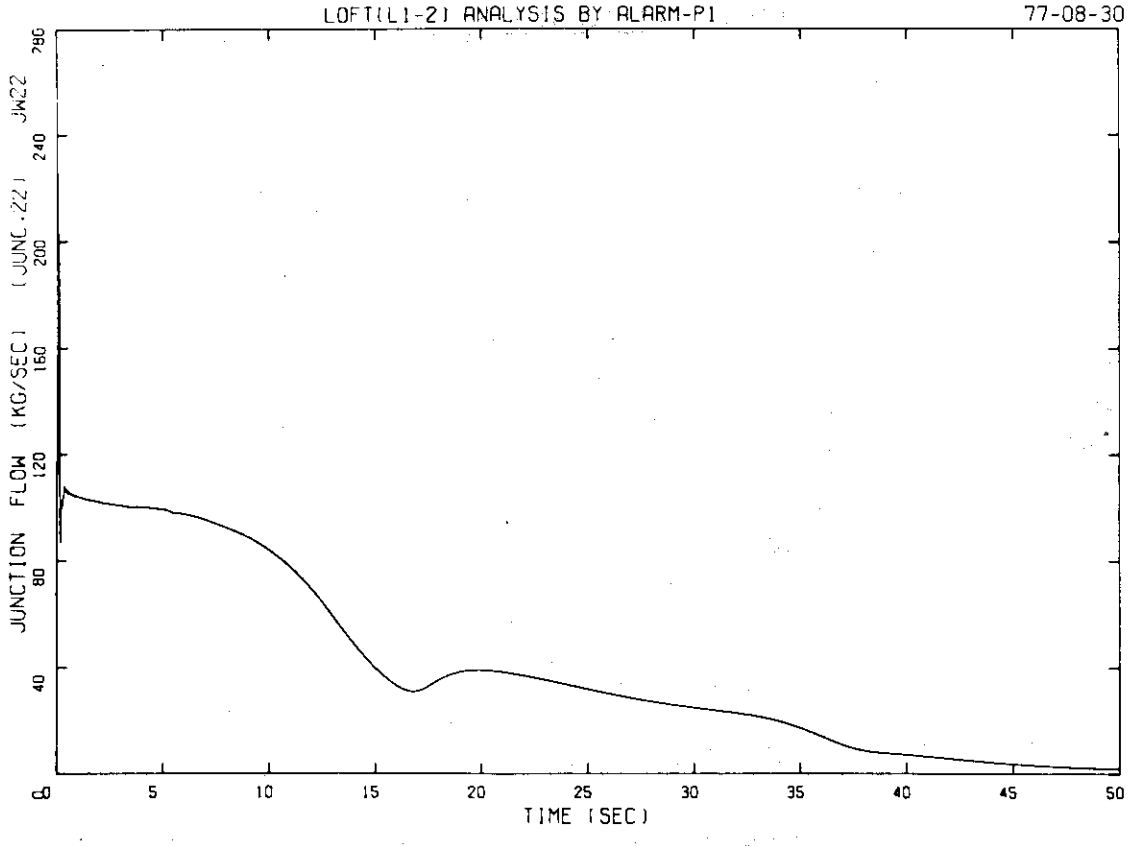

Fig. 15 Mass Flow Rate at Pump Simulator Outlet

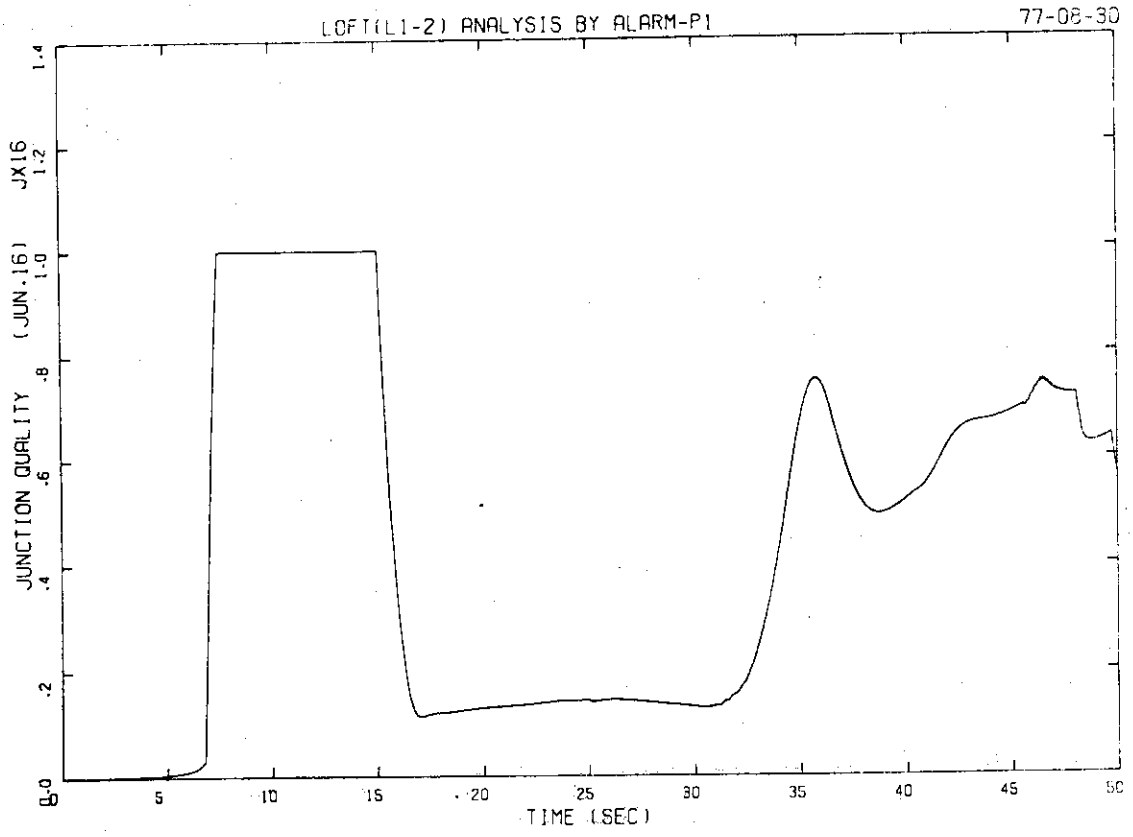

Fig. 16 Junction Quality between Upper-Plenum and Broken Loop Hot Leg

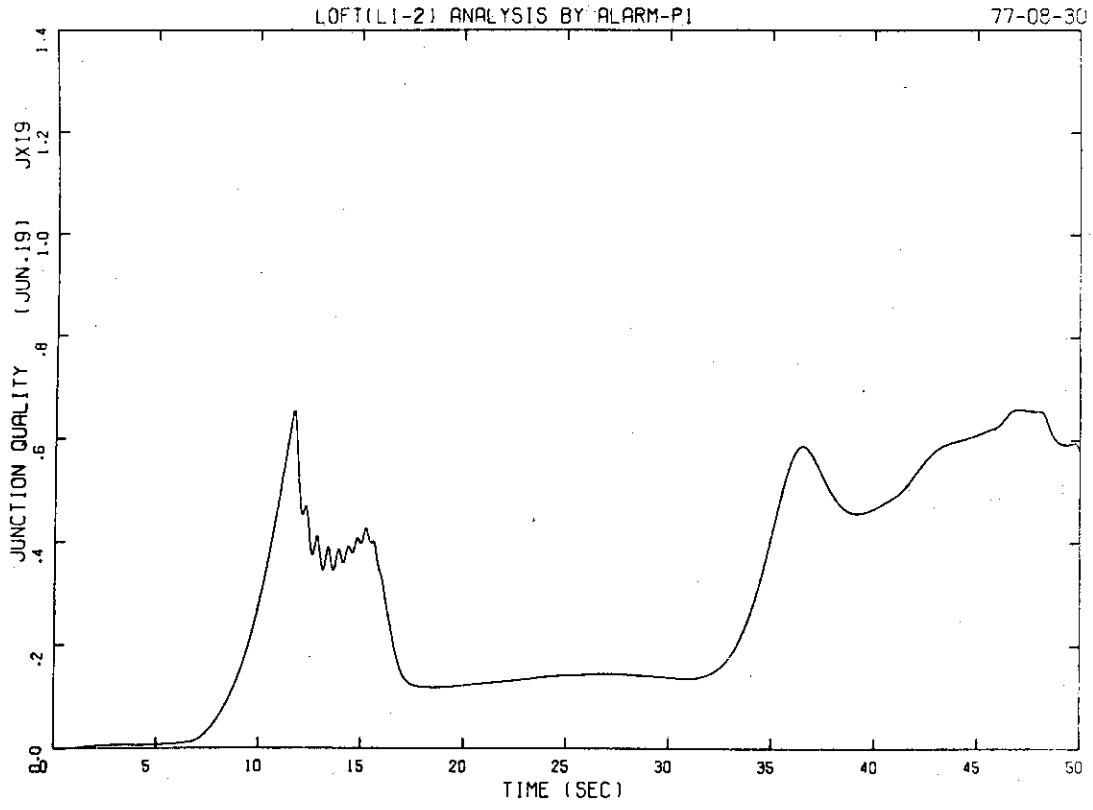

Fig. 17 Junction Quality at Steam Generator Simulator Inlet

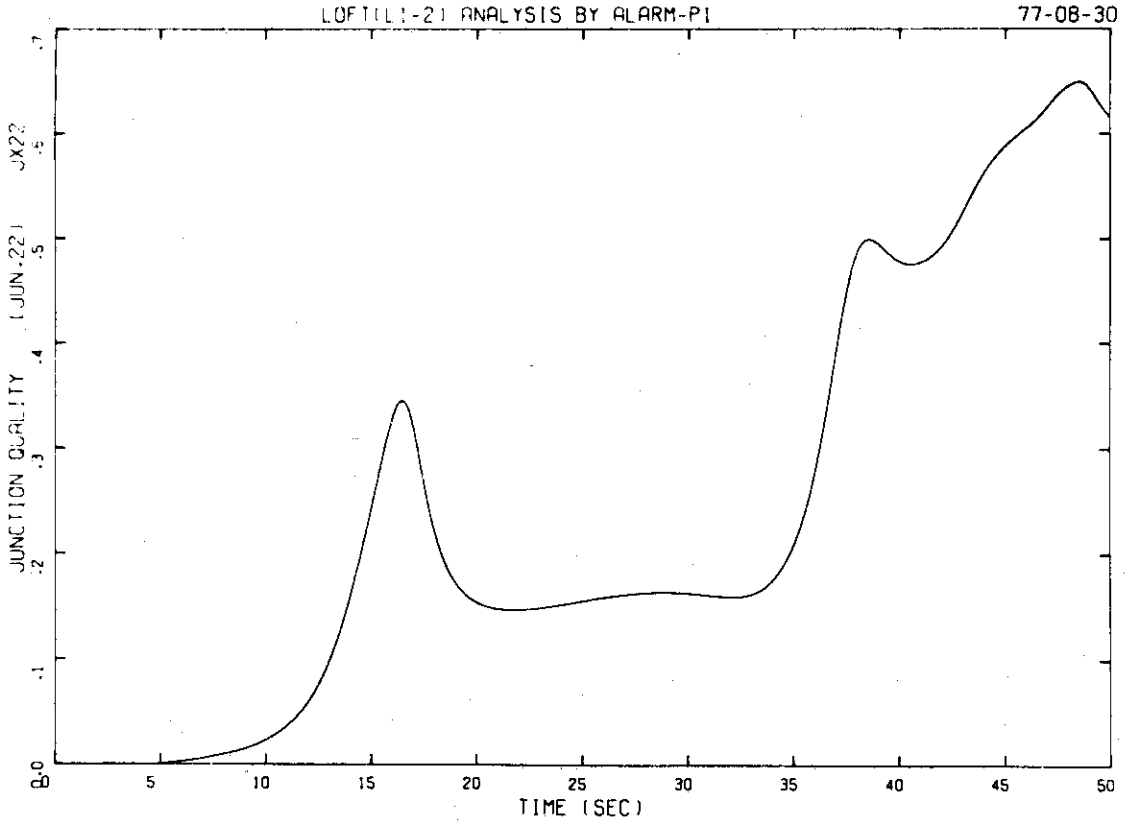

Fig. 18 Junction Quality at Pump Simulator Outlet

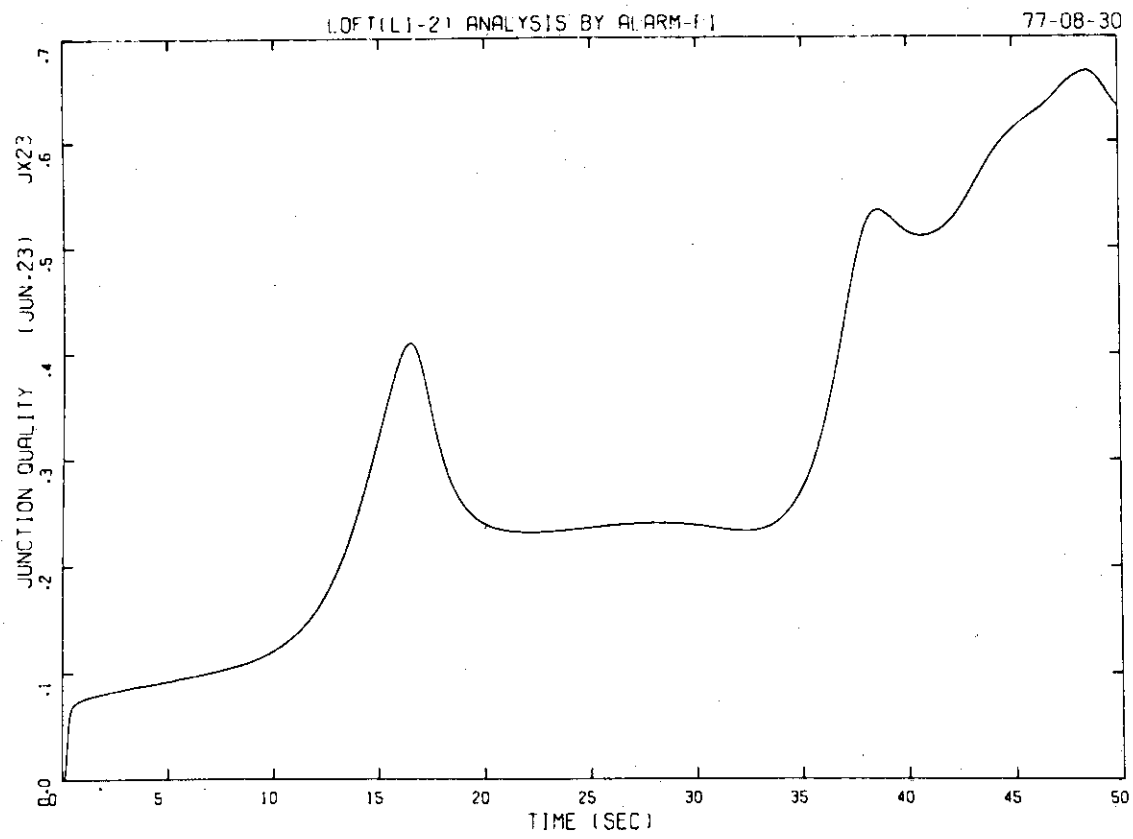

Fig. 19 Discharge Flow Quality at Hot Let Break Plane

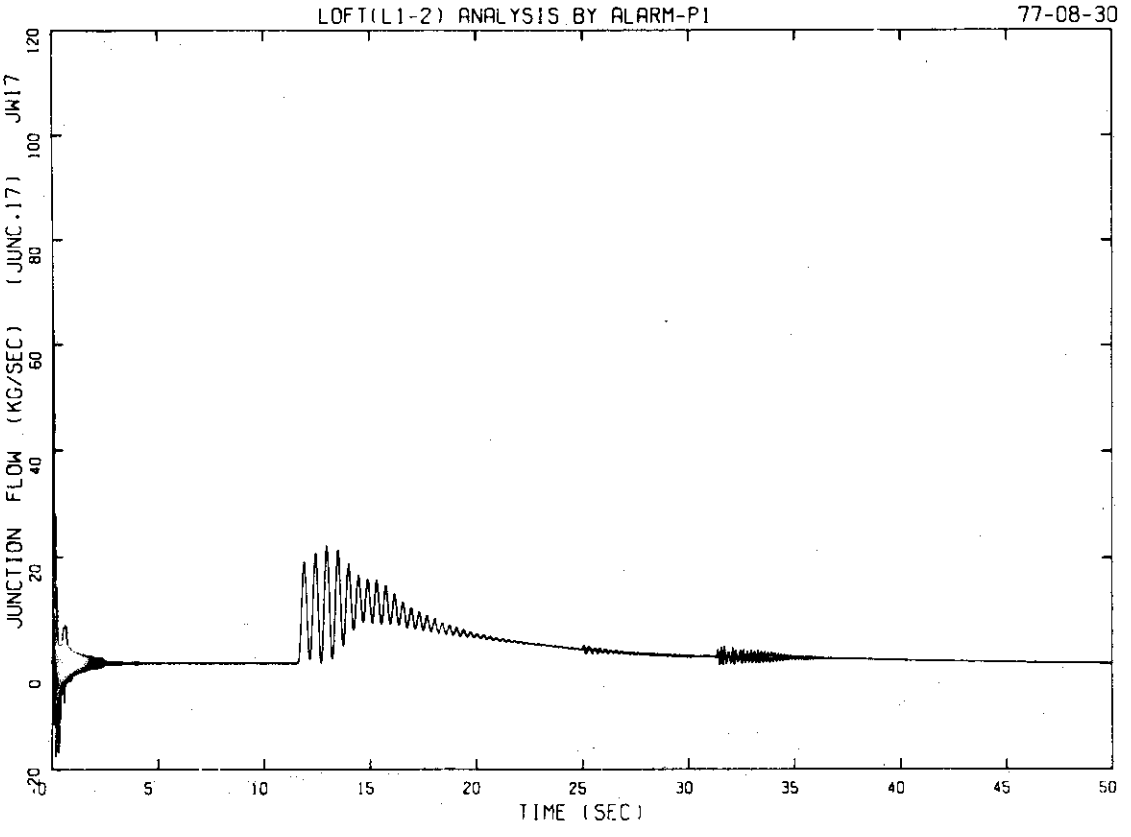

Fig. 20 Mass Flow Rate at Reflood Assist Line Outlet

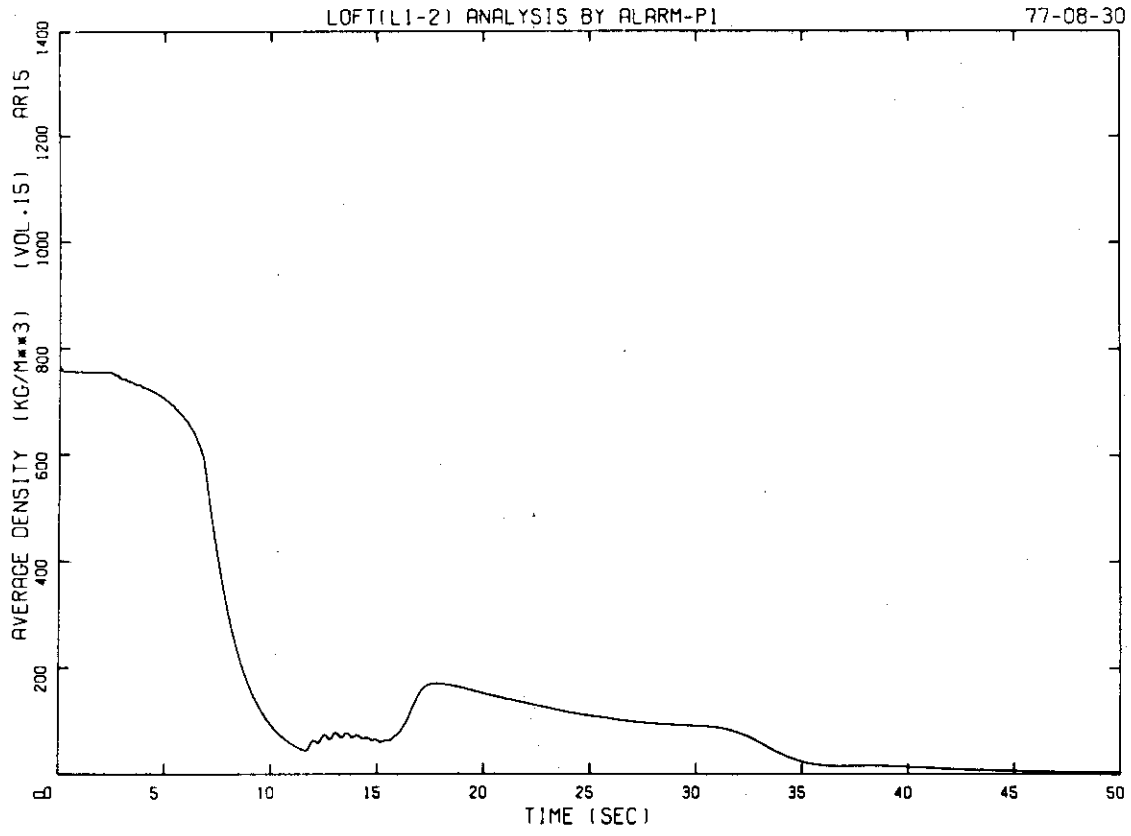

Fig. 21 Average Density in Broken Loop Hot Leg

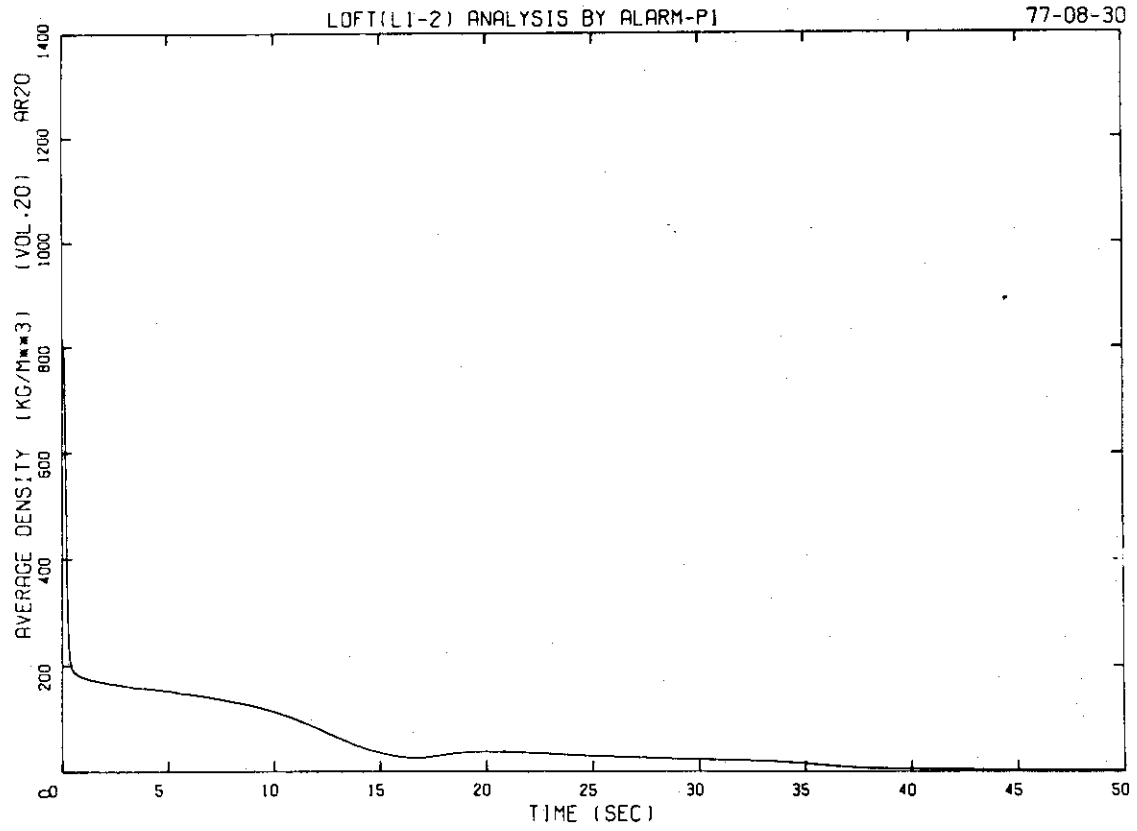

Fig. 22 Average Density in Break Node

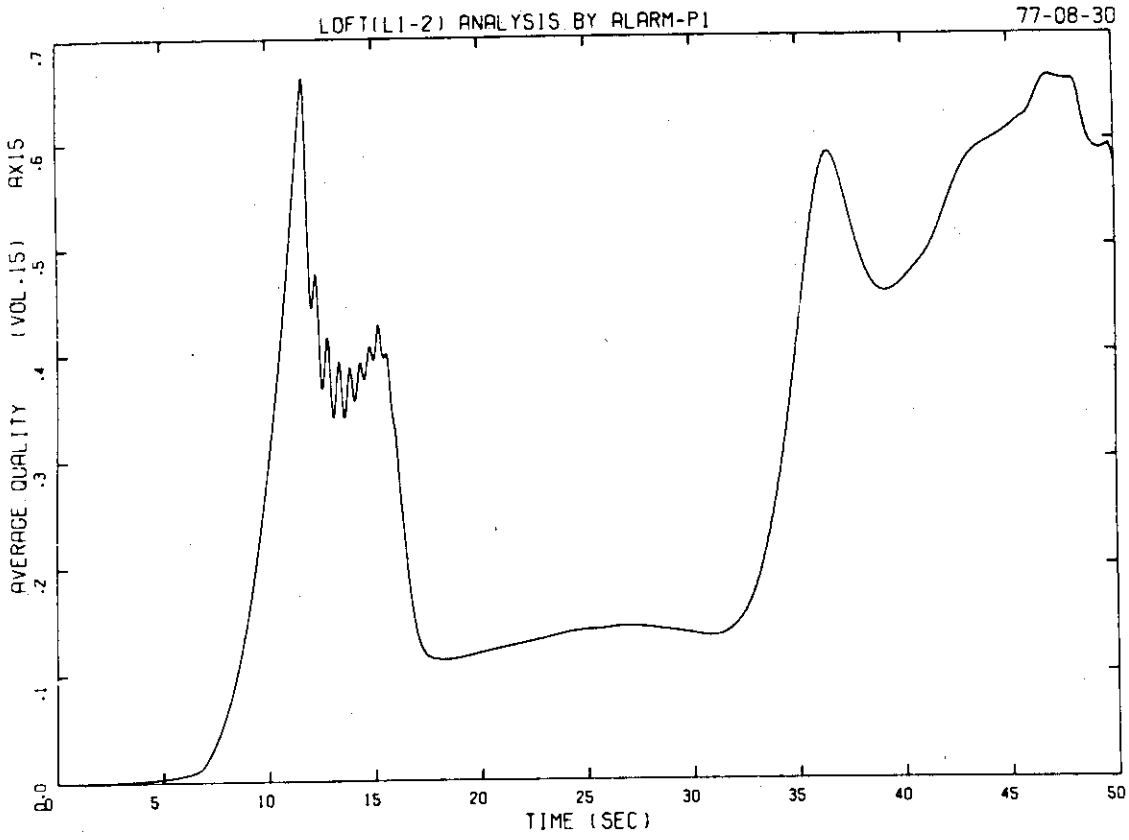

Fig. 23 Average Quality in Broken Loop Hot Leg

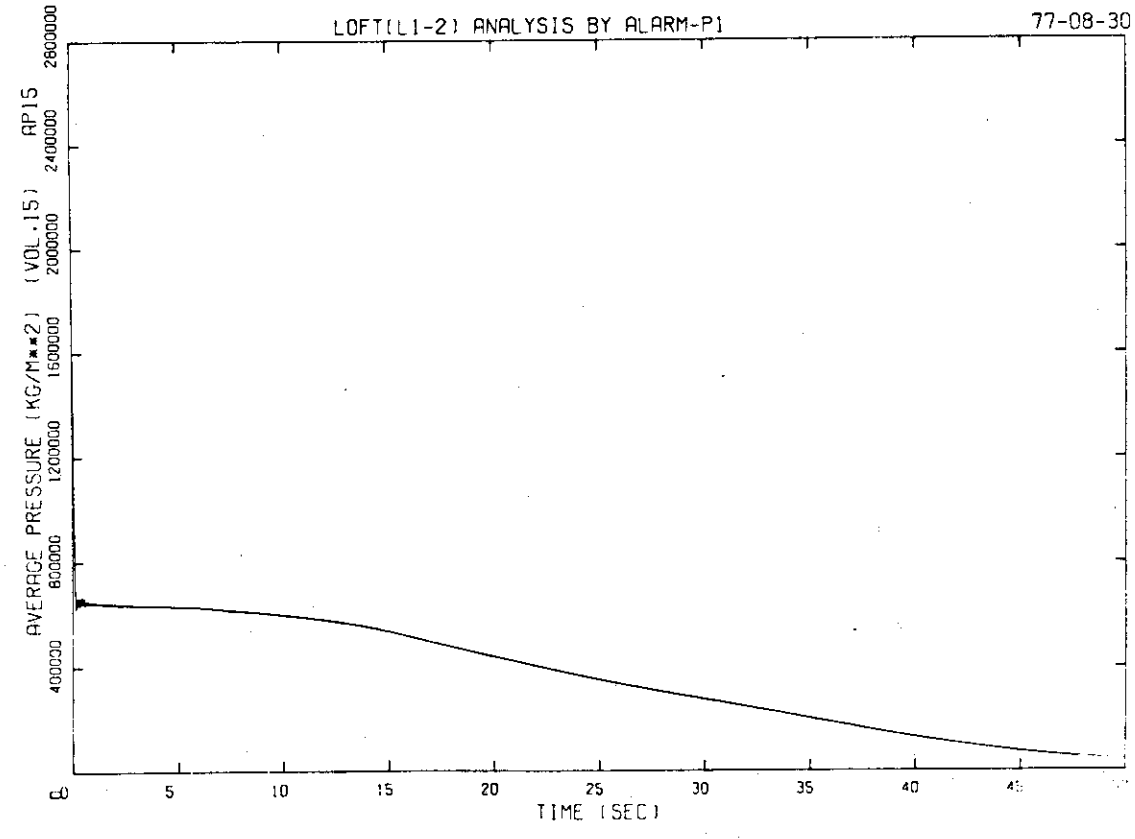

Fig. 24 Average Pressure in Broken Loop Hot Leg

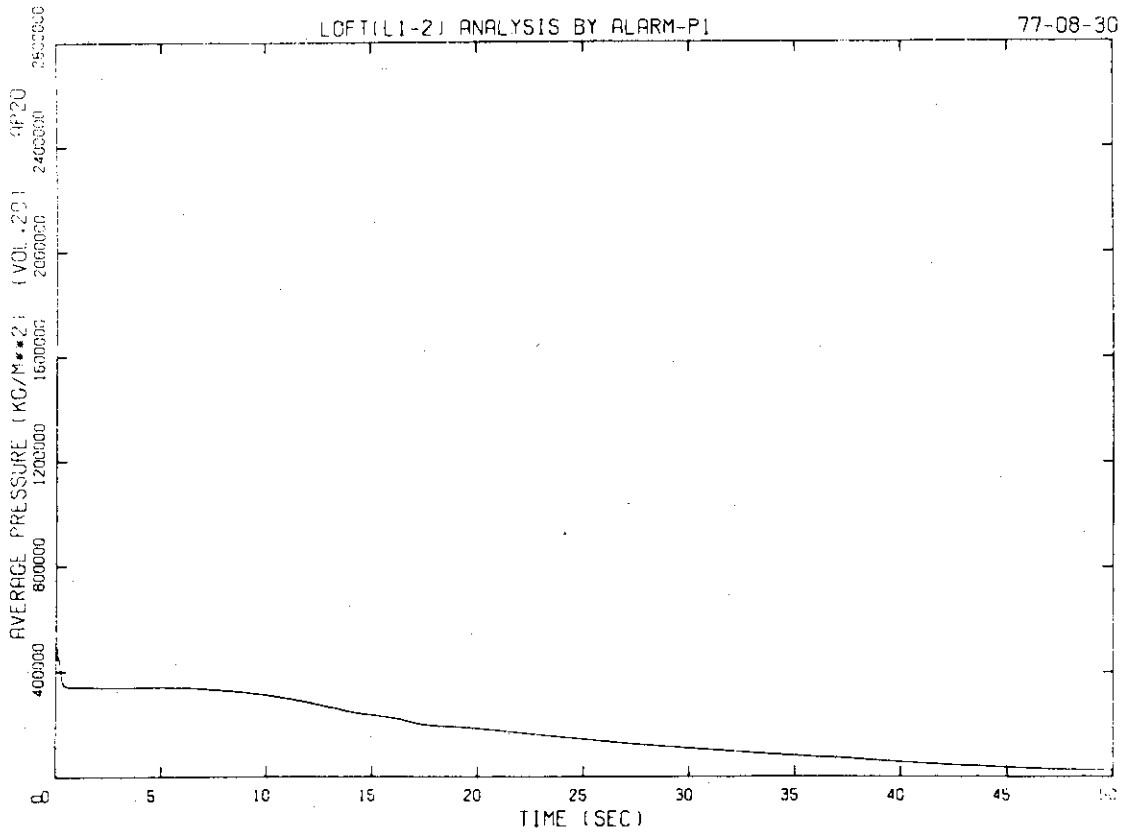

Fig. 25 Average Pressure in Break Node

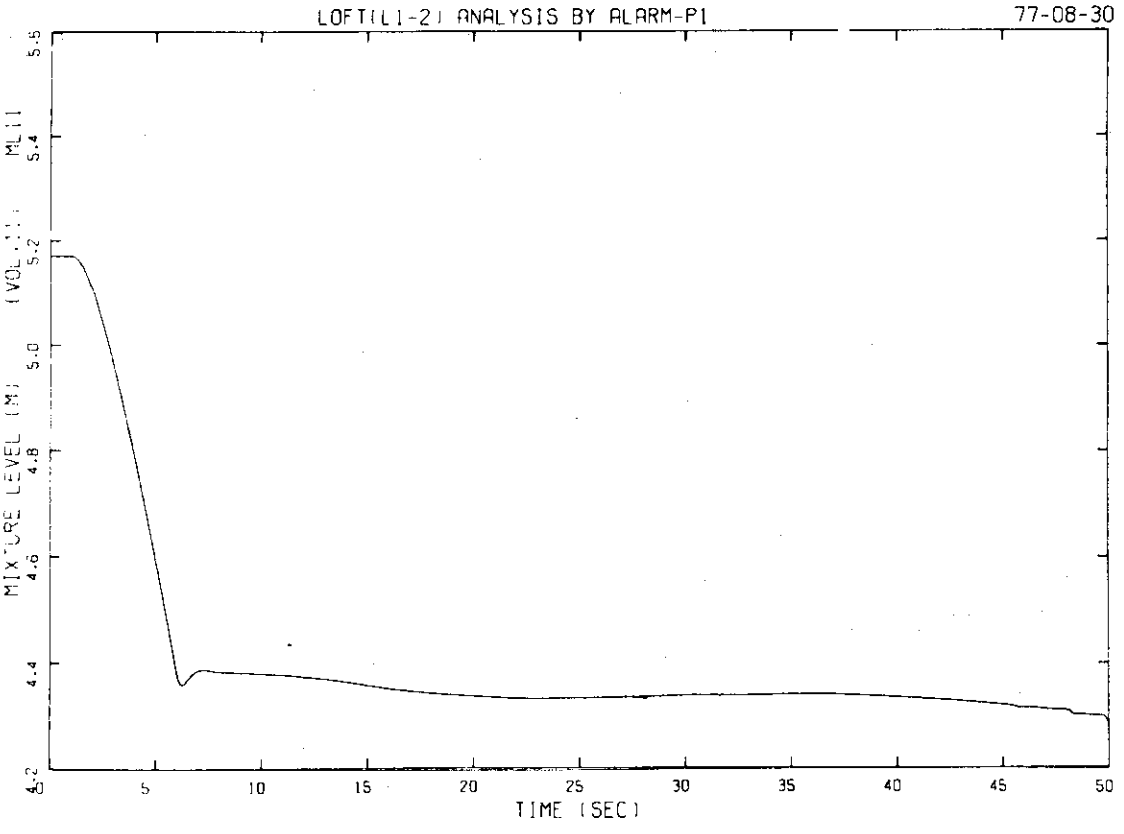

Fig. 26 Mixture Level in Downcomer

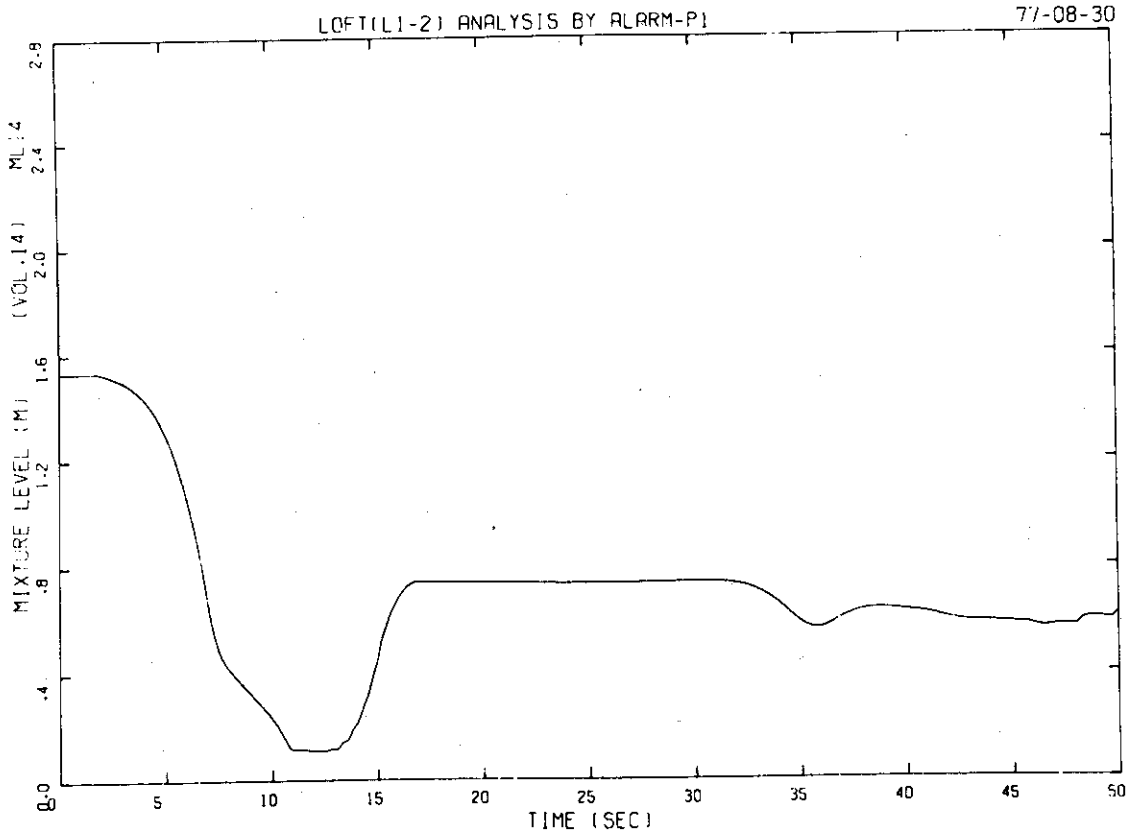

Fig. 27 Mixture Level in Upper-Plenum

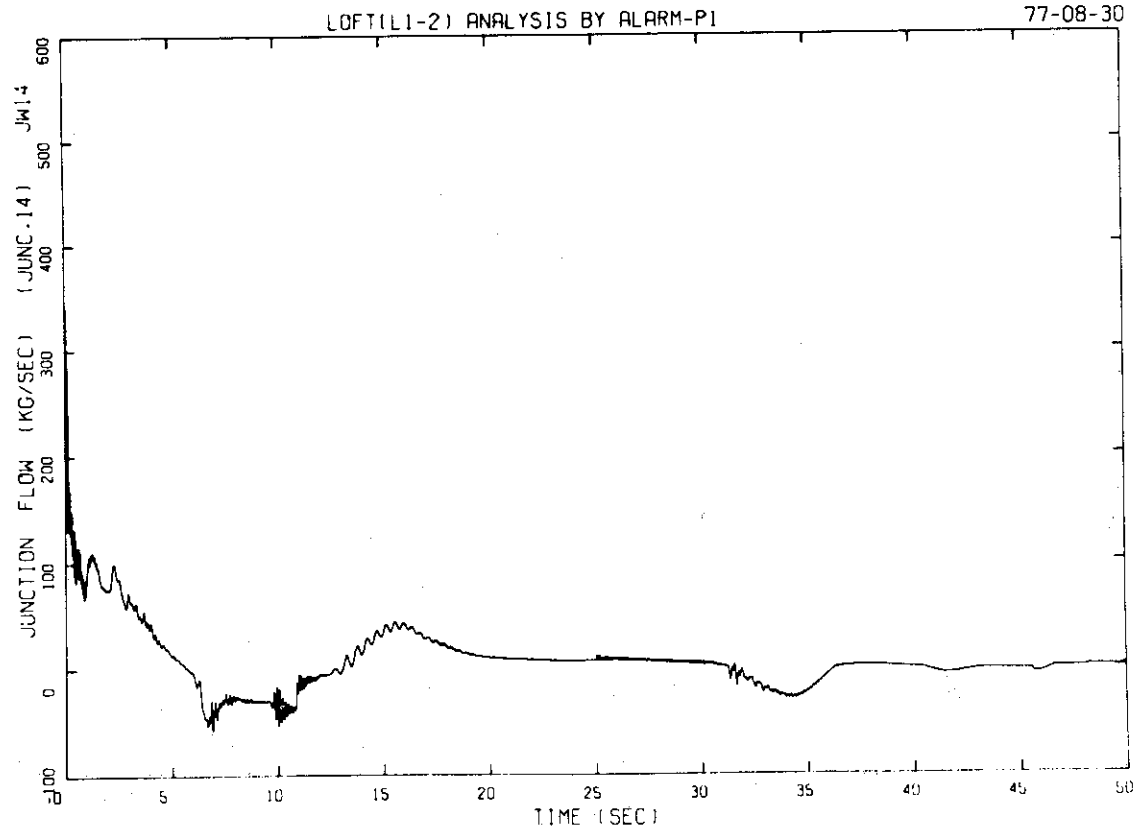

Fig. 28 Mass Flow Rate from Core to Upper-Plenum

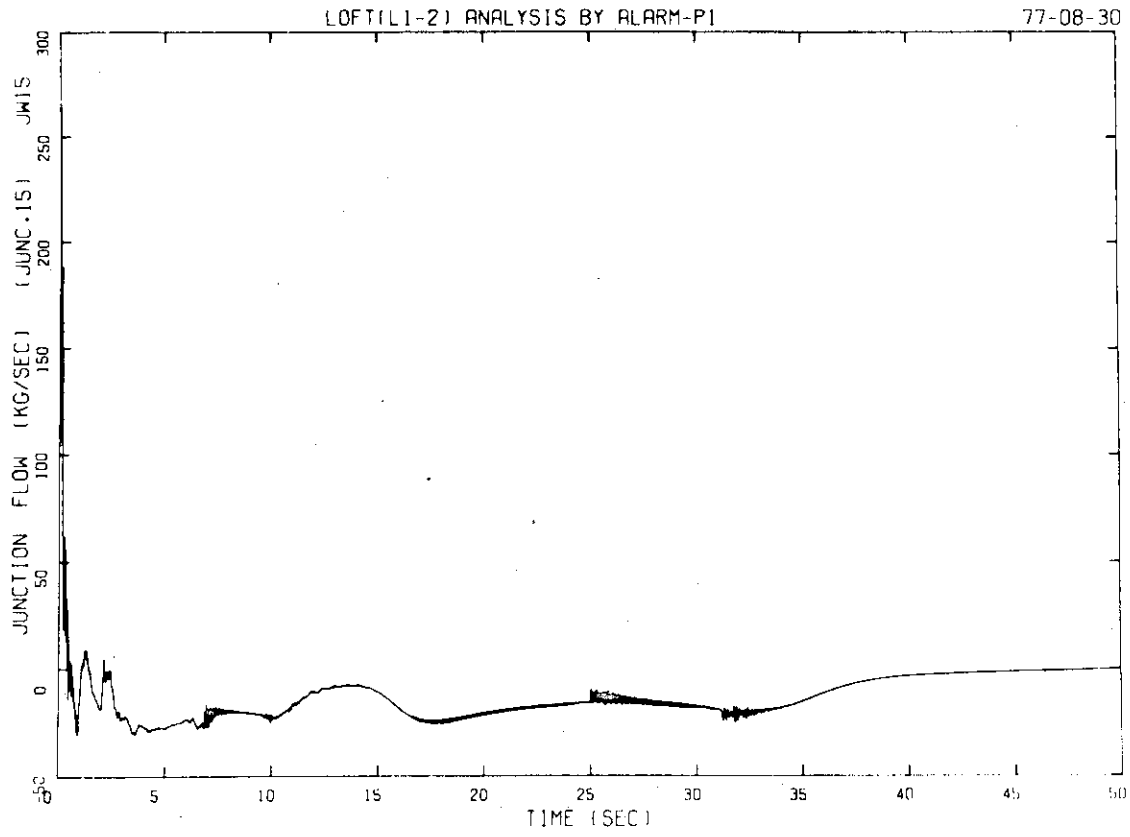

Fig. 29 Mass Flow Rate from Upper-Plenum to Intact Loop Hot Leg

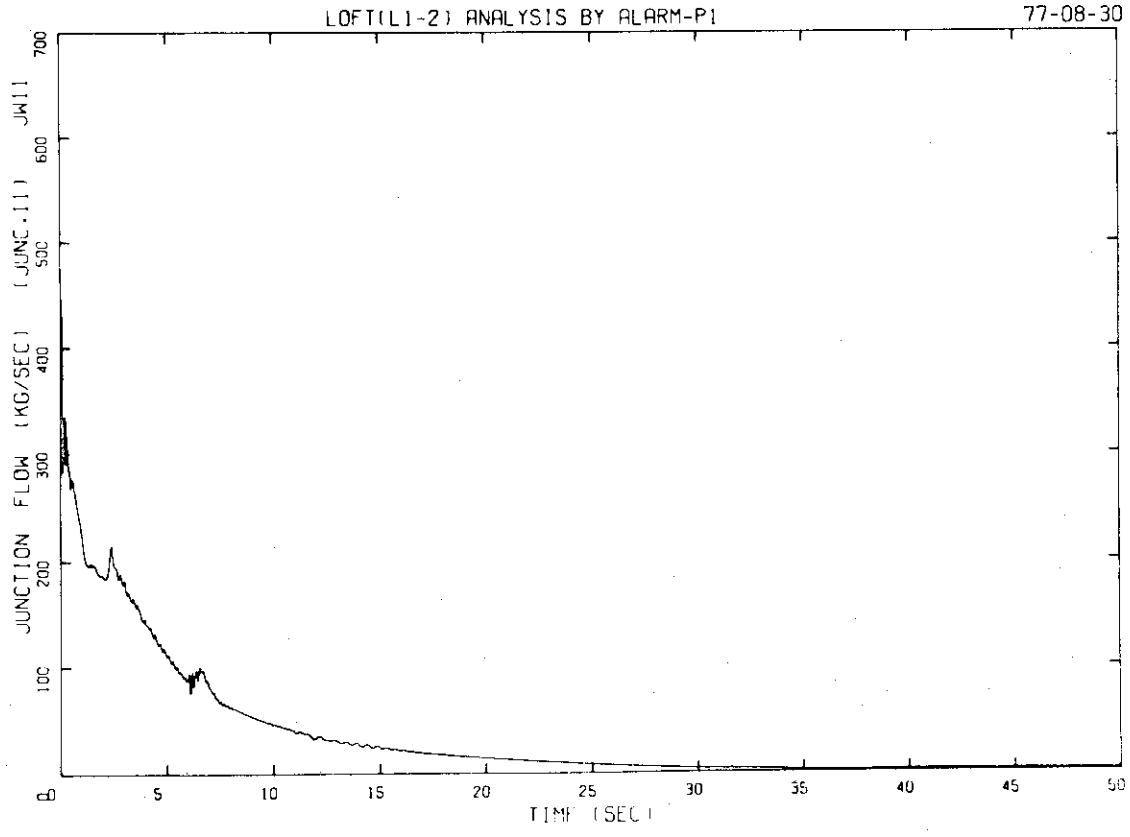

Fig. 30 Mass Flow Rate from Intact Loop Cold Leg to Downcomer

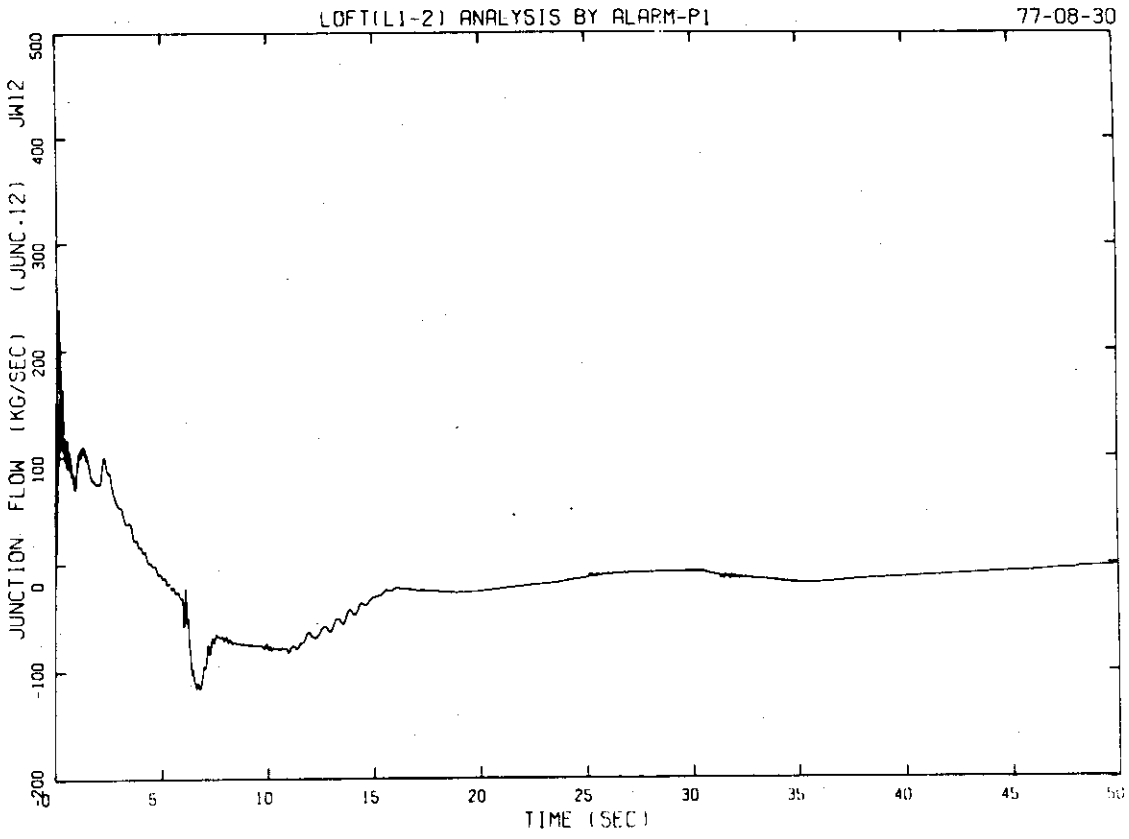

Fig. 31 Mass Flow Rate from Downcomer to Lower-Plenum

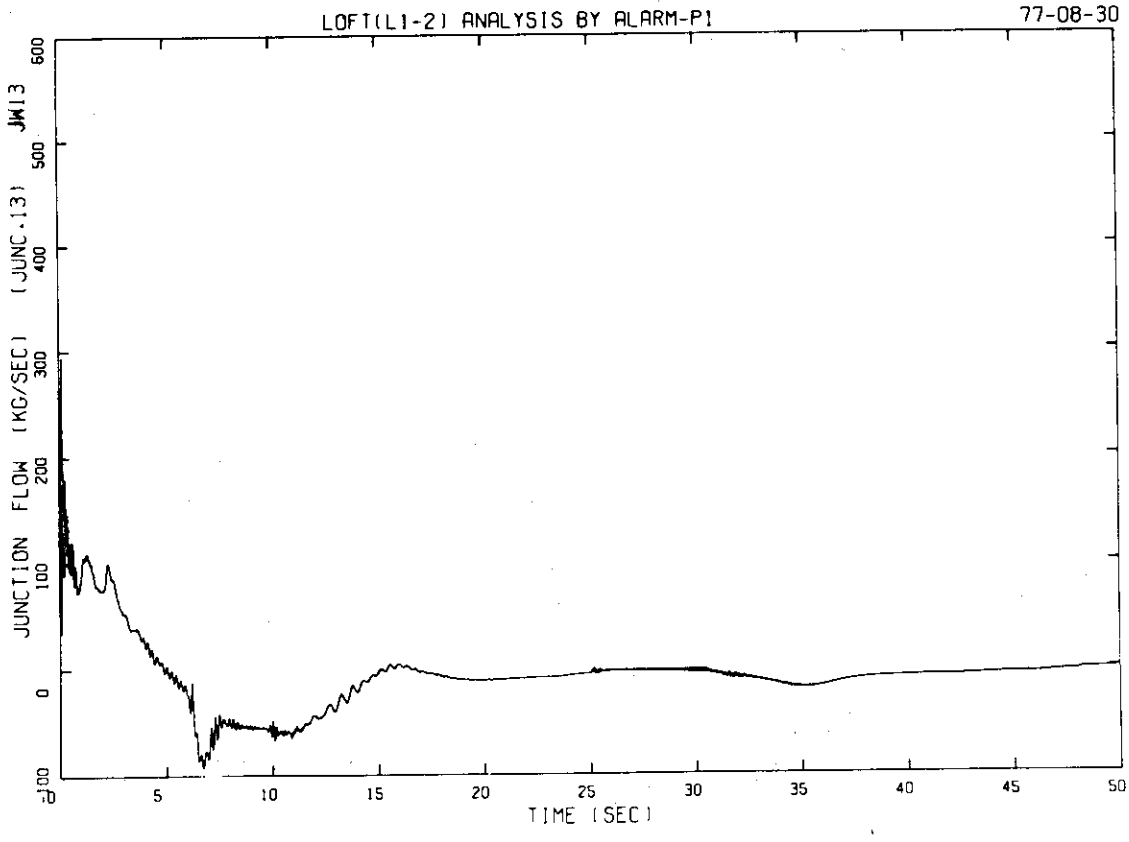

Fig. 32 Mass Flow Rate from Lower-Plenum to Core

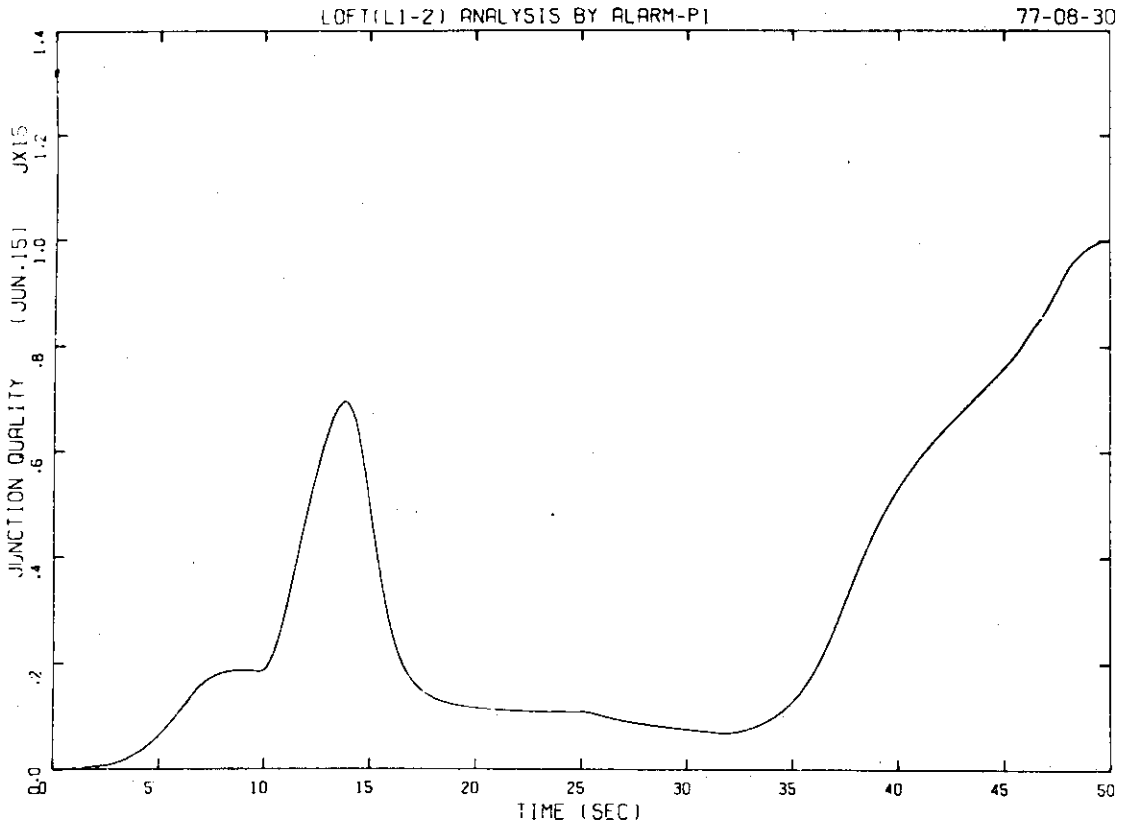

Fig. 33 Junction Quality between Intact Loop Hot Leg and Upper-Plenum

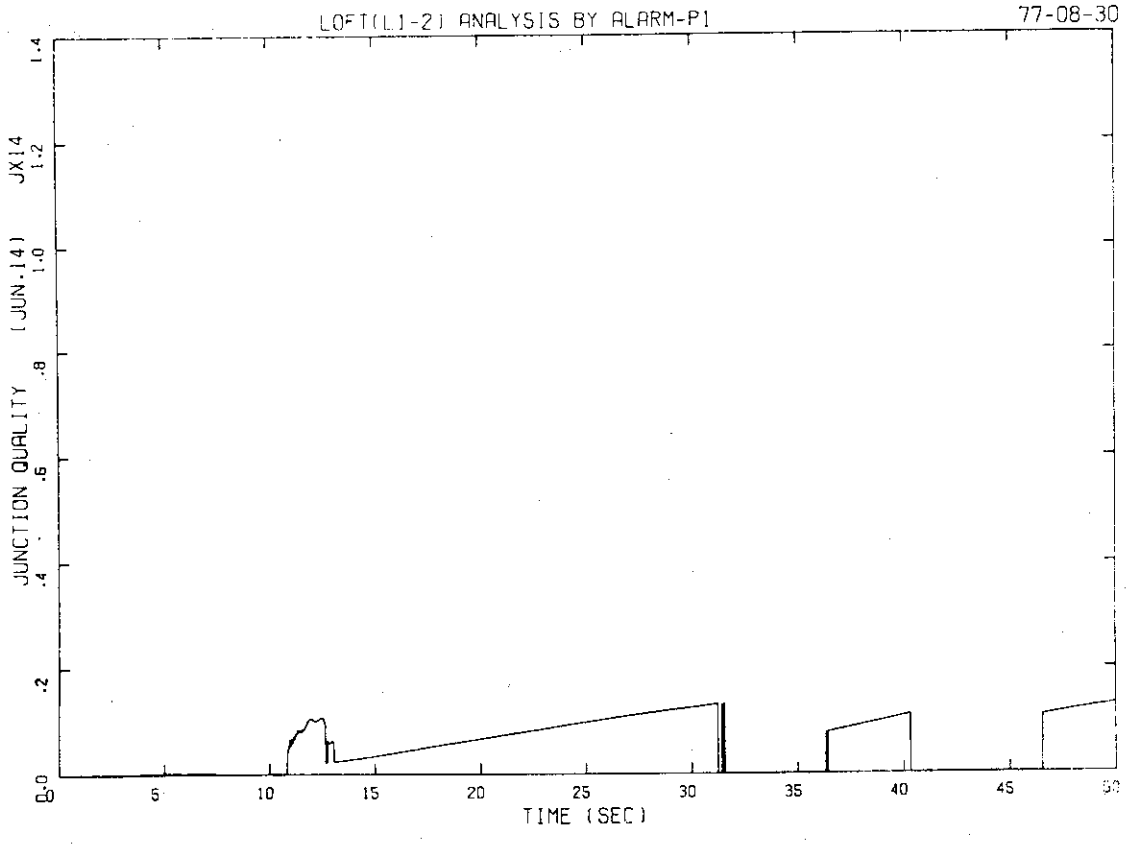

Fig. 34 Junction Quality between Core and Upper-Plenum

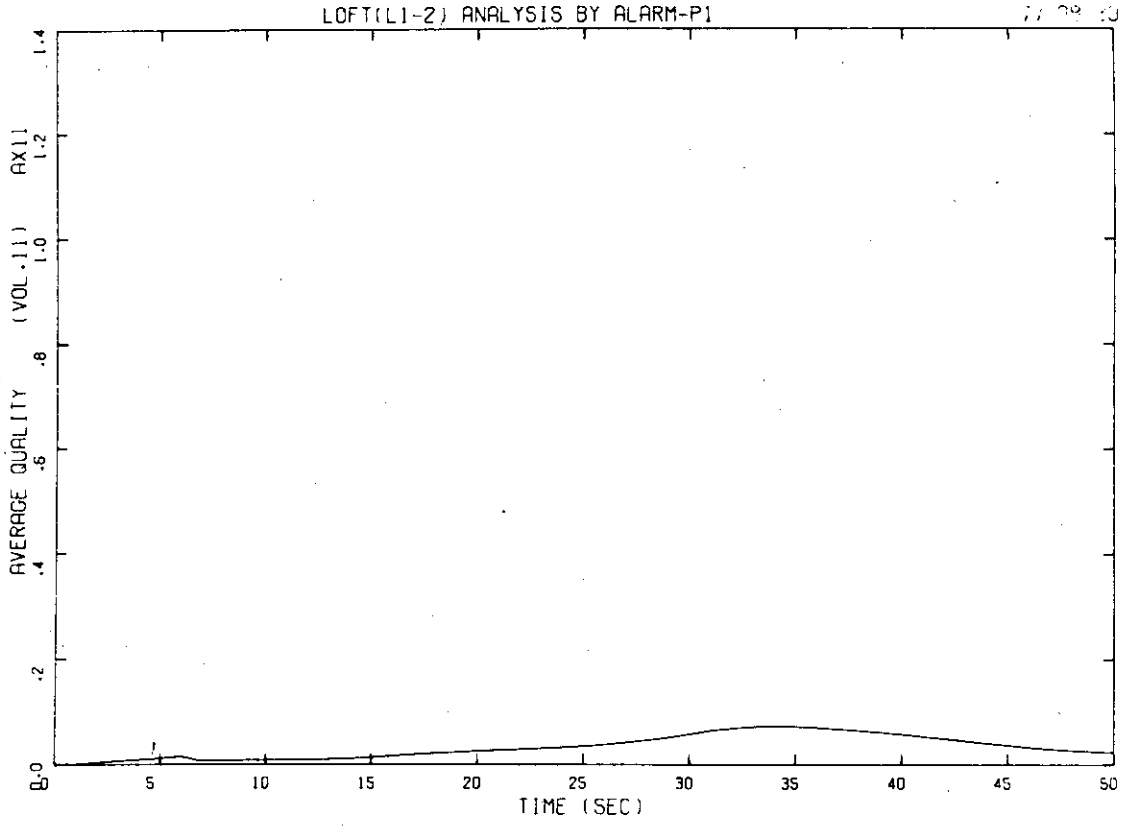

Fig. 35 Average Quality in Downcomer

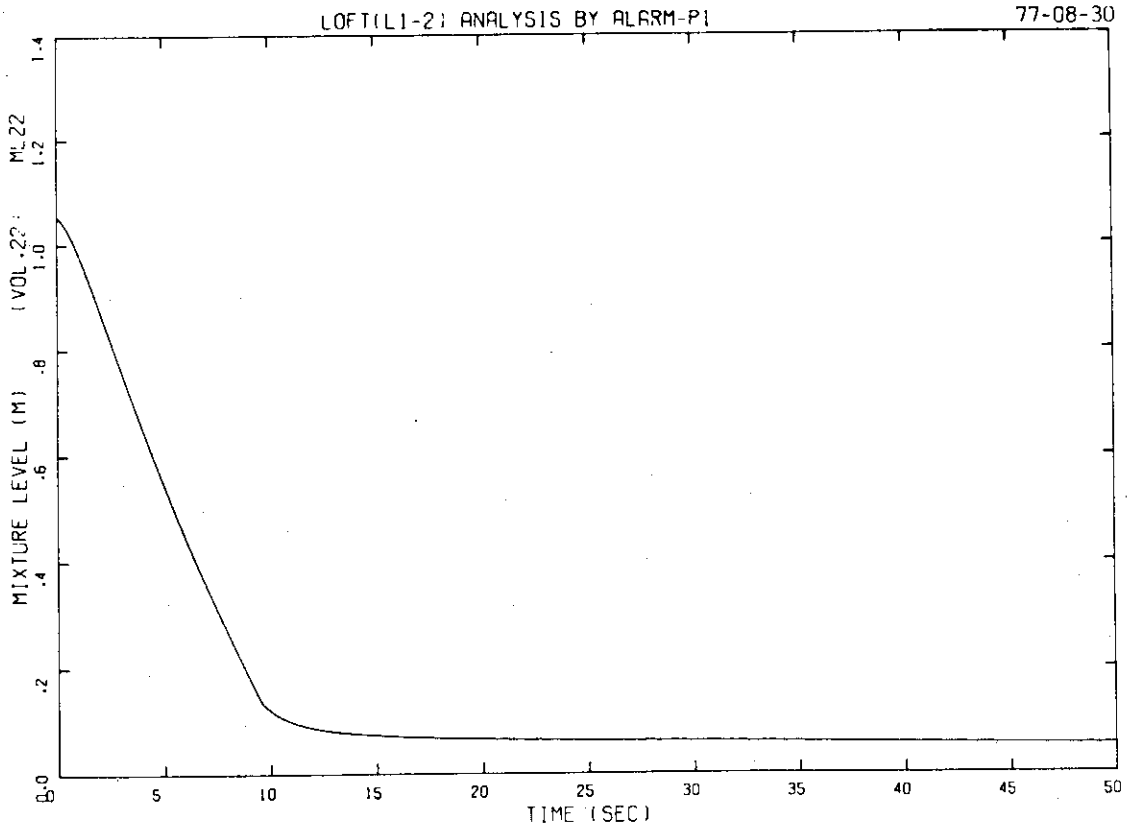

Fig. 36 Mixture Level in Pressurizer

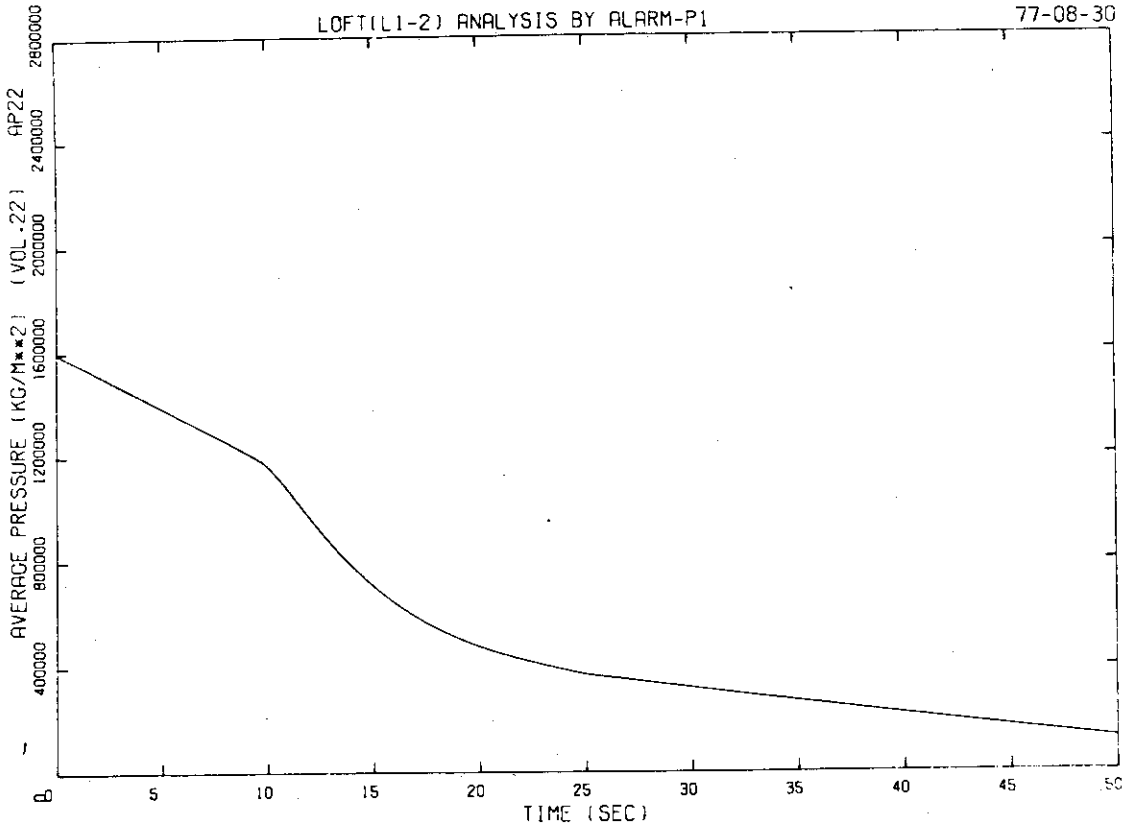

Fig. 37 Average Pressure in Pressurizer

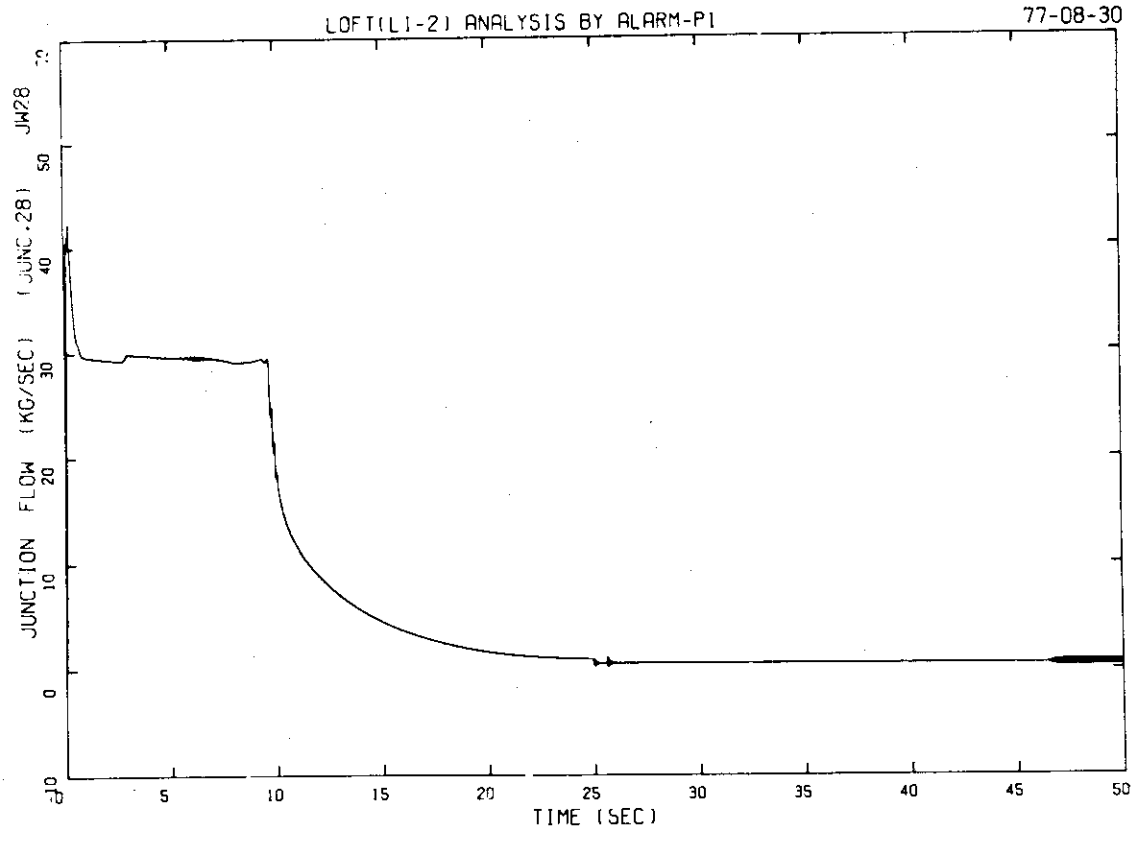

Fig. 38 Mass flow Rate at Surge Line Outlet

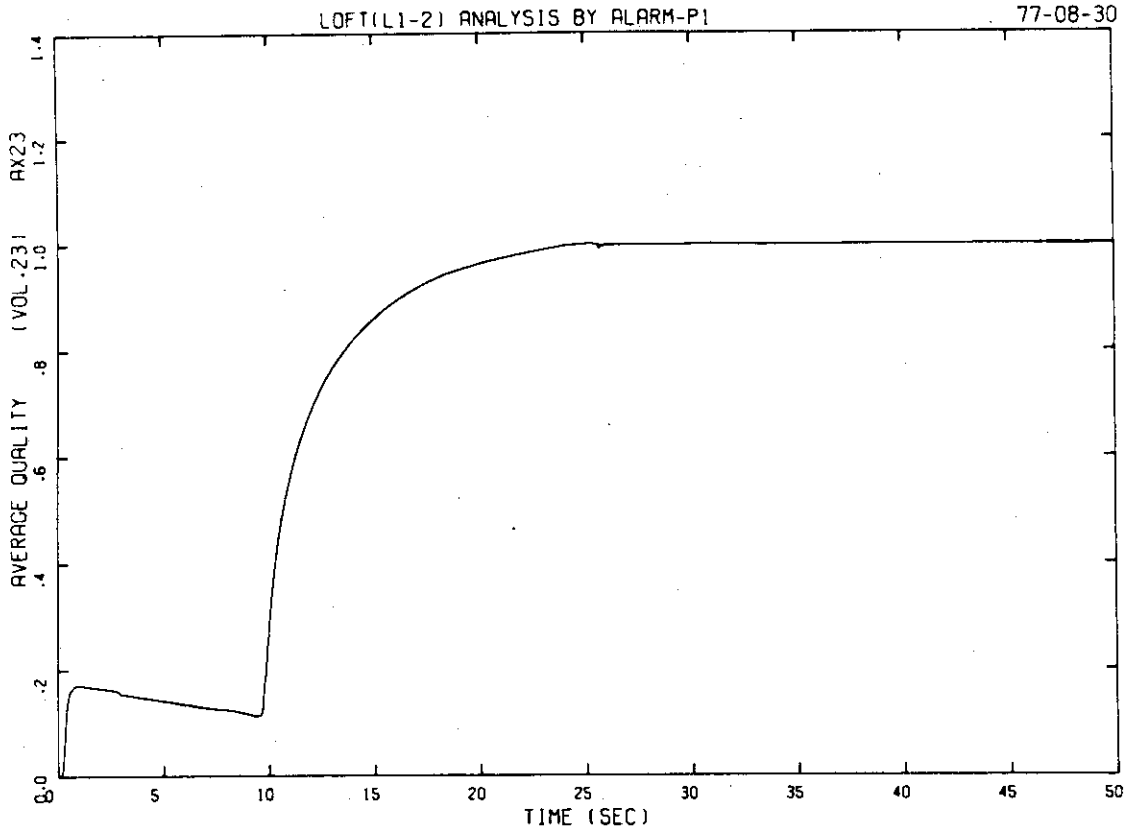

Fig. 39 Average Quality in Surge Line

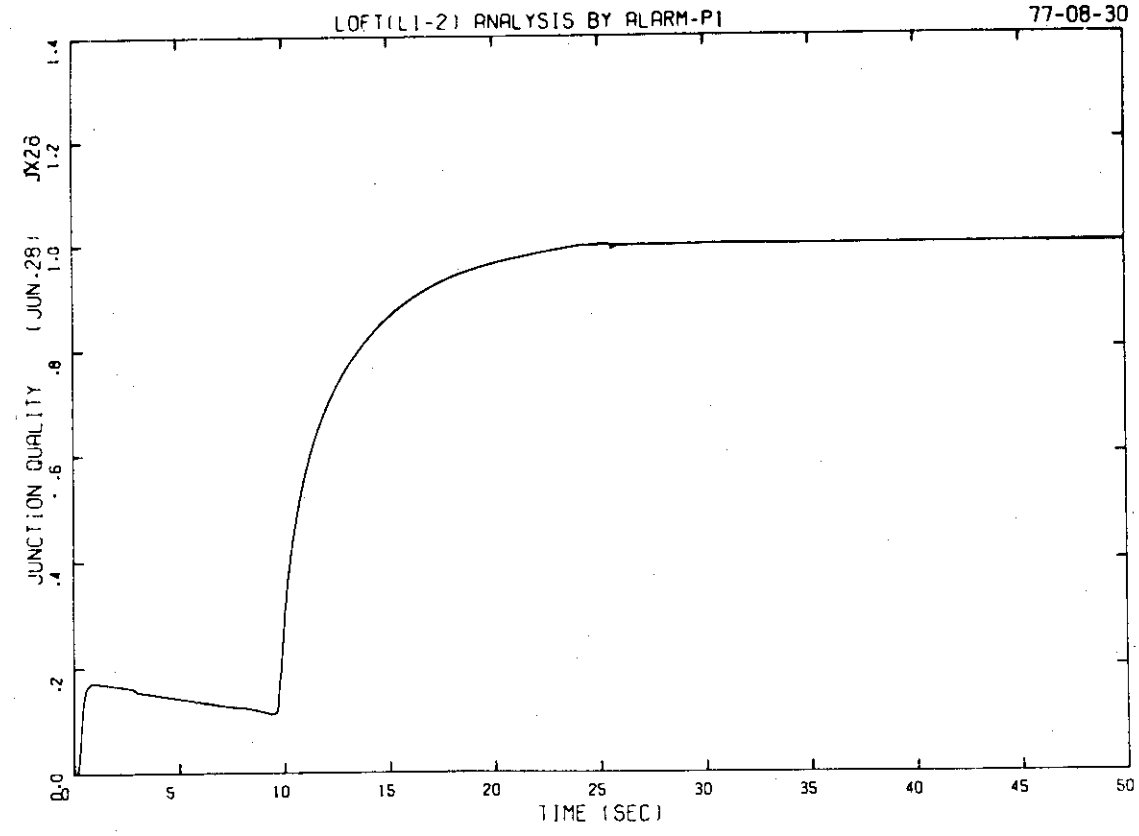

Fig. 40 Junction Quality at Surge Line Outlet

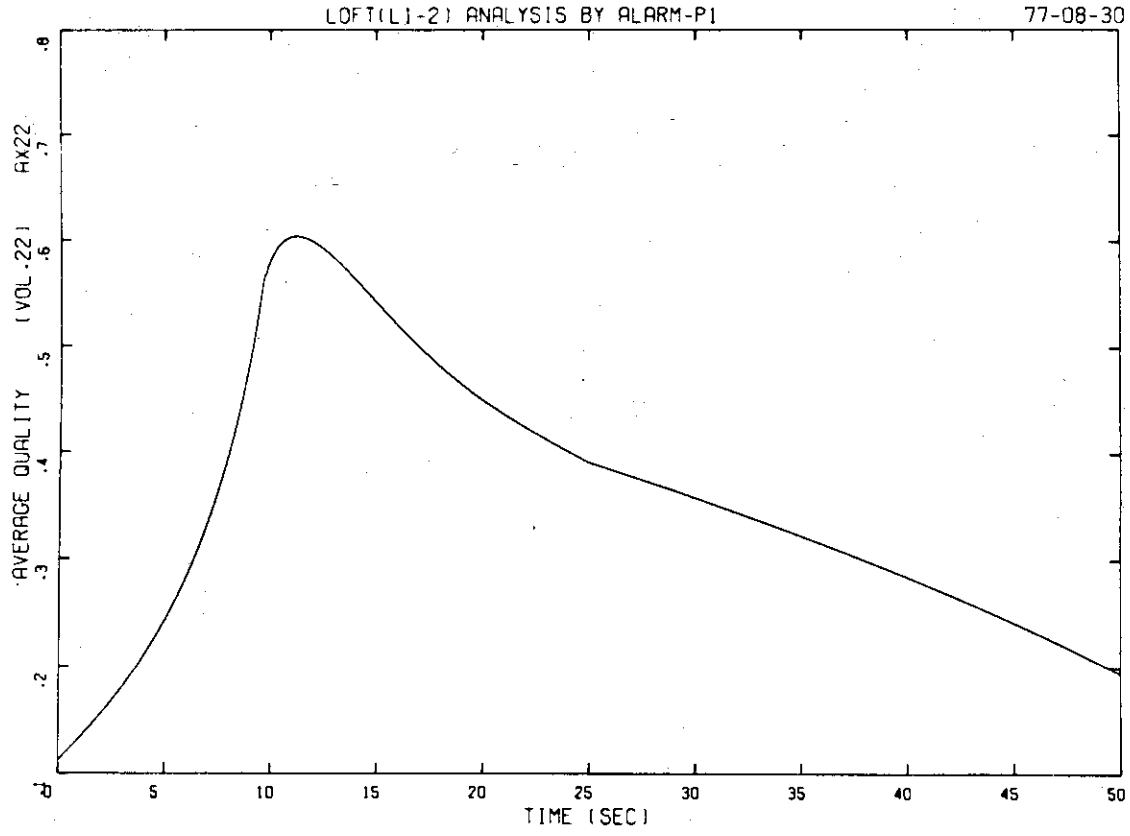

Fig. 41 Average Quality in Pressurizer

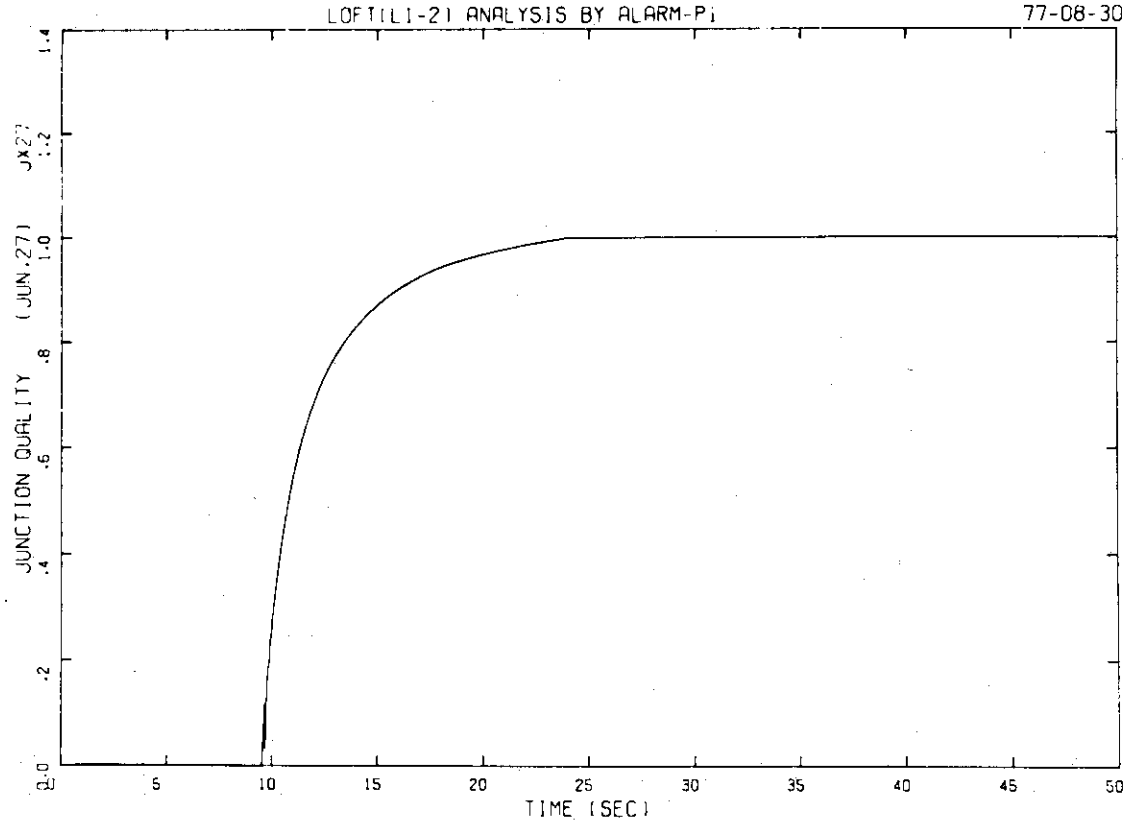

Fig. 42 Junction Quality at Surge Line Inlet

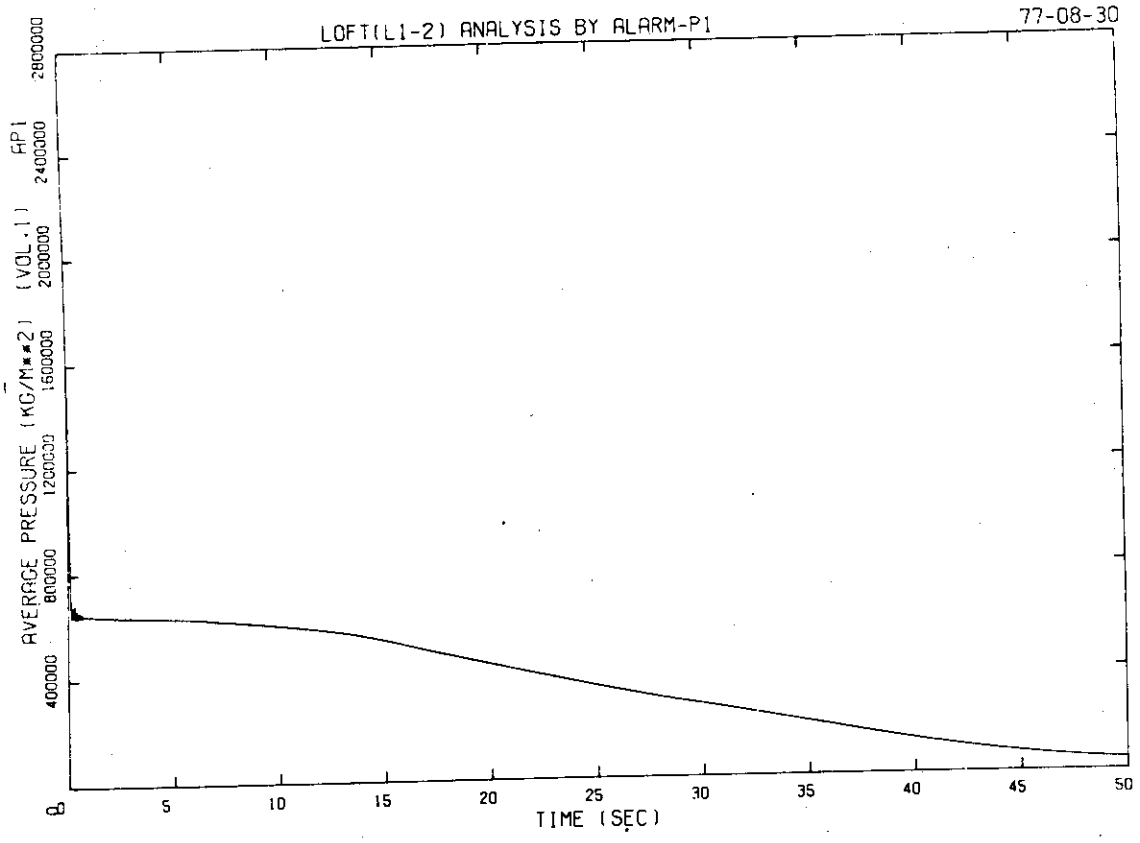

Fig. 43 Average Pressure in Intact Loop Hot Leg

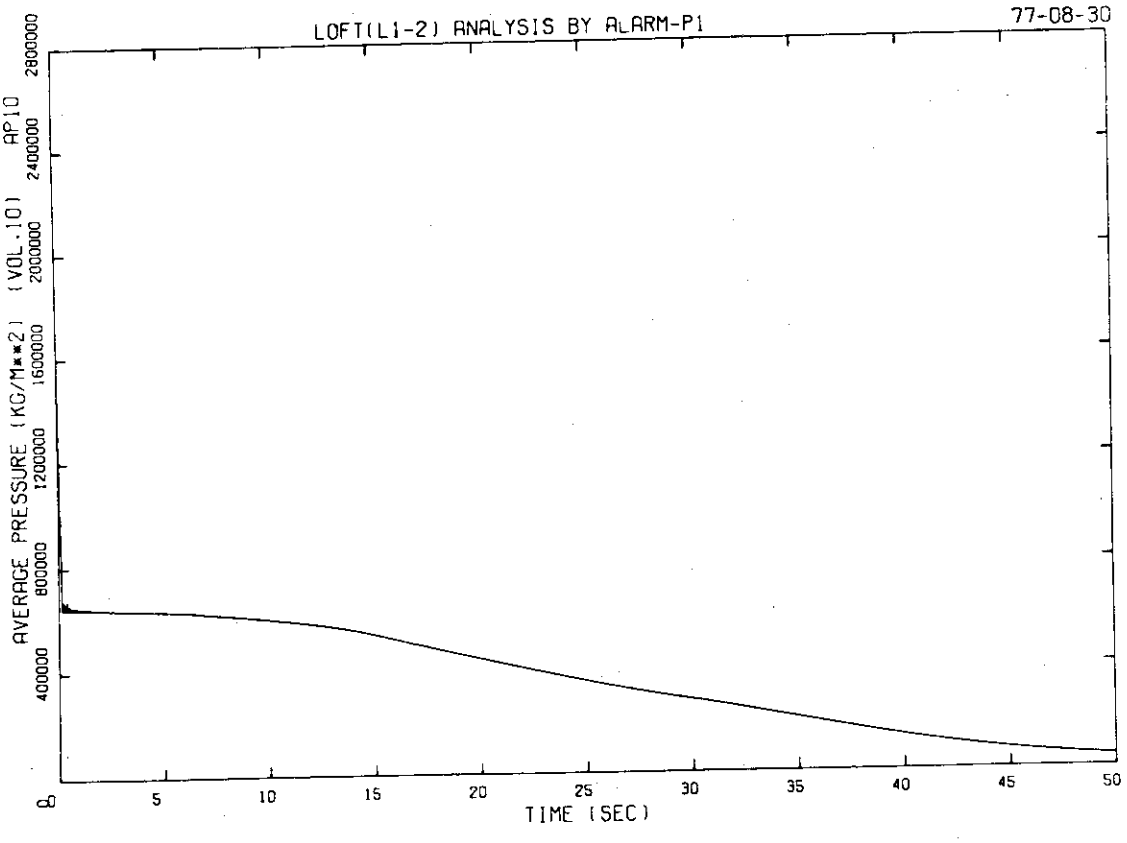

Fig. 44 Average Pressure in Intact Loop Cold Leg

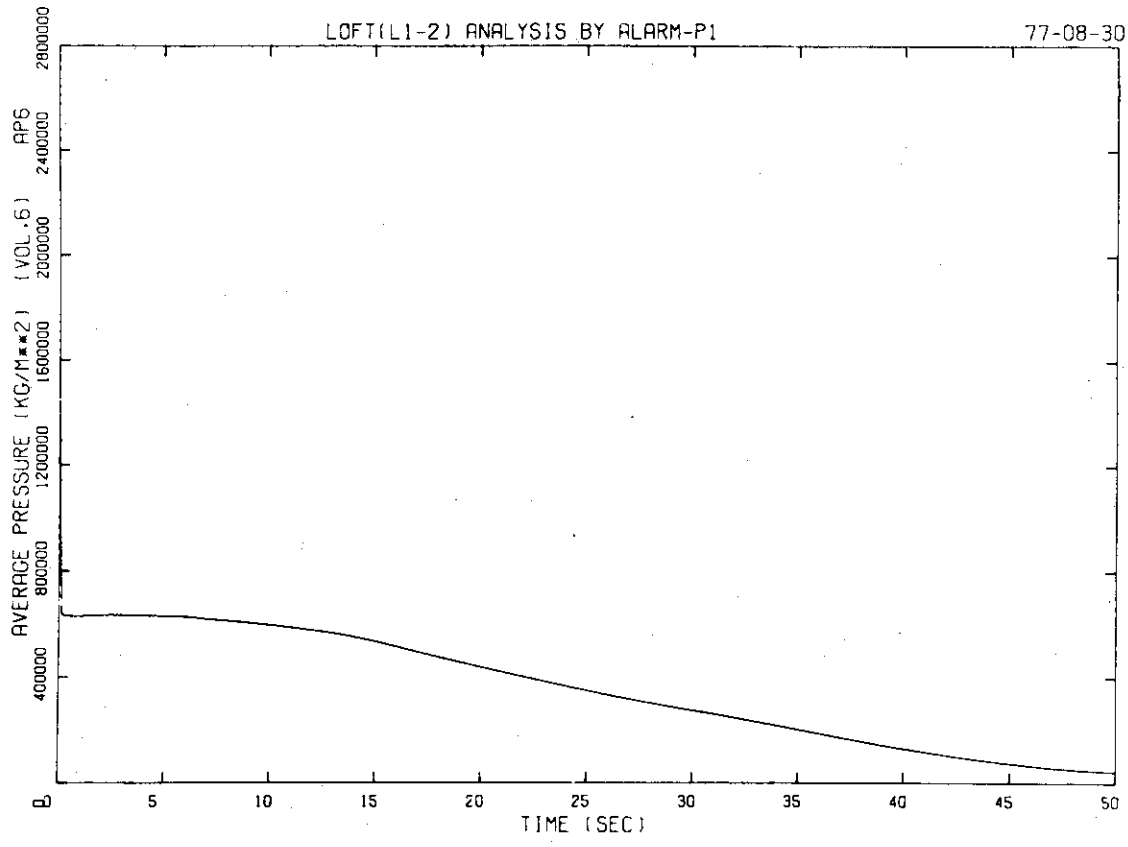

Fig. 45 Average Pressure between Steam Generator and Pump

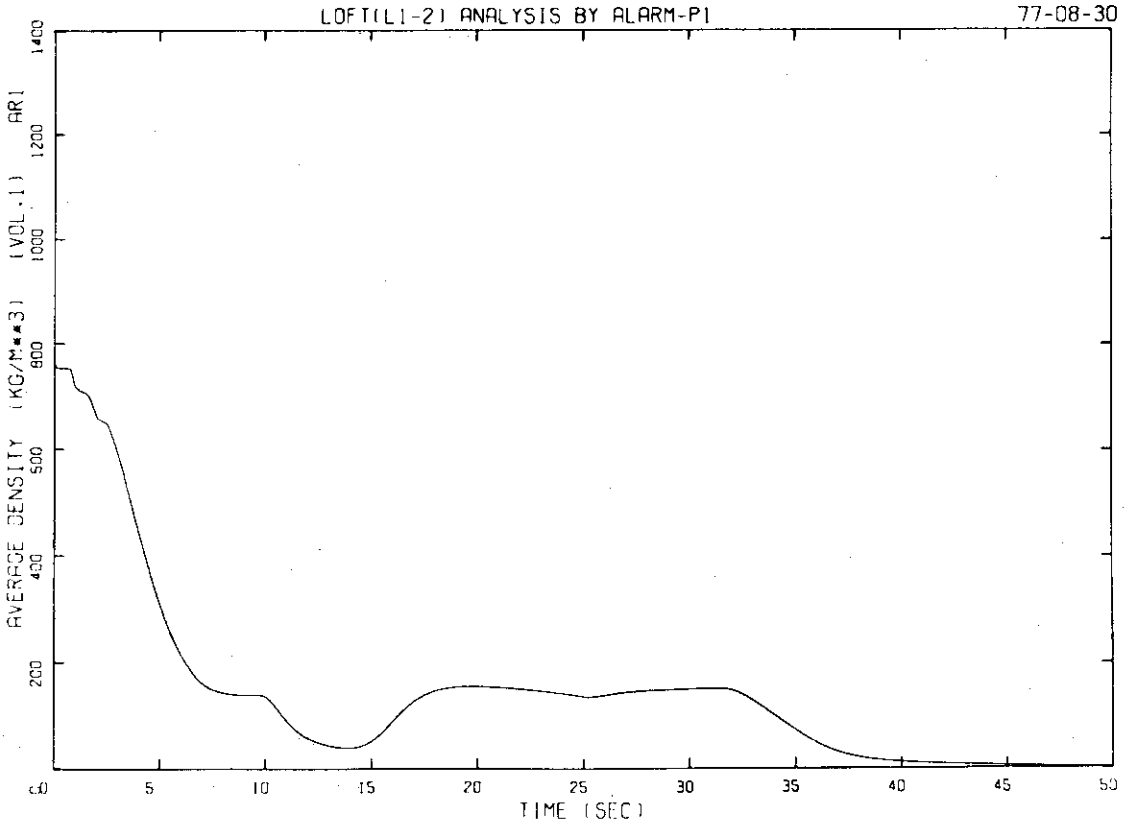

Fig. 46 Average Density in Intact Loop Hot Leg

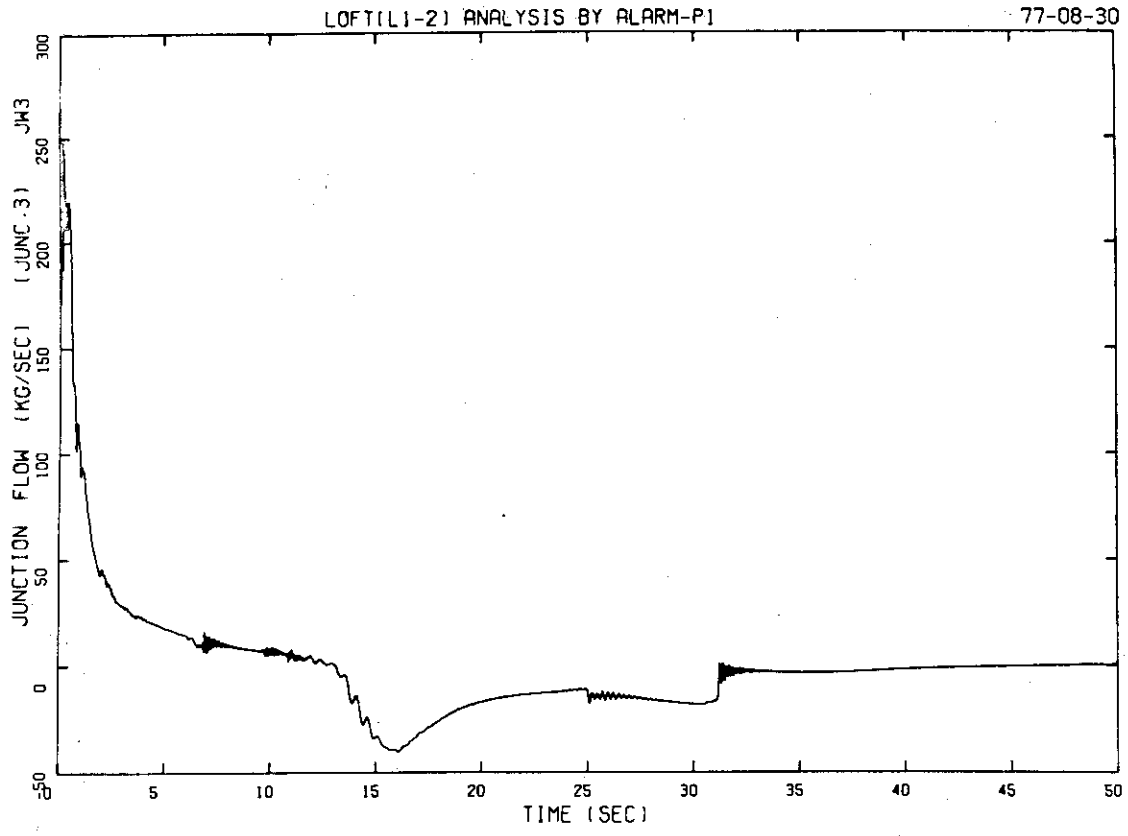

Fig. 47 Mass flow Rate at Steam Generator Inlet

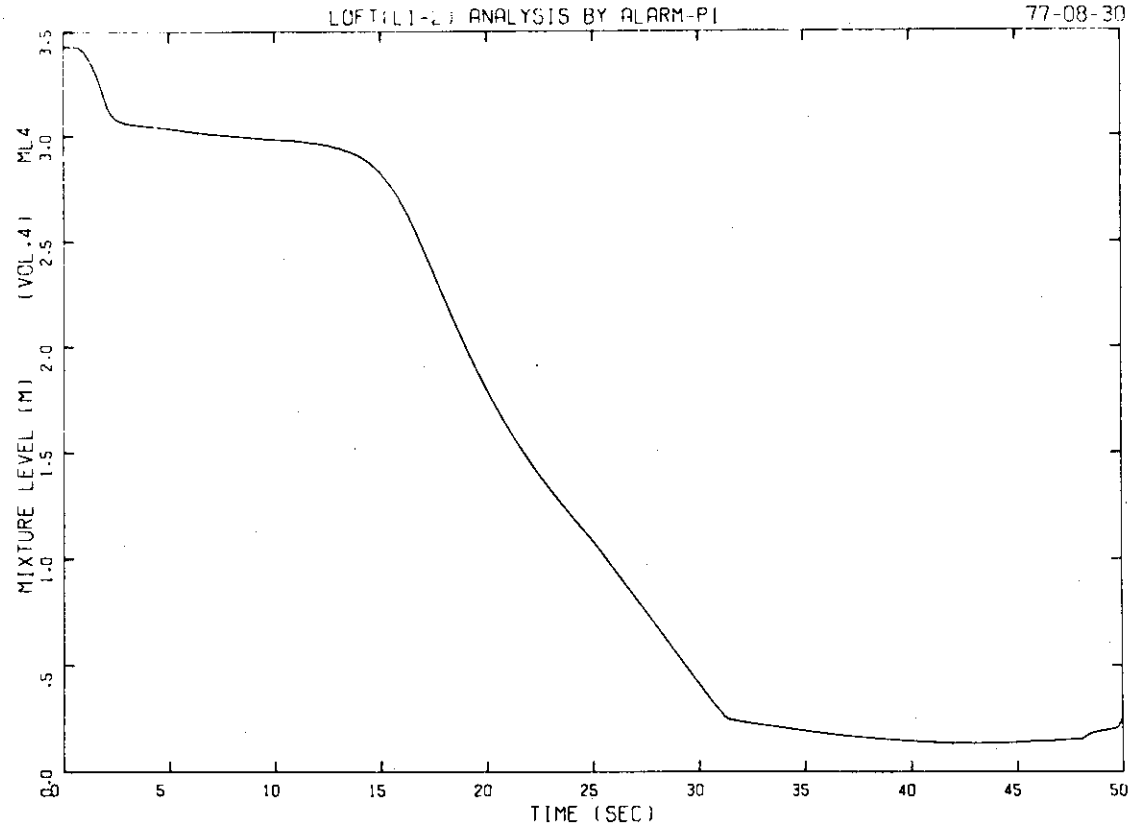

Fig. 48 Mixture Level in Steam Generator Inlet Volume

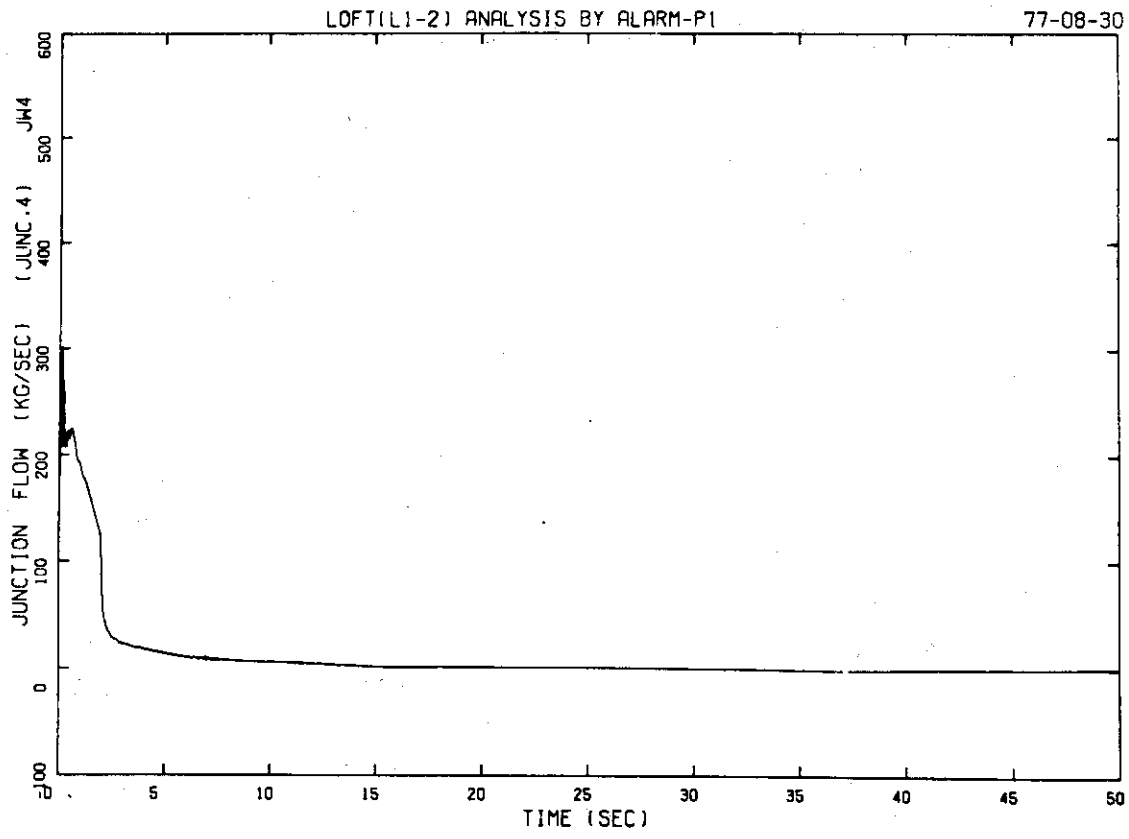

Fig. 49 Mass Flow Rate at Top of Steam Generator

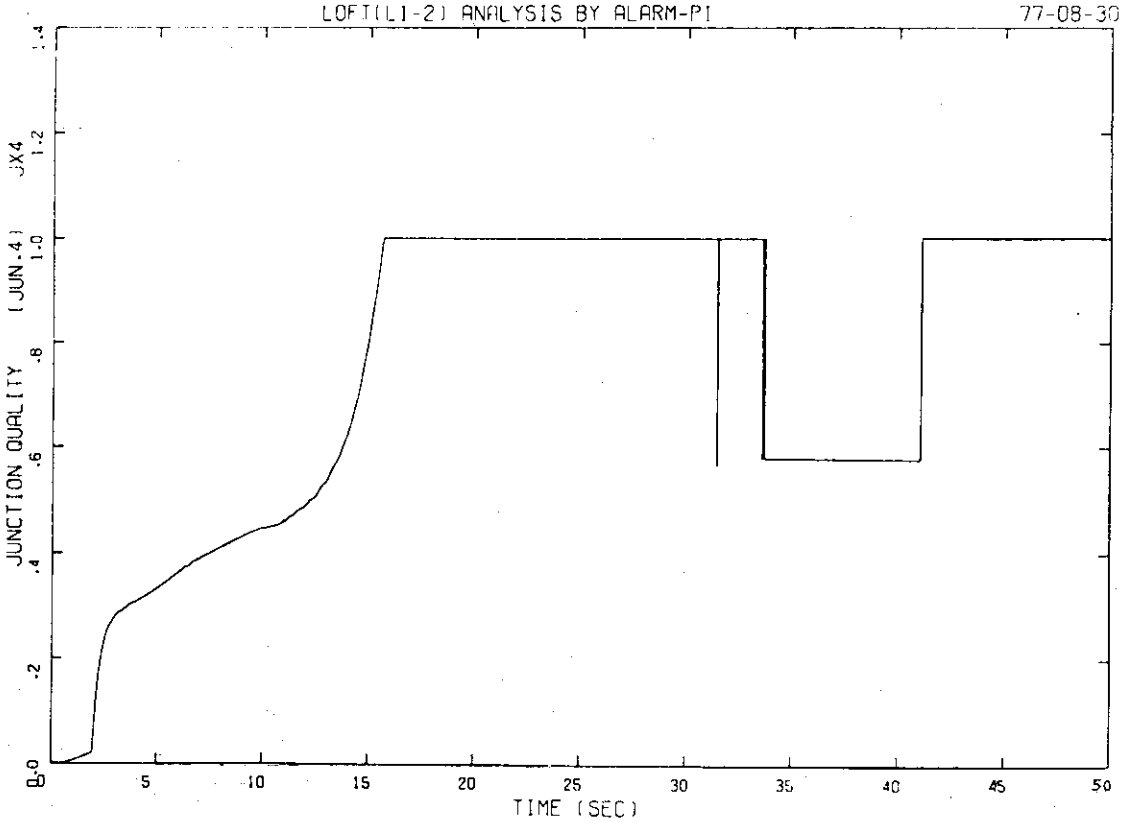

Fig. 50 Junction Quality at Top of Steam Generator

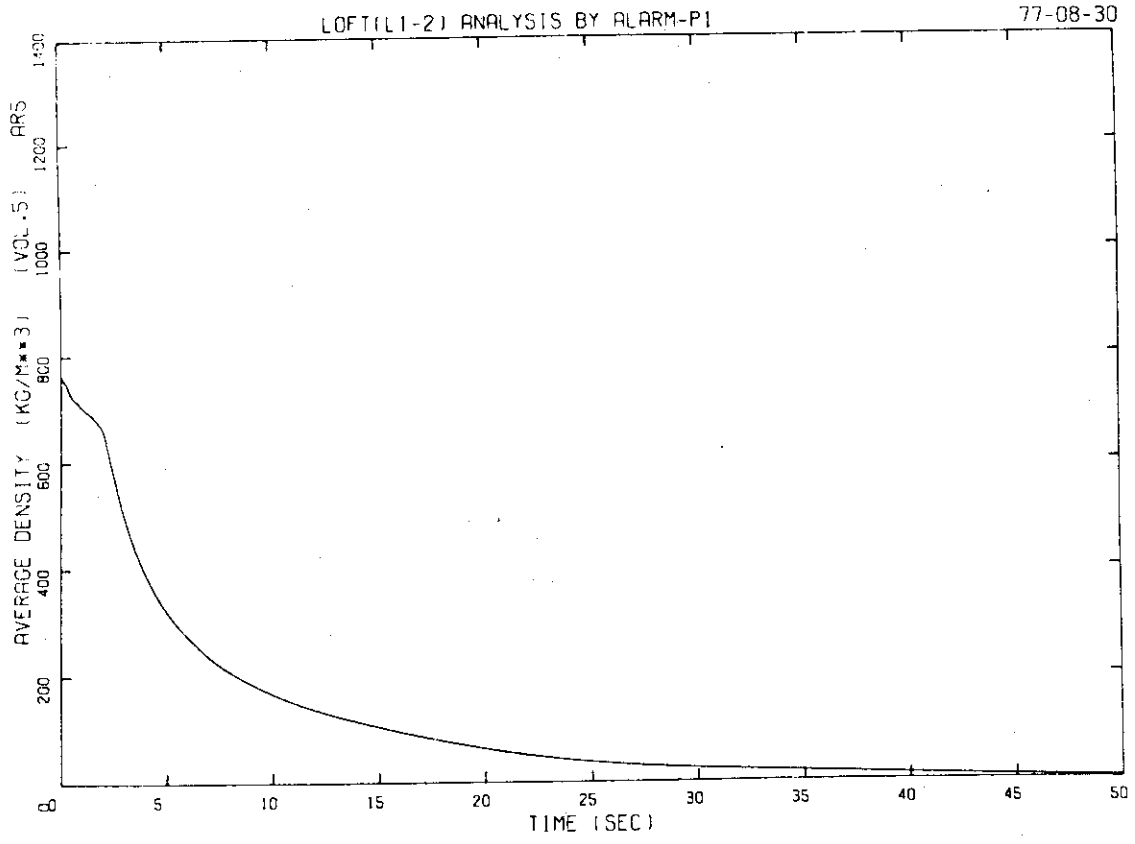

Fig. 51 Average Density in Steam Generator Outlet Volume

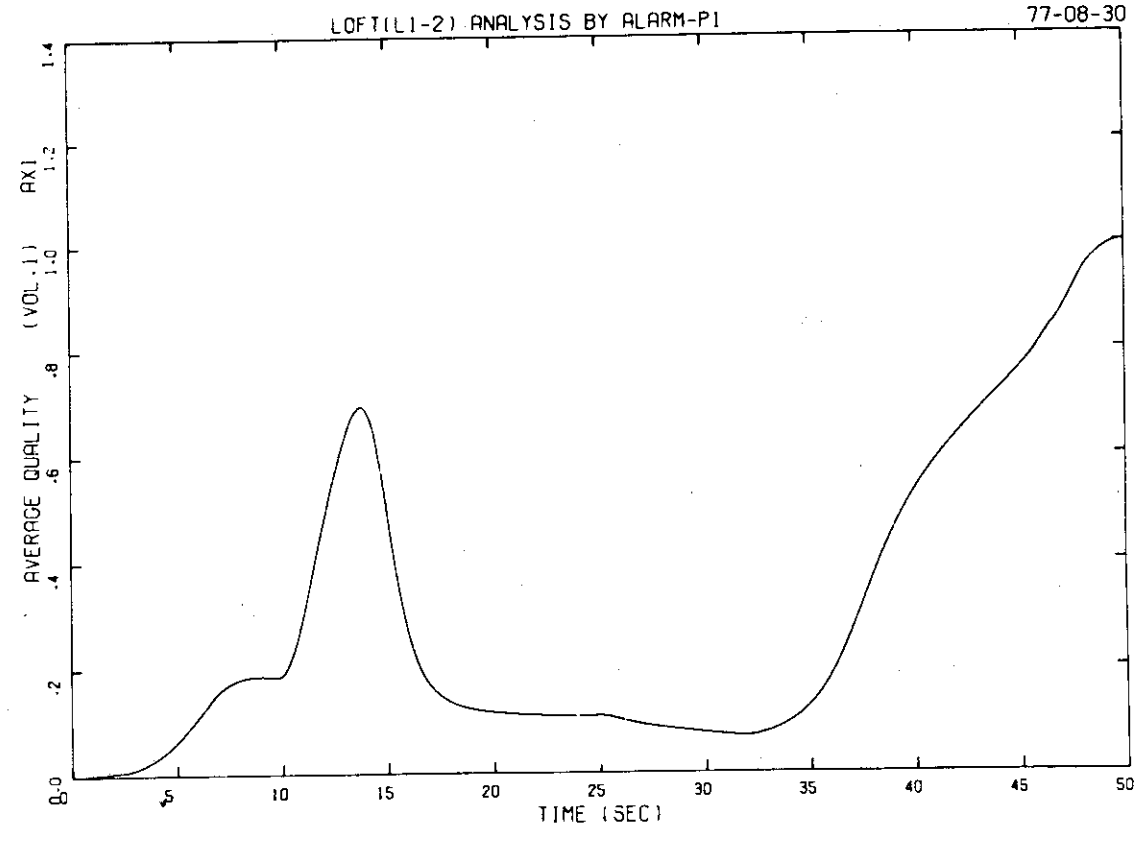

Fig. 52 Average Quality in Intact Loop Hot Leg

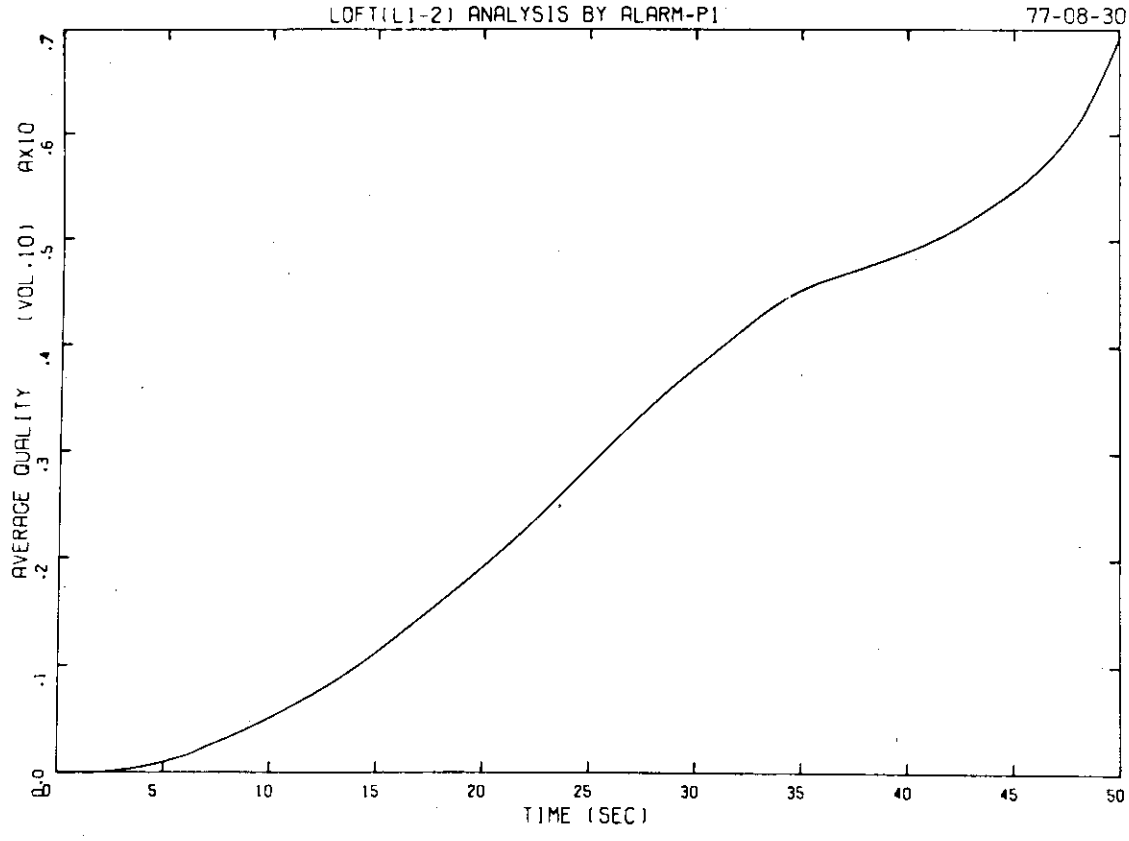

Fig. 53 Average Quality in Intact Loop Cold Leg

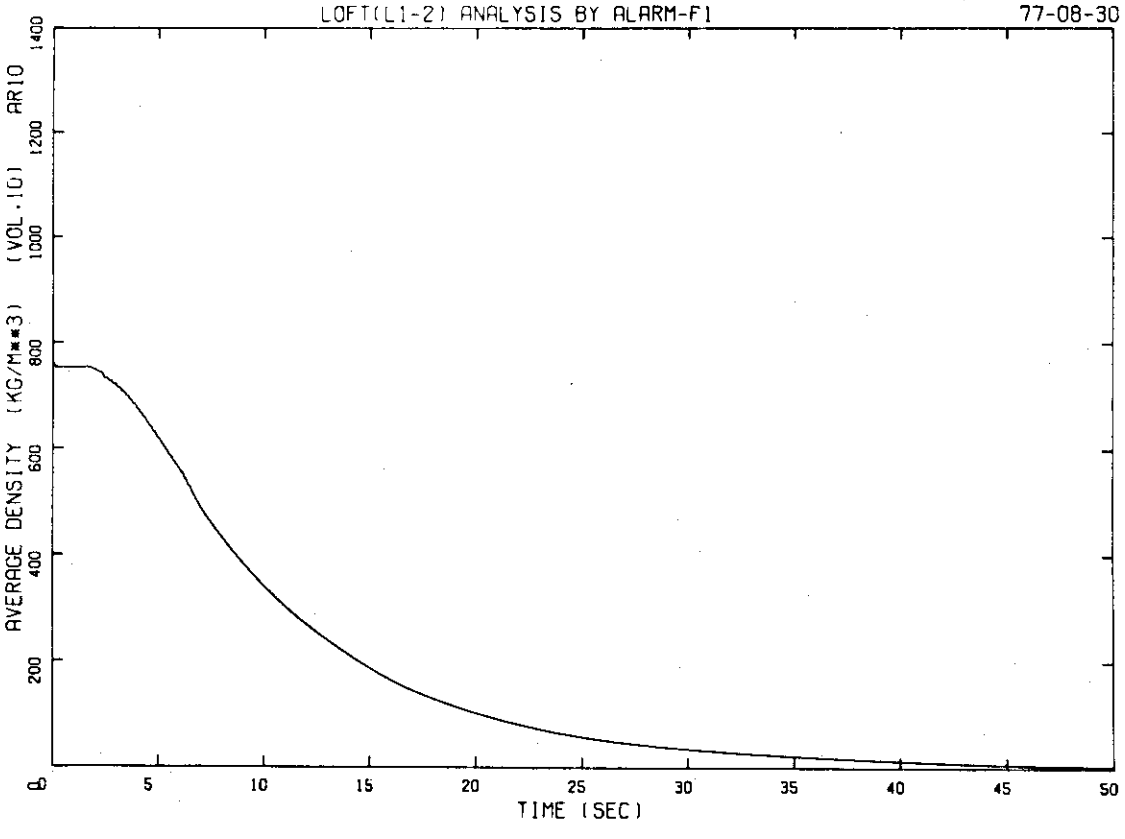

Fig. 54 Average Density in Intact Loop Cold Leg

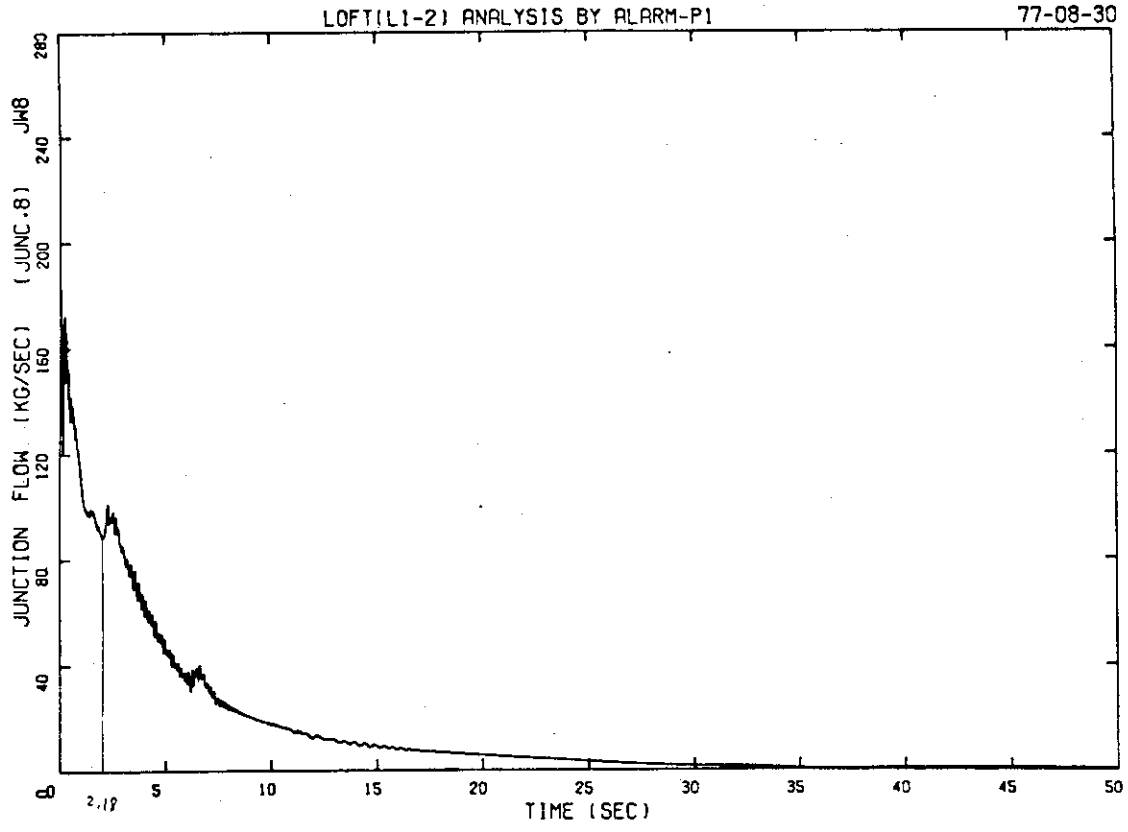

Fig. 55 Mass Flow Rate at Pump Outlet

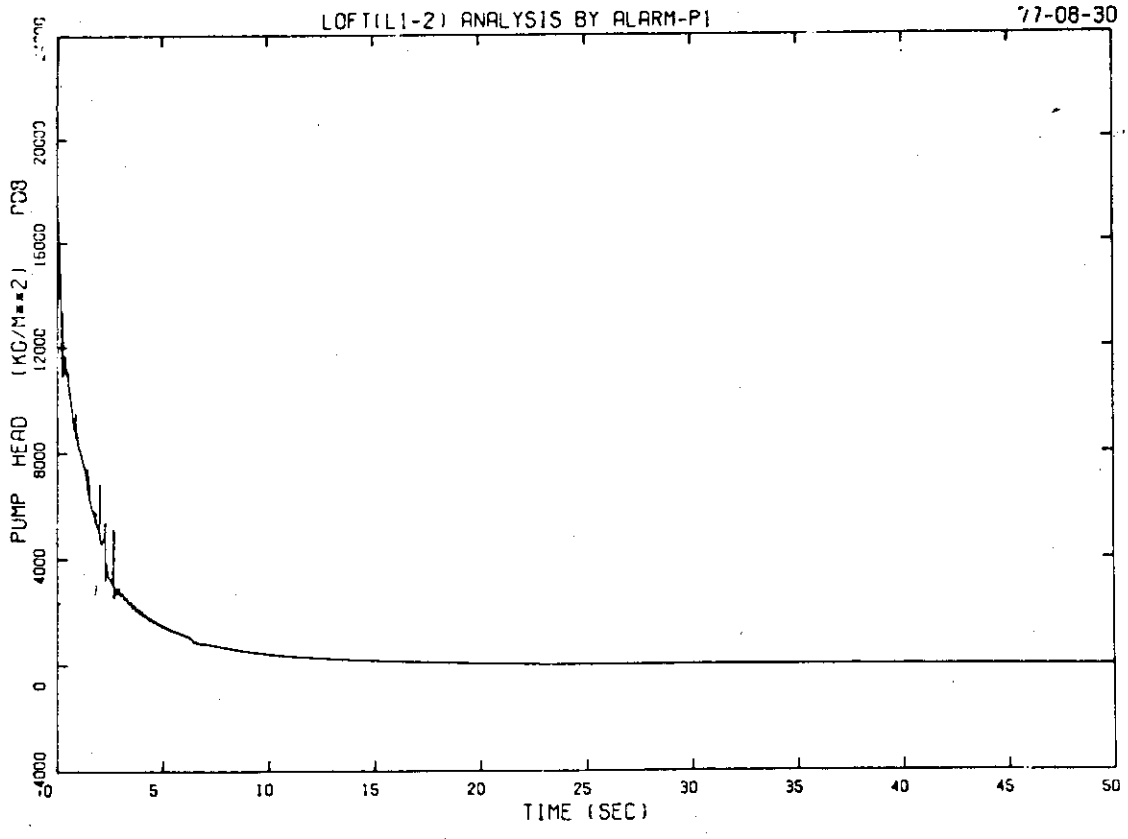

Fig. 56 Pump Head

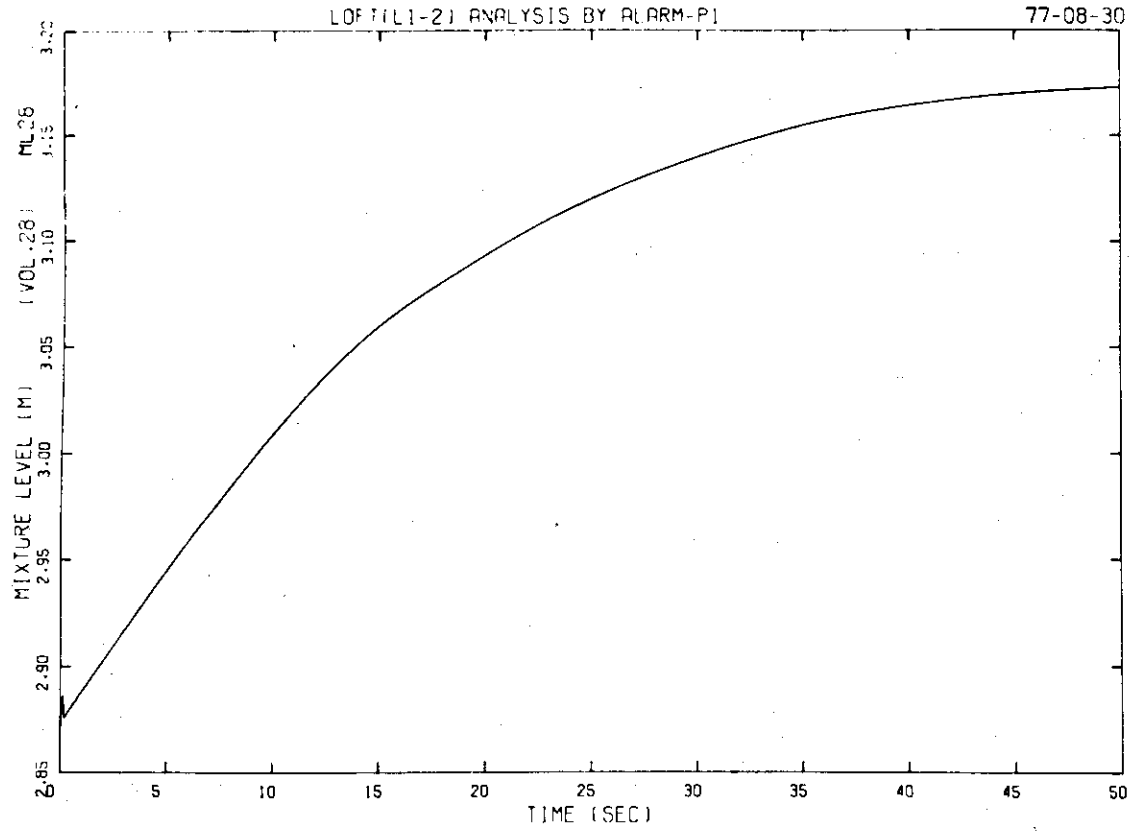

Fig. 57 Mixture Level in Suppression Tank

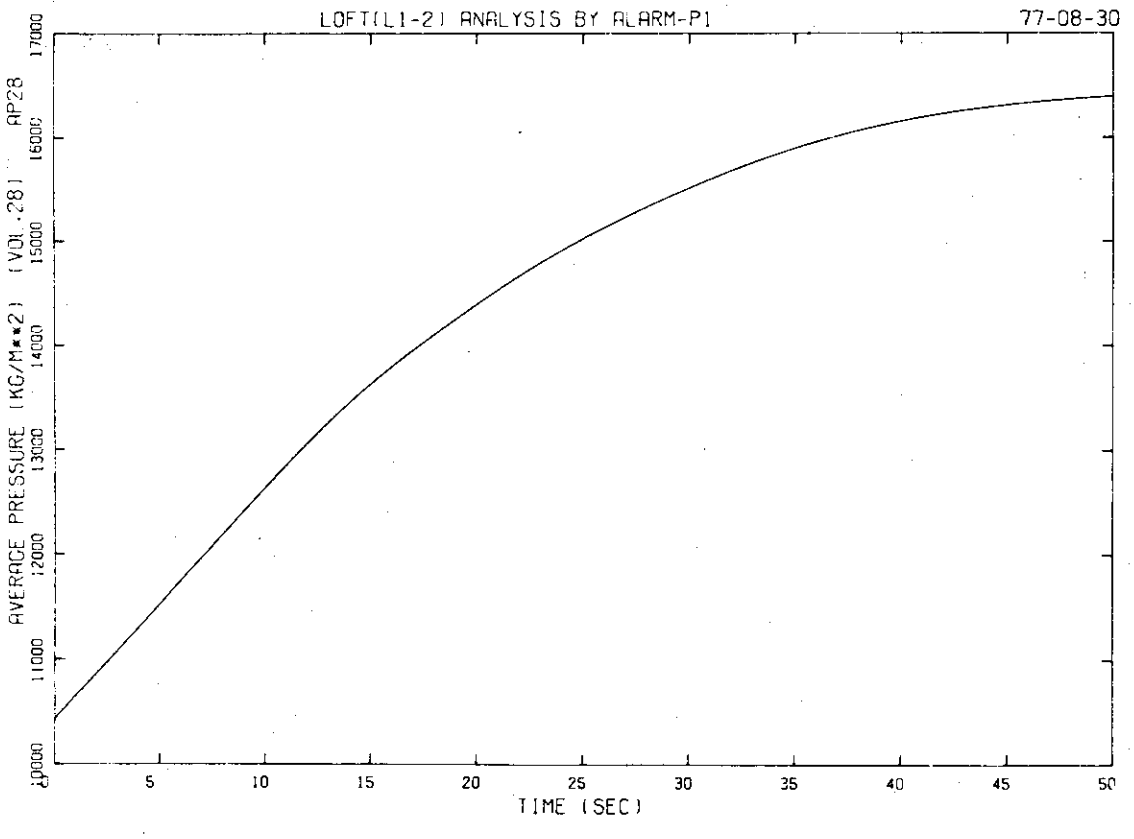

Fig. 58 Average Pressure in Suppression Tank

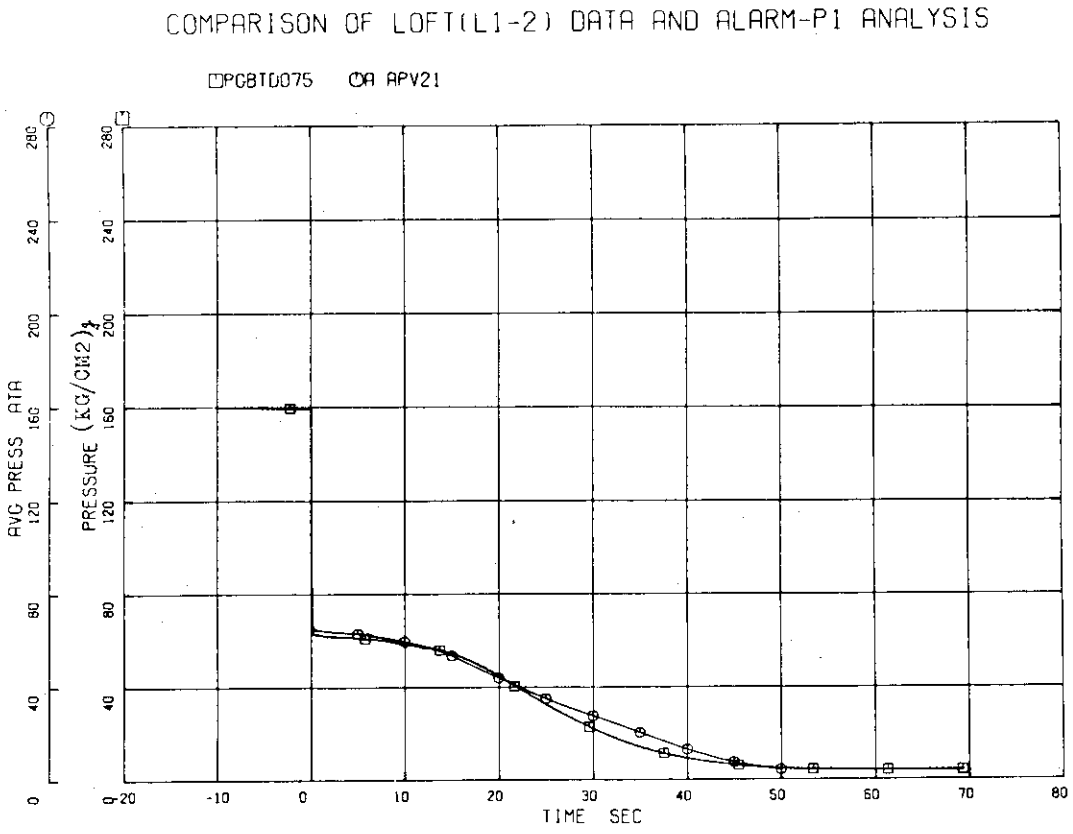

Fig. 59 Average Pressure in Blowdown Loop Cold Leg

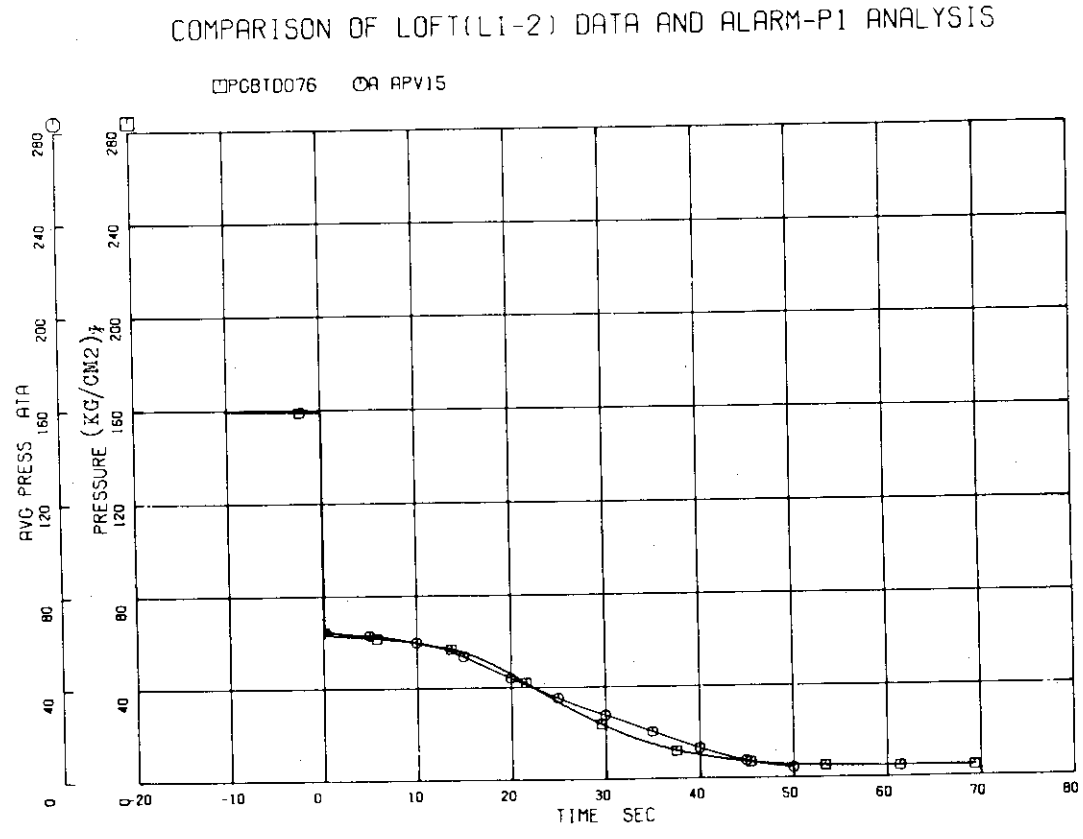

Fig. 60 Average Pressure in Blowdown Loop Hot Leg

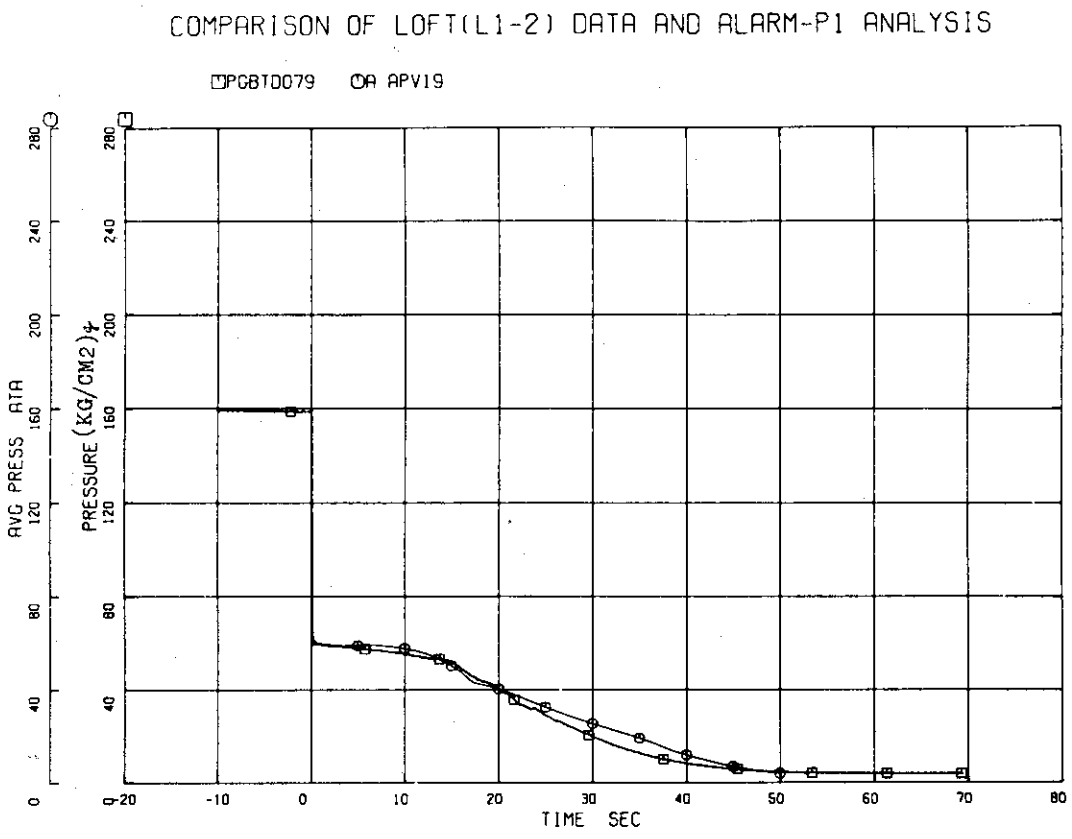

Fig. 61 Average Pressure in Blowdown Loop Pump Simulator Inlet Volume

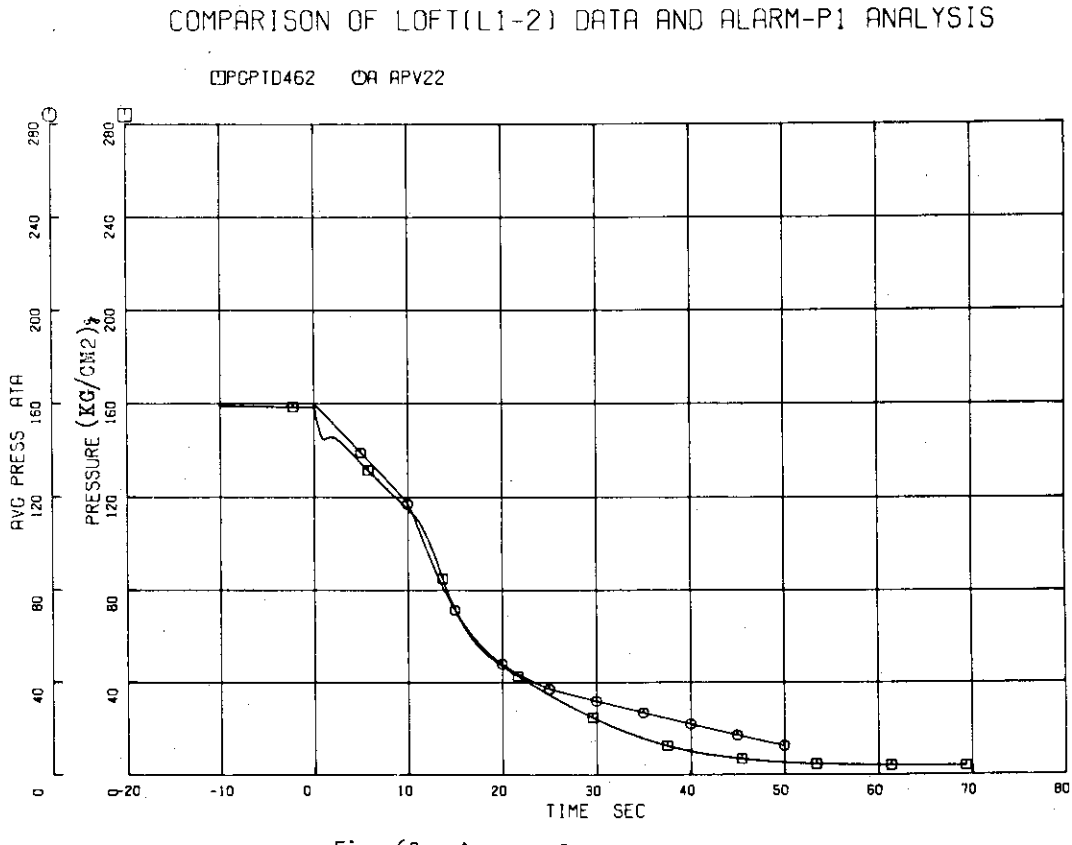

Fig. 62 Average Pressure in Pressurizer

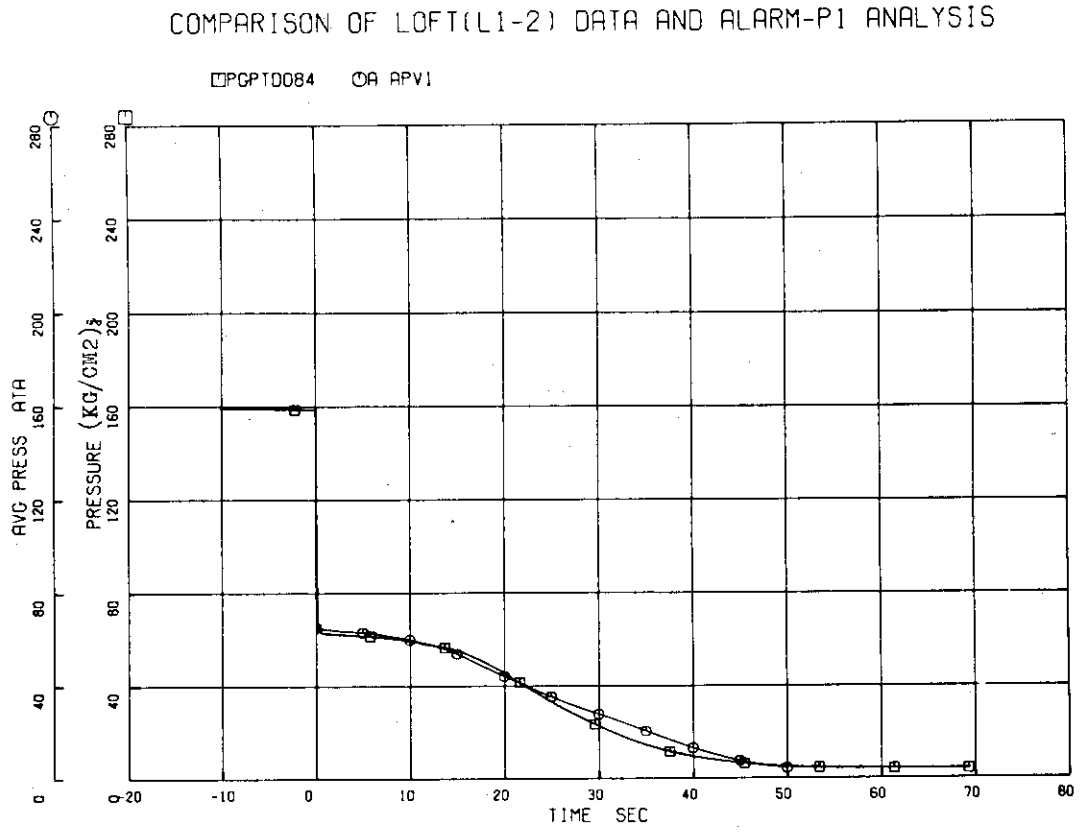

Fig. 63 Average Pressure in Intact Loop Hot Leg

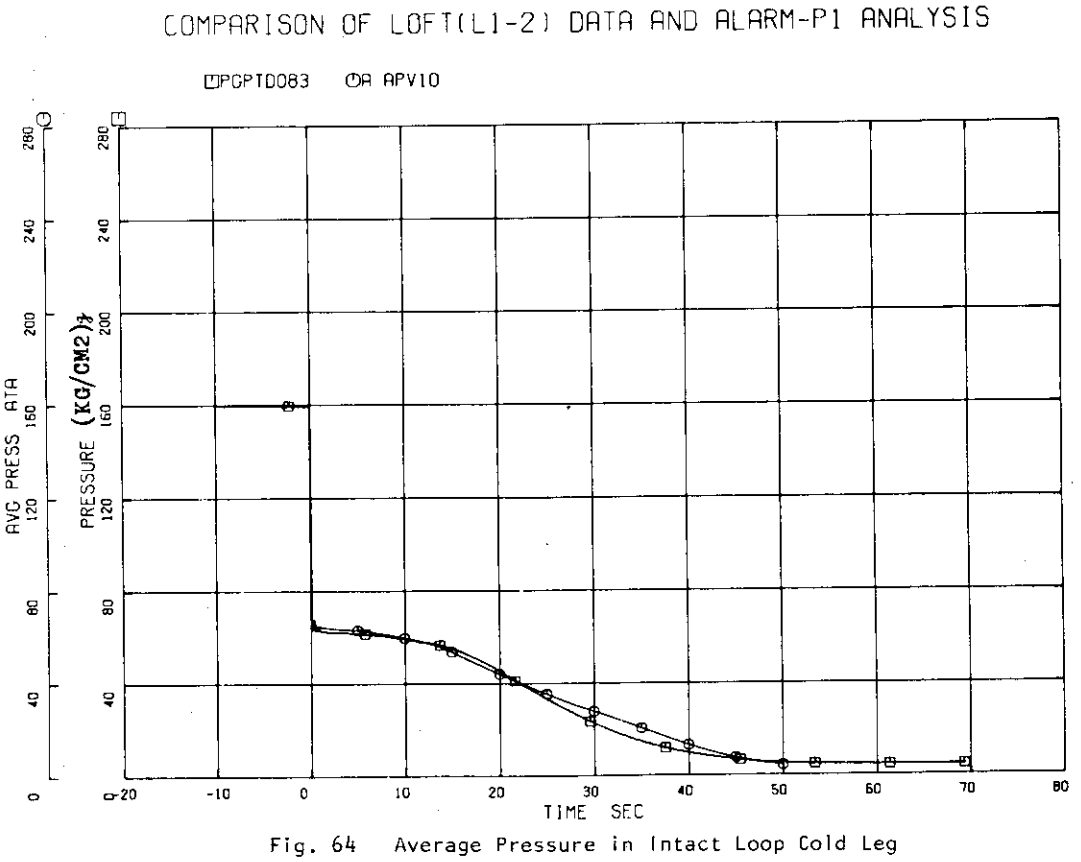

Fig. 64 Average Pressure in Intact Loop Cold Leg

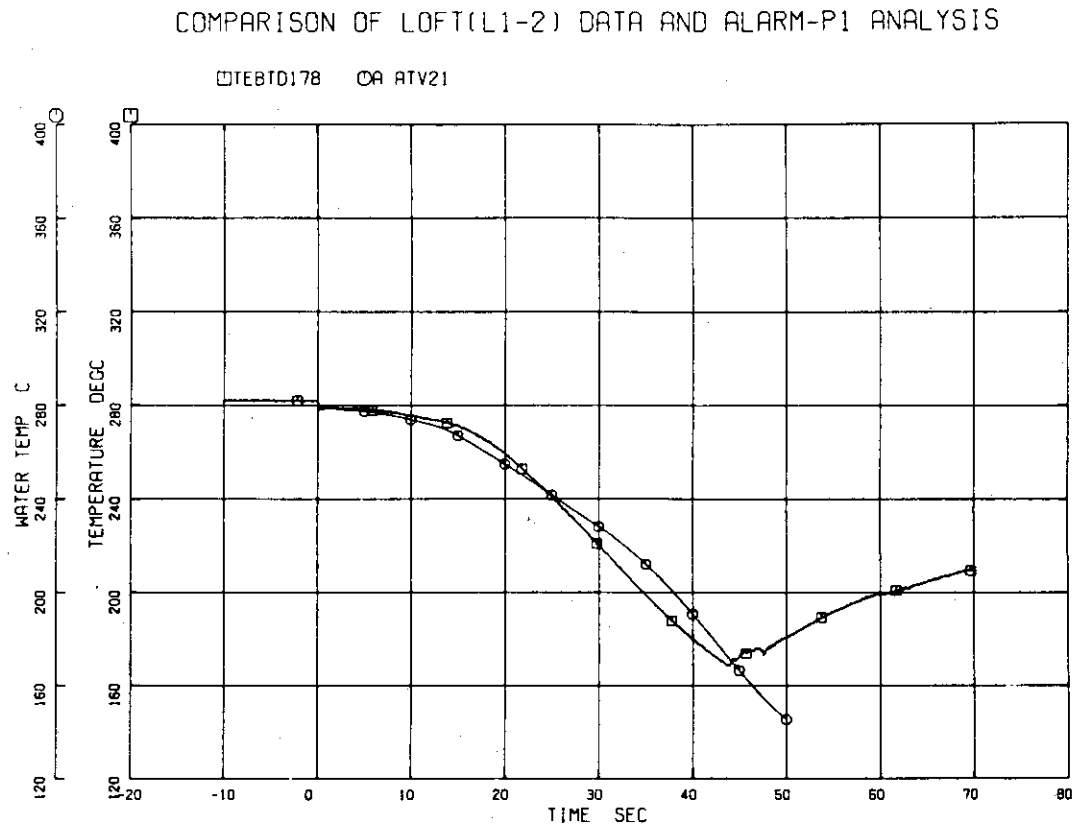

Fig. 65 Average Temperature in Broken Loop Cold Leg

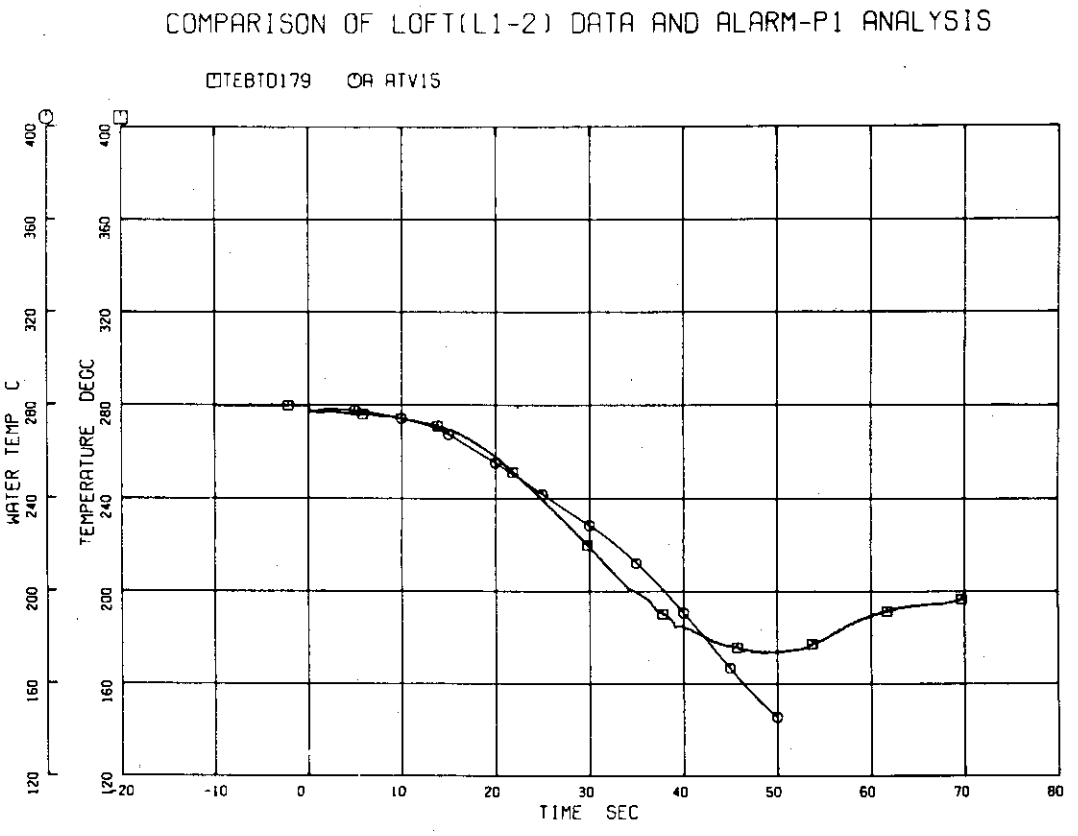

Fig. 66 Average Temperature in Broken Loop Hot Leg

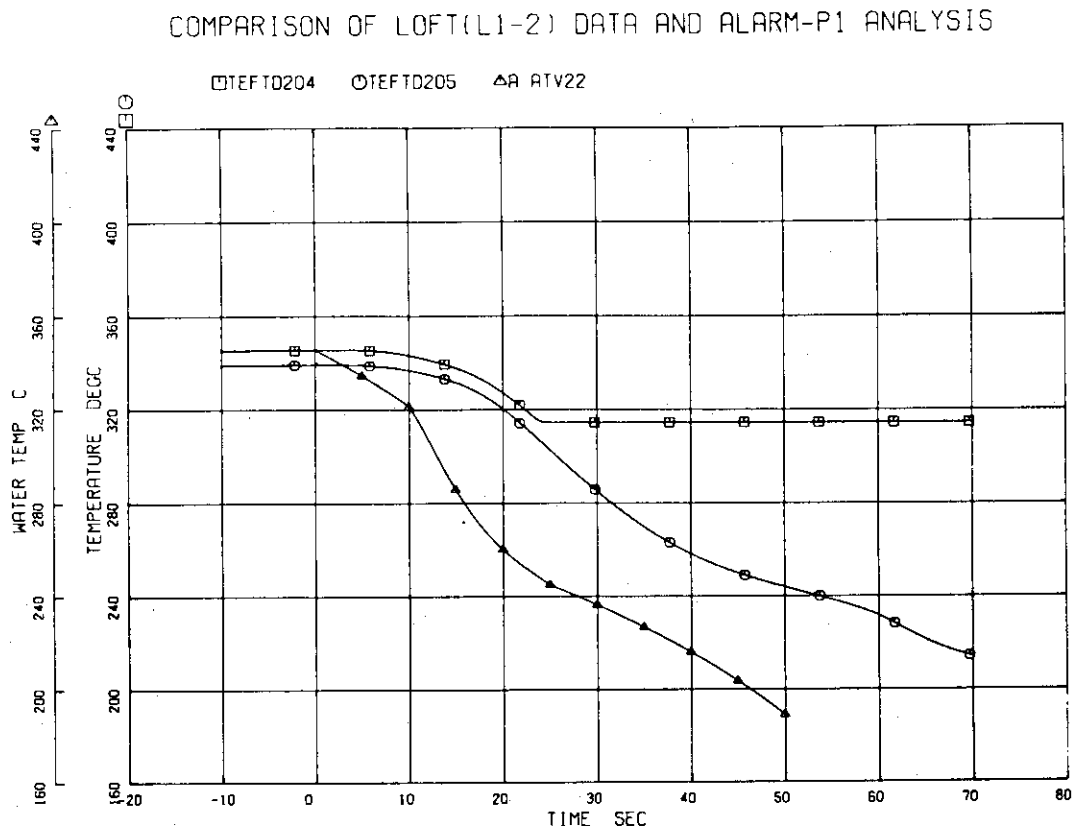

Fig. 67 Average Temperature in Pressurizer

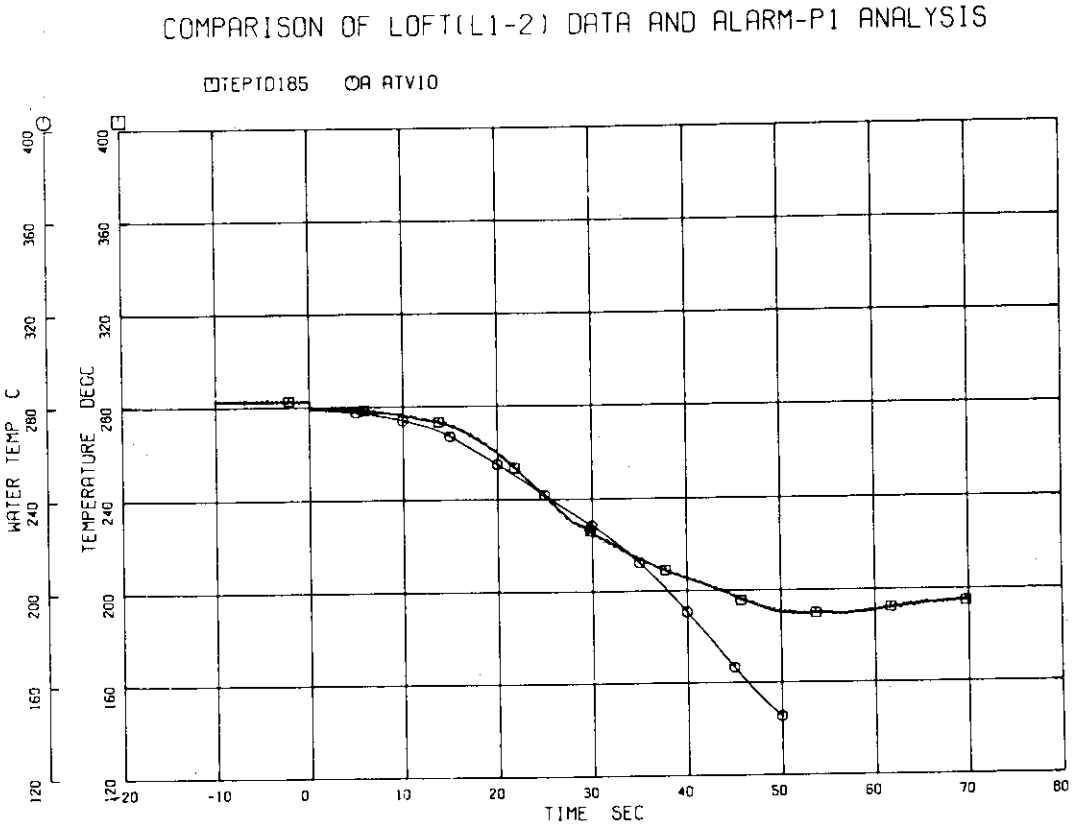

Fig. 68 Average Temperature in Intact Loop Cold Leg

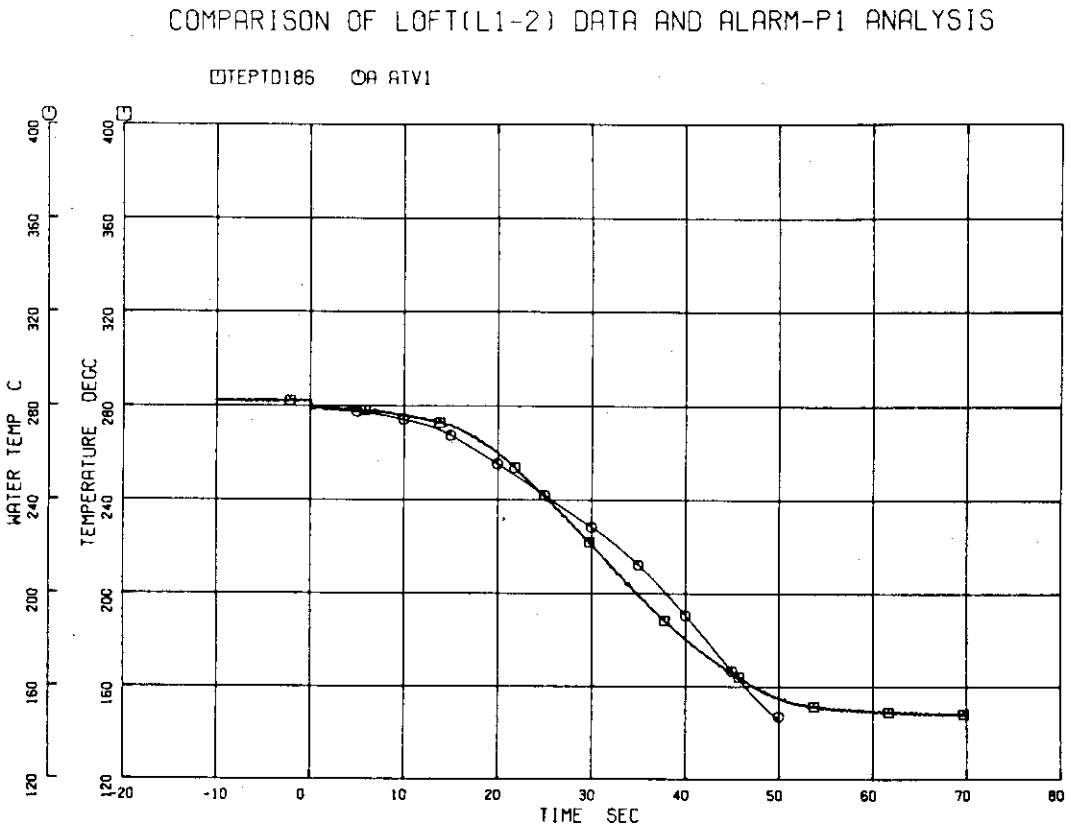

Fig. 69 Average Temperature in Intact Loop Hot Leg

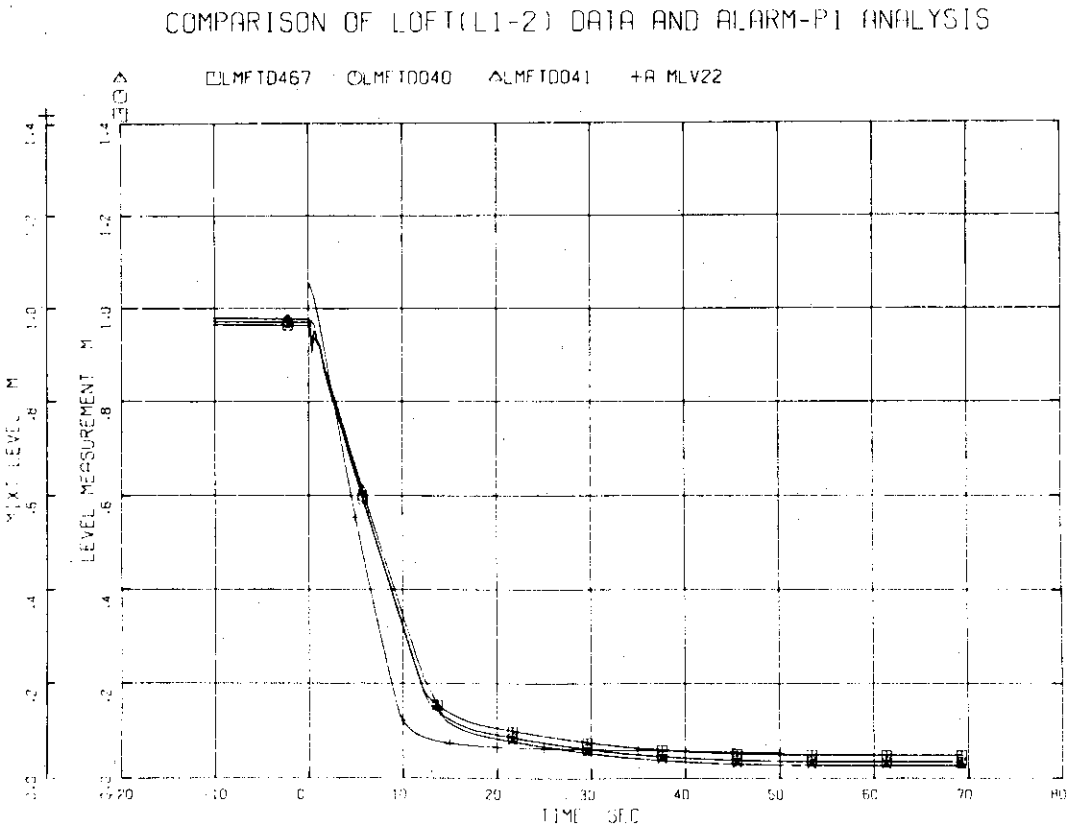

Fig. 70 Average Mixture Level in Pressurizer

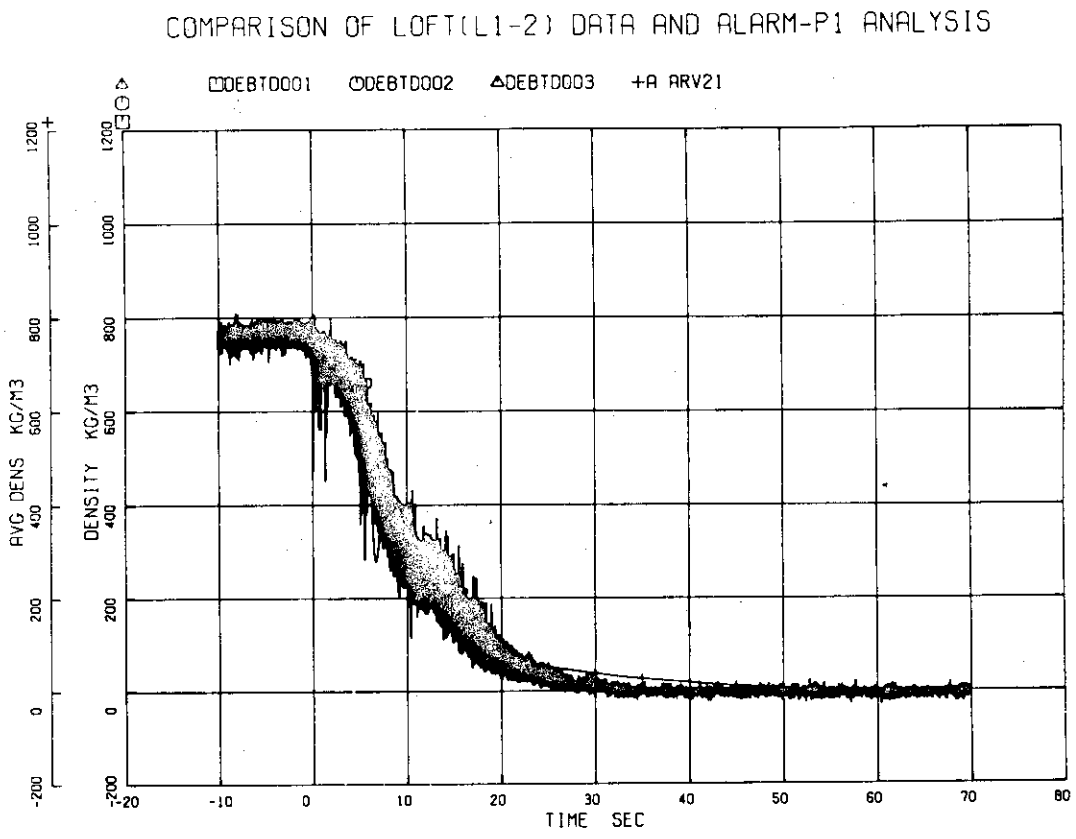

Fig. 71 Average Density in Broken Loop Cold Leg

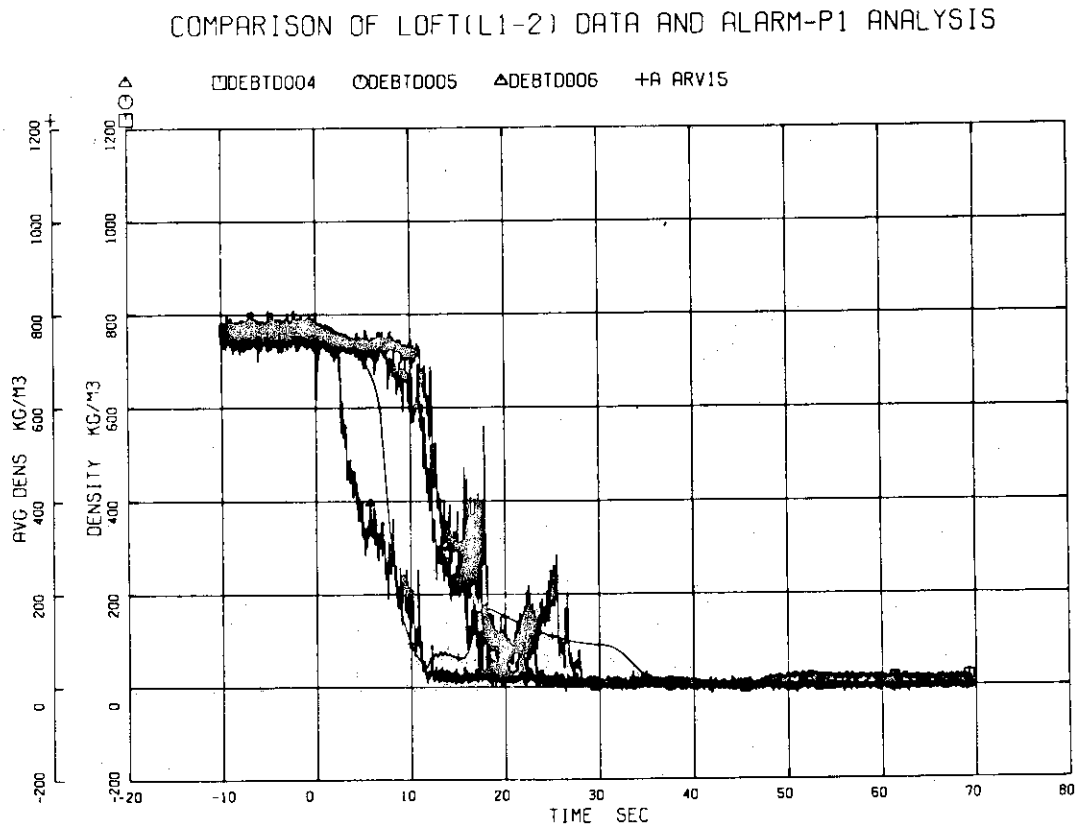

Fig. 72 Average Density in Broken Loop Hot Leg

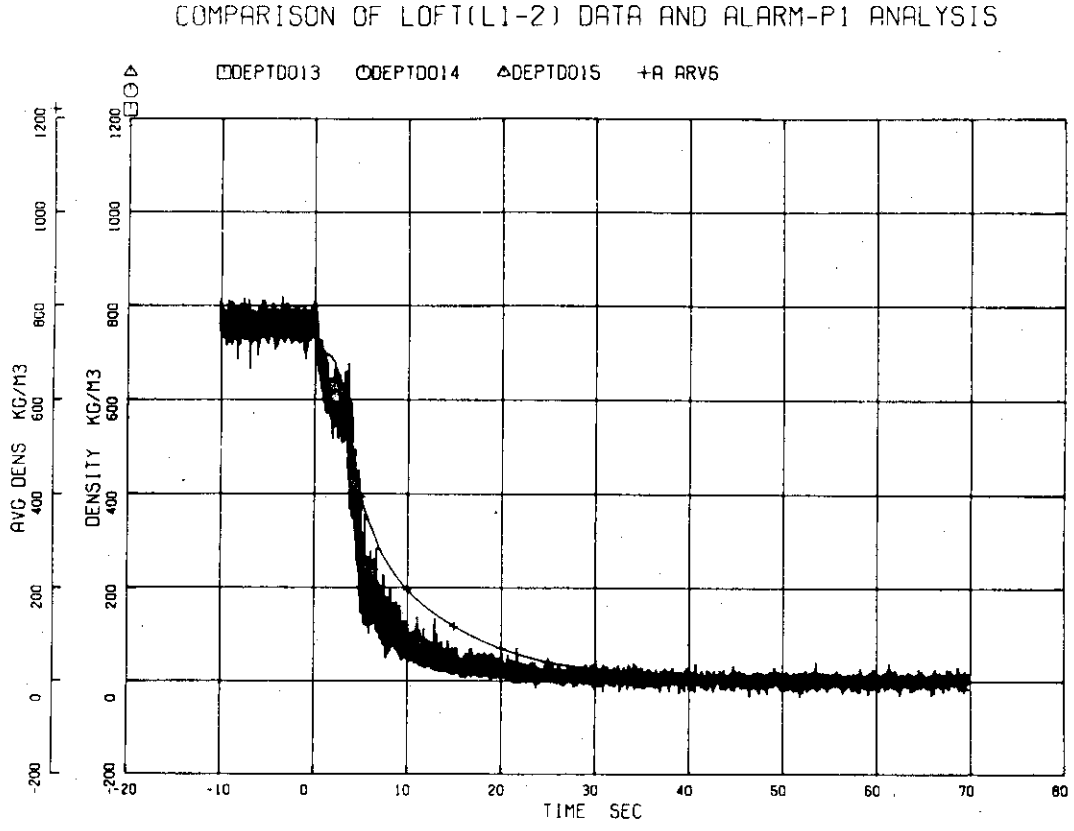

Fig. 73 Average Density in Intact Loop Pump Inlet Volume

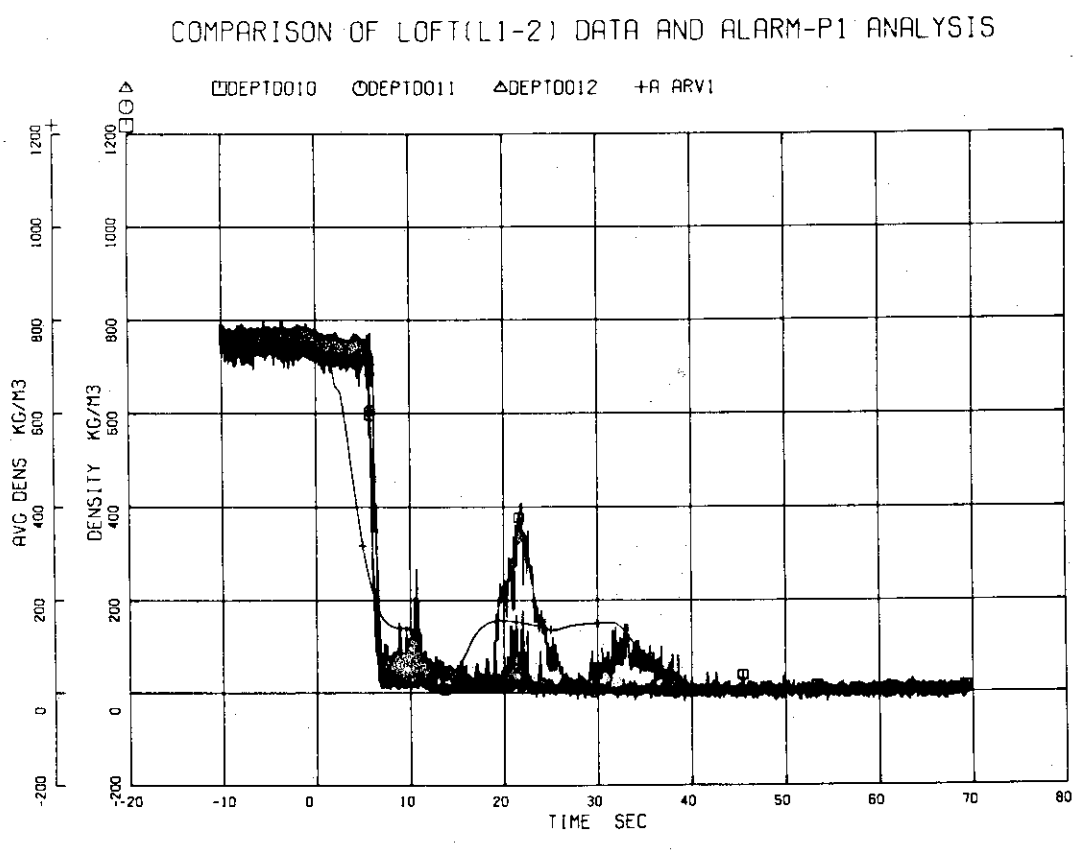

Fig. 74 Average Density in Intact Loop Hot Leg

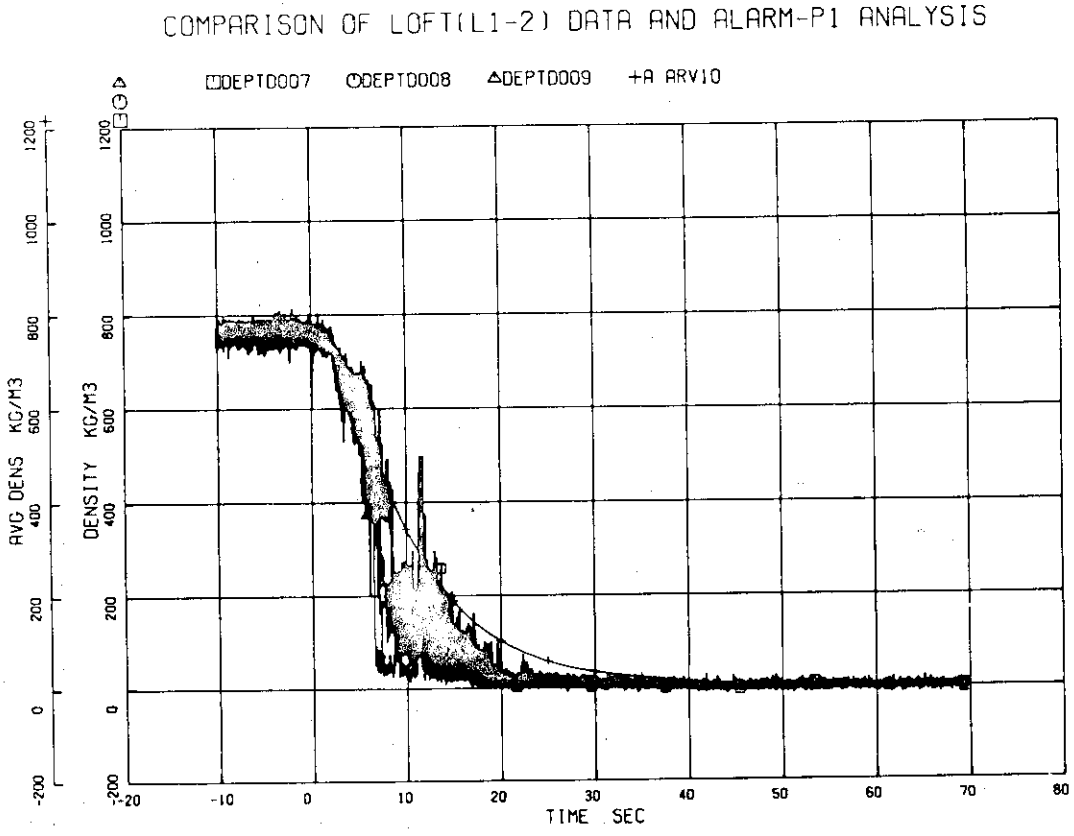

Fig. 75 Average Density in Intact Loop Cold Leg

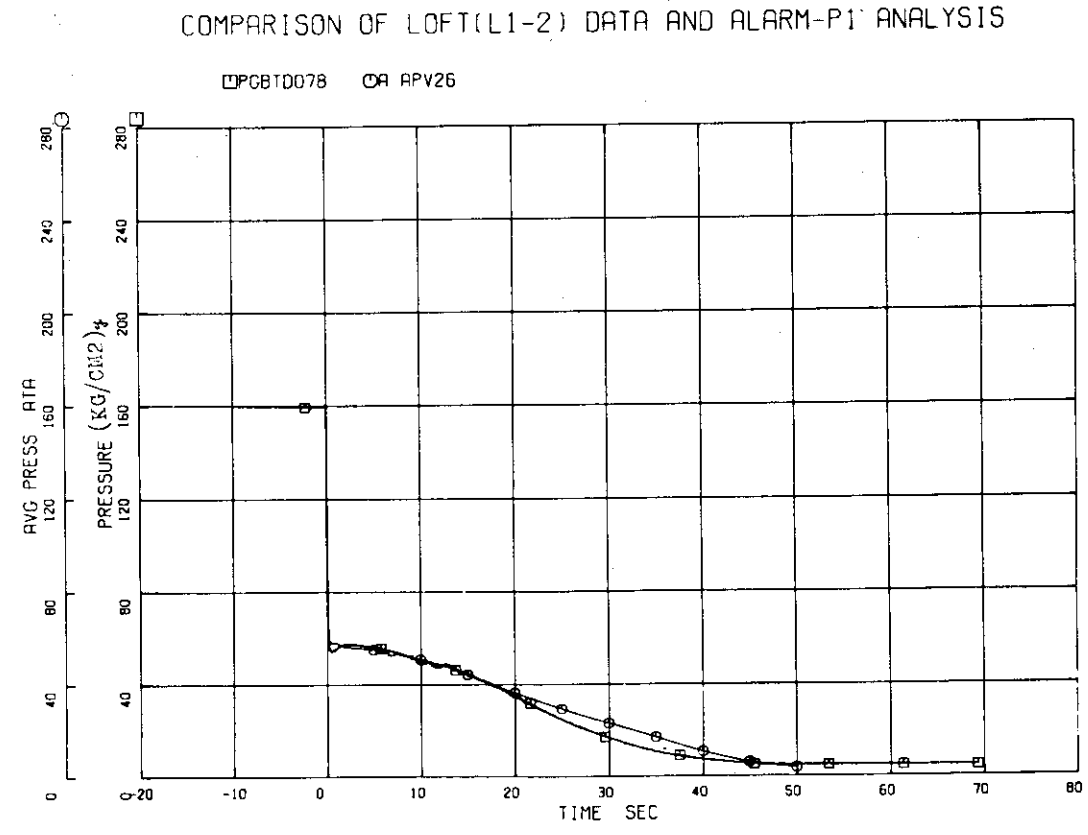

Fig. 76 Average Pressure at The Nozzle of The Broken Loop

Appendix 1

ALARM-P (VERSION 1) PWR LOSS OF COOLANT ANALYSIS PROGRAM

***** LISTING OF INPUT DATA *****

```
NO.      ....*....1....*....2....*....3....*....4....*....5....*....6....*....7....*....8

  1      /*                                                                    LFT00100
  2      /*          LOFT(L1-2) ANALYSIS BY ALARM-P1                           LFT00200
  3      /*                                                                    LFT00300
  4                  LOFT(L1-2) ANALYSIS BY ALARM-P1                           LFT00400
  5      /*                                                                    LFT00500
  6      /*    PROBLEM DIMENSION                                               LFT00600
  7      /*                                                                    LFT00700
  8           -3   9   5   6  28  1  30  2  1  2  0  0  1  0  1  1  0  0,0     LFT00800
  9      /*                                                                    LFT00900
 10      /*    EDIT VARIABLE                                                   LFT01000
 11      /*                                                                    LFT01100
 12      AP  N1  AP  N10 AP  N15 AP  N21 AP  N22 AR  N1  AR  N10 AR  N15 AR  N21 LFT01200
 13      /*                                                                    LFT01300
 14      /*    TIME STEP CONTROL                                               LFT01400
 15      /*                                                                    LFT01500
 16           10      100    1      1000   0,00001   0.05                     LFT01600
 17            2      100    1       200   0,00005   0.30                     LFT01700
 18           10       10    1       100   0,0001    1.00                     LFT01800
 19           20      100    1        20   0,0005    5.00                     LFT01900
 20           10      100    1        10   0,001    70.00                     LFT02000
 21      /*                                                                    LFT02100
 22      /*    TRIP  CONTROL                                                   LFT02200
 23      /*                                                                    LFT02300
 24          1    1    0    0    50.0     0.0  / END OF PROBLEM               LFT02400
 25          1   -4    1    0     1.89E4  0.0  / LOW PRESSURE                 LFT02500
 26         41    1    0    0     0.0     0.0  /   PUMP                       LFT02600
 27         42    1    0    0     0.0     0.0  /   PUMP                       LFT02700
 28          6    1    0    0     0.0     0.0  /  BREAK VALVE                 LFT02800
 29          7    1    0    0     0.0     0.0  /  BREAK VALVE                 LFT02900
 30      /*                                                                    LFT03000
 31      /*    VOLUME DATA                                                     LFT03100
 32      /*                                                                    LFT03200
 33        0      0 159.8241912E+4 281.667   -1.0   0.13933   0.2840736       LFT03300
 34          0.2840736      0.06342     0.2840736    -0.1420368          0.0  LFT03400
 35        0      0 159.7749648E+4 282.222   -1.0   0.06853   0.2840736       LFT03500
 36          0.2840736      0.06342     0.2840736    -0.1420368          0.0  LFT03600
 37        0      0 159.7257383E+4 282.222   -1.0   0.16567   0.384048        LFT03700
 38          0.384048       0.06342     0.2840736    -0.1420368          0.0  LFT03800
 39        1      0 159.0787623E+4 281.944   -1.0   0.70517   3.429           LFT03900
 40          3.429          0.15107     0.0102108     0.0950976          3.56 LFT04000
 41        0      0 157.7426160E+4 281.667   -1.0   0.70517   3.429           LFT04100
 42          3.429          0.15107     0.0102108     0.0950976          3.56 LFT04200
 43        0      0 157.2925457E+4 281.111   -1.0   0.17473   1.685544        LFT04300
 44          1.685544       0.06342     0.2840736    -1.4121384          0.0  LFT04400
 45        0      1 159.0717294E+4 282.222   -1.0   0.19413   1.5200376       LFT04500
 46          1.5200376      0.06342     0.2840736    -1.4121384          0.0  LFT04600
 47            240.871                                                       LFT04700
 48        0      1 159.0717294E+4 282.222   -1.0   0.22755   1.5200376       LFT04800
 49          1.5200376      0.06342     0.2840736    -1.4121384          0.0  LFT04900
 50            240.871                                                       LFT05000
```

***** LISTING OF INPUT DATA *****

```
NO.       ....*....1....*....2....*....3....*....4....*....5....*....6....*...,7....*....8

 51            0     0 160,4922644E+4 282.222   -1.0   0.11385   0.2840736          LFT05100
 52              0.2840736      0.06342     0.2840736     -0.1420368          0.0  LFT05200
 53            0     0 160,4571026E+4 282.222   -1.0   0.14981   0.2840736          LFT05300
 54              0.2840736      0.06342     0.2840736     -0.1420368          0.0  LFT05400
 55            1     0 160,5133614E+4 281.667   -1.0   0.94306   5.1703224          LFT05500
 56              5.1703224      0.18230     0.0495776     -4.255006           0.0  LFT05600
 57            0     0 160,6047819E+4 281.111   -1.0   0.64315   0.8238744          LFT05700
 58              0.8238744      0.78055     0.9970006     -4.988052           0.0  LFT05800
 59            0     0 160,3656821E+4 281.667   -1.0   0.91474   3.5317176          LFT05900
 60              3.5317176      0.25901     0.5742432     -4.1641776          0.0  LFT06000
 61            1     0 160,1195499E+4 282.222   -1.0   0.30669   1.5325344          LFT06100
 62              1.5325344      0.23067     0.5419344     -0.63246            0.0  LFT06200
 63            0     0 159,8241912E+4 279.444   -1.0   0.16406   0.2840736          LFT06300
 64              0.2840736      0.06342     0.2840736     -0.1420368          0.0  LFT06400
 65            0     0 159,7187060E+4 276.667   -1.0   0.01269   0.7690104          LFT06500
 66              0.7690104      0.00836     0.1033272     -0.0515112          0.0  LFT06600
 67            0     0 159,6132205E+4 271.111   -1.0   0.33672   2.8882848          LFT06700
 68              2.8882848      0.10563     0.3666744      0.7174992          0.0  LFT06800
 69            0     0 159,6132205E+4 271.111   -1.0   0.33672   2.8882848          LFT06900
 70              2.8882848      0.10563     0.3666744      0.7174992          0.0  LFT07000
 71            0     0 159,8241912E+4 260.000   -1.0   0.04996   2.07264            LFT07100
 72              2.07264        0.02564     0.1807464     -1.354836           0.0  LFT07200
 73            0     0 159,8241912E+4 246.111   -1.0   0.01575   1.2643104          LFT07300
 74              1.2643104      0.00836     0.10333       -1.2643104          0.0  LFT07400
 75            0     0 160,4571026E+4 280,556   -1.0   0.13857   0.2840736          LFT07500
 76              0.2840736      0.06342     0.2840736     -0.1420368          0.0  LFT07600
 77            1     0 159,6132206E+4   0.0       0.0   1.02802   1.819656           LFT07700
 78              1.0527791      0.56483     0.847344       1.1728704          0.0  LFT07800
 79            0     0 159,7116736E+4 301,667   -1.0   0.00634   1.0308336          LFT07900
 80              1.0306336      0.00145     0.0429768      0.1420368          0.0  LFT08000
 81            0     0 159,6874824E+4 275,556   -1.0   0.16576   0.8619744          LFT08100
 82              0.8619744      0.03865     0.2221992     -0.11113008         0.0  LFT08200
 83            0     0 160,5203936E+4 275,556   -1.0   0.19235   0.6074664          LFT08300
 84              0.6074664      0.03883     0.2221992      0.1420368          0.0  LFT08400
 85            0     0 160,4571026E+4 252,222   -1.0   0.00408   0.10320528         LFT08500
 86              0.10320528     0.00836     0.10320528    -0.0515112          0.0  LFT08600
 87            0     0 159,6132208E+4 321,111   -1.0   0.00634   0.2023872          LFT08700
 88              0.2023872      0.00144     0.042672       1.1298936          0.0  LFT08800
 89            1     0   1,0407876E+4  71.0       0.0 104.809   4.9054512          LFT08900
 90              2.871216      21.367       5.21208       -4.13004            0.0  LFT09000
 91       /*                                                                       LFT09100
 92       /*   BUBBLE DATA                                                         LFT09200
 93       /*                                                                       LFT09300
 94              0.8     0.9144                                                    LFT09400
 95       /*                                                                       LFT09500
 96       /*   PUMP DATA                                                           LFT09600
 97       /*                                                                       LFT09700
 98            11  12  13  17  11   7  10  17  2                                  LFT09800
 99            0.0   1.0E-5  769.134  100.564  0.3154  369.661  9.748  0.412  0.0LFT09900
100       /*                                                                       LFT10000
```

***** LISTING OF INPUT DATA *****

```
NO.  ....*....1....*....2....*....3....*....4....*....5....*....6....*....7....*....8
101  /*    HEAD                                                                  LFT10100
102  /*                                                                          LFT10200
103      -1.0       2.4722   -0.80574   2.0474   -0.6069   1.831              LFT10300
104      -0.40683   1.624    -0.200171  1.4705    0.0      1.4036             LFT10400
105       0.19061   1.3636    0.38963   1.3186    0.59396  1.2328             LFT10500
106       0.7902    1.1336    1.0       1.0078                                LFT10600
107  /*                                                                          LFT10700
108      -1.0      -1.0      -0.80      -0.63     -0.60     -0.30              LFT10800
109      -0.40     -0.05     -0.20       0.15      0.0       0.25              LFT10900
110       0.20      0.28      0.40       0.34      0.4118    0.2768            LFT11000
111       0.59763   0.4584    0.763467   0.6992    1.0       0.9465            LFT11100
112  /*                                                                          LFT11200
113      -1.0      -1.0      -0.80      -0.97     -0.60     -0.95              LFT11300
114      -0.40     -0.85     -0.20      -0.80      0.0      -0.67              LFT11400
115       0.20     -0.50      0.40      -0.25      0.57554   0.0               LFT11500
116       0.74437   0.2563    0.77345    0.3778    0.86313   0.6326            LFT11600
117       1.0       1.0076                                                     LFT11700
118  /*                                                                          LFT11800
119      -1.0       2.4722   -0.82297   1.9968   -0.63332  1.5897             LFT11900
120      -0.45534   1.3279   -0.27109   1.1949   -0.17716  1.0605             LFT12000
121      -0.09073   1.0156    0.0       0.934279  0.091099  0.9229            LFT12100
122       0.186509  0.6963    0.271762  0.875     0.455872  0.6433            LFT12200
123       0.574406  0.8355    0.740576  0.8466    0.766619  0.8469            LFT12300
124       0.871471  0.8638    1.0       0.9465                                LFT12400
125  /*                                                                          LFT12500
126  /*    TORQUE                                                              LFT12600
127  /*                                                                          LFT12700
128      -1.0       1.9843   -0.80096   1.394    -0.60638  1.0975             LFT12800
129      -0.40686   0.822    -0.19928   0.6648    0.0      0.6032             LFT12900
130       0.1930    0.8325    0.393     0.7369    0.59552  0.8331             LFT13000
131       0.79782   0.9229    1.0       0.9672                                LFT13100
132  /*                                                                          LFT13200
133      -1.0      -1.0      -0.30      -0.90     -0.10     -0.50              LFT13300
134       0.0      -0.45      0.40      -0.25      0.50      0.0               LFT13400
135       1.0       0.3569                                                     LFT13500
136  /*                                                                          LFT13600
137      -1.0      -1.0      -0.25      -0.90     -0.08     -0.80              LFT13700
138       0.0      -0.67      0.40      -0.25      0.50      0.15              LFT13800
139       0.737255  0.526586  0.768049   0.606594  0.86723   0.74366           LFT13900
140       1.0       0.9672                                                     LFT14000
141  /*                                                                          LFT14100
142      -1.0       1.9843   -0.82234   1.8508   -0.63371  1.6824             LFT14200
143      -0.45655   1.557    -0.267023  1.4362   -0.176107 1.3879             LFT14300
144      -0.08931   1.3481    0.0       1.23361   0.090643  1.1965            LFT14400
145       0.188569  1.1096    0.27347   1.0416    0.458669  0.8958            LFT14500
146       0.57448   0.7807    0.73816   0.6134    0.76852   0.5649            LFT14600
147       0.870057  0.4877    1.0       0.3569                                LFT14700
148  /*                                                                          LFT14800
149       0.0       0.0       1.E+8     0.0                                   LFT14900
150  /*                                                                          LFT15000
```

***** LISTING OF INPUT DATA *****

```
NO.  ....*....1....*....2....*....3....*....4....*....5....*....6....*....7....*....8

151  /*   JUNCTION DATA                                                              LFT15100
152  /*                                                                              LFT15200
153       1    2    0   0   0   1   265.855   0.06342     0.0          0.0         LFT15300
154                       1.0E-5   1.0E-5   0.0  0.85  0.0                        LFT15400
155       2    3    0   0   0   1   265.855   0.06342     0.0          0.0         LFT15500
156                       1.0E-5   1.0E-5   0.0  0.85  0.0                        LFT15600
157       3    4    0   0   0   1   265.855   0.05169     0.2420112    0.0         LFT15700
158                       1.0E-5   1.0E-5   0.0  0.85  0.0                        LFT15800
159       4    5    0   0   0   1   265.855   0.15143     3.057144     0.0         LFT15900
160                       1.0E-5   1.0E-5   0.0  0.85  0.0                        LFT16000
161       5    6    0   0   0   1   265.855   0.05169     0.2734056    0.0         LFT16100
162                       1.0E-5   1.0E-5   0.0  0.85  0.0                        LFT16200
163       6    7   -1   0   0   1   132.950   0.06342    -1.2701016    0.0         LFT16300
164                       1.0E-5   1.0E-5   0.0  0.85  0.0                        LFT16400
165       6    8   -2   0   0   1   132.905   0.06342    -1.2701016    0.0         LFT16500
166                       1.0E-5   1.0E-5   0.0  0.85  0.0                        LFT16600
167       7    9    1   0   0   1   132.950   0.03661     0.0          0.0         LFT16700
168                       1.0E-5   1.0E-5   0.0  0.85  0.0                        LFT16800
169       8    9    2   0   0   1   132.905   0.03661     0.0          0.0         LFT16900
170                       1.0E-5   1.0E-5   0.0  0.85  0.0                        LFT17000
171       9   10    0   0   0   1   265.855   0.06342     0.0          0.0         LFT17100
172                       1.0E-5   1.0E-5   0.0  0.85  0.0                        LFT17200
173      10   11    0   0   0   1   265.855   0.06342     0.0          0.0         LFT17300
174                       1.0E-5   1.0E-5   0.0  0.85  0.0                        LFT17400
175      11   12    0   0   0   1   265.855   0.17094    -4.255008     0.0         LFT17500
176                       1.0E-5   1.0E-5   0.0  0.85  0.0                        LFT17600
177      12   13    0   0   0   1   265.855   0.26254    -4.1641776    0.0         LFT17700
178                       1.0E-5   1.0E-5   0.0  0.85  0.0                        LFT17800
179      13   14    0   0   0   1   265.855   0.04779    -0.63246      0.0         LFT17900
180                       1.0E-5   1.0E-5   0.0  0.85  0.0                        LFT18000
181      14    1    0   0   0   1   265.855   0.06342     0.0          0.0         LFT18100
182                       1.0E-5   1.0E-5   0.0  0.85  0.0                        LFT18200
183      14   15    0   0   0   1     0.0     0.06342     0.0          0.0         LFT18300
184       0.0   0.0   0.0   0.85  0.0                                             LFT18400
185      24   15    0   0   0   1     0.0     0.03880     0.0          0.0         LFT18500
186                 0.5   0.5   0.0  0.85  0.0                                   LFT18600
187      15   16    0   0   0   1     0.0     0.00836     0.0          0.0         LFT18700
188       0.0   0.0   0.0   0.85  0.0                                             LFT18800
189      16   17    0   0   0   1     0.0     0.00836     0.7174992    0.0         LFT18900
190                 1.52  1.09  0.0  0.85  0.0                                   LFT19000
191      17   18    0   0   0   1     0.0     0.01914     3.4222944    0.0         LFT19100
192                 7.02  7.02  0.0  0.85  0.0                                   LFT19200
193      18   19    0   0   0   1     0.0     0.00836     0.7174992    0.0         LFT19300
194                 1.09  1.52  0.0  0.85  0.0                                   LFT19400
195      19   20    0   0   0   1     0.0     0.00836    -1.2127992    0.0         LFT19500
196                17.10 17.10  0.0  0.85  0.0                                   LFT19600
197      20   28    0   1   0   1   0.0     0.00836     0.0     0.0               LFT19700
198         0.0   0.0   0.0   0.85  0.6                                           LFT19800
199      11   21    0   0   0   1     0.0     0.06342     0.0          0.0         LFT19900
200       0.0   0.0   0.0   0.85  0.0                                             LFT20000
```

ALARM-P (VERSION 1) PWR LOSS OF COOLANT ANALYSIS PROGRAM

***** LISTING OF INPUT DATA *****

```
NO.      ....*....1....*....2....*....3....*....4....*....5....*....6....*....7....*....8
201          25   21   0   0   0   1      0.0      0.03880      0.1420368     0.0     LFT20100
202                     0.5     0.5    0.0  0.85   0.0                                LFT20200
203          21   26   0   0   0   1      0.0      0.00836      0.0           0.0     LFT20300
204           0.0   0.0   0.0   0.85  0.0                                             LFT20400
205          22   27   0   0   0   1      0.0      0.00468      1.2743688     0.0     LFT20500
206           0.0   0.0   0.0   0.85  0.6                                             LFT20600
207          23    2   0   0   0   1      0.0      0.00145      0.1420368     0.0     LFT20700
208                    0.95    0.44   0.0  0.85   0.6                                LFT20800
209          26   28   0   2   0   1     0.0     0.00836     0.0     0.0              LFT20900
210           0.0   0.0   0.0   0.85  0.6                                             LFT21000
211          27   23   0   0   0   1     0.0     0.00145     1.1515344 0.0           LFT21100
212                9.00    9.00    0.0  0.85   0.6                                  LFT21200
213     /*                                                                           LFT21300
214     /*    CHECK VALVE DATA                                                       LFT21400
215     /*                                                                           LFT21500
216          -6       0.0      0.0     0.0     0.0                                  LFT21600
217          -7       0.0      0.0     0.0     0.0                                  LFT21700
218     /*                                                                           LFT21800
219     /*    HEAT SLAB DATA                                                         LFT21900
220     /*                                                                           LFT22000
221          0   11  1     0.0    76.206     13.6644     0.0    0.0                 LFT22100
222     /*                                                                           LFT22200
223     /*    SLAB GEOMETRY DATA                                                     LFT22300
224     /*                                                                           LFT22400
225          1   1  0  1   5     0.2560    0.0    0.0                               LFT22500
226     /*                                                                           LFT22600
227     /*    MATERIAL THERMAL PROPERTY DATA                                         LFT22700
228     /*                                                                           LFT22800
229     /*    SS304  THERMAL CONDUCTIVITY                                            LFT22900
230     /*                                                                           LFT23000
231          2                                                                       LFT23100
232          100.0     3.95725E-3      1300.0      7.97485E-3                       LFT23200
233     /*                                                                           LFT23300
234     /*    SS304  HEAT CAPACITY                                                   LFT23400
235     /*                                                                           LFT23500
236          13                                                                      LFT23600
237          76.667     712.1265   121.111   710.0256   204.444   712.5495         LFT23700
238         315.556     727.0415   426.667   751.3652   537.778   782.2920         LFT23800
239         648.889     816.7132   760.000   851.4400   871.111   883.3040         LFT23900
240         982.222     909.1364  1093.333   925.7688  1204.444   930.0322         LFT24000
241        1315.556     918.7580                                                    LFT24100
242     /*                                                                           LFT24200
243     /*    GAP CONDUCTANCE  DATA                                                  LFT24300
244     /*                                                                           LFT24400
245          2                                                                       LFT24500
246          0.0   0.0     1000.0   0.0                                             LFT24600
247     /*                                                                           LFT24700
248     /*    END  OF DATA                                                           LFT24800
```

END OF INPUT DATA

ELAPSED TIME 0.0 SEC TIME STEP NUMBER 0

********** TOTAL SYSTEM BALANCE **********

NORM POWER	POWER (MW)	HEAT REMOV. (KCAL/SEC)	ENERGY LEAK (KCAL)	MASS LEAK (KG)	ENERGY BAL. (KCAL)	MASS BAL. (KG)	TOTAL REAC. ($)	PERIOD (SEC)
0.19000D+01	0.0	0.0	0.0	0.0	0.87291D+07	0.65645D+05	0.0	0.0

********** VOLUME QUANTITIES **********

VOL NO.	AVG. PRES (KG/M2)	TOT. MASS (KG)	AVG. ENTH (KCAL/KG)	AVG. DENS (KG/M3)	AVG. TEMP (DEG C)	AVG. QUAL	BUBL MASS (KG)	MIX. LEVEL (M)	LIQ. MASS (KG)
1	0.15982D+07	0.10621D+03	0.29648D+03	0.76228D+03	0.28167D+03	0.0	0.0	0.28407D+00	0.10621D+03
2	0.15977D+07	0.52171D+02	0.29716D+03	0.76129D+03	0.28222D+03	0.0	0.0	0.28407D+00	0.52171D+02
3	0.15973D+07	0.12612D+03	0.29716D+03	0.76139D+03	0.28222D+03	0.0	0.0	0.38405D+00	0.12612D+03
4	0.15980D+07	0.53712D+03	0.29683D+03	0.76169D+03	0.28194D+03	0.0	0.0	0.34290D+01	0.53712D+03
5	0.15974D+07	0.53733D+03	0.29650D+03	0.76196D+03	0.28167D+03	0.0	0.0	0.34290D+01	0.53733D+03
6	0.15979D+07	0.13330D+03	0.29583D+03	0.76269D+03	0.28111D+03	0.0	0.0	0.16855D+01	0.13330D+03
7	0.15907D+07	0.14777D+03	0.29717D+03	0.76119D+03	0.28222D+03	0.0	0.0	0.15200D+01	0.14777D+03
8	0.15907D+07	0.17321D+03	0.29717D+03	0.76119D+03	0.28222D+03	0.0	0.0	0.15200D+01	0.17321D+03
9	0.16049D+07	0.86685D+02	0.29715D+03	0.76140D+03	0.28222D+03	0.0	0.0	0.28407D+00	0.86685D+02
10	0.16046D+07	0.11406D+03	0.29715D+03	0.76139D+03	0.28222D+03	0.0	0.0	0.28407D+00	0.11406D+03
11	0.16051D+07	0.71897D+03	0.29648D+03	0.76238D+03	0.28167D+03	0.0	0.0	0.51703D+01	0.71897D+03
12	0.16036D+07	0.49096D+03	0.29580D+03	0.76337D+03	0.28111D+03	0.0	0.0	0.82367D+00	0.49096D+03
13	0.16037D+07	0.69736D+03	0.29643D+03	0.76236D+03	0.28167D+03	0.0	0.0	0.35317D+01	0.69736D+03
14	0.16013D+07	0.23502D+03	0.29716D+03	0.76134D+03	0.28222D+03	0.0	0.0	0.15325D+01	0.23502D+03
15	0.15962D+07	0.12569D+03	0.29376D+03	0.76611D+03	0.27944D+03	0.0	0.0	0.28407D+00	0.12569D+03
16	0.15972D+07	0.97796D+01	0.29040D+03	0.77066D+03	0.27667D+03	0.0	0.0	0.76901D+00	0.97796D+01
17	0.15961D+07	0.26268D+03	0.28382D+03	0.78010D+03	0.27111D+03	0.0	0.0	0.28883D+01	0.26268D+03
18	0.15961D+07	0.26268D+03	0.28382D+03	0.78010D+03	0.27111D+03	0.0	0.0	0.20726D+01	0.39846D+02
19	0.15962D+07	0.39846D+02	0.27066D+03	0.79756D+03	0.26000D+03	0.0	0.0	0.12643D+01	0.12678D+02
20	0.15982D+07	0.12878D+02	0.25507D+03	0.81767D+03	0.24611D+03	0.0	0.0	0.28407D+00	0.10591D+03
21	0.16046D+07	0.10591D+03	0.29512D+03	0.76431D+03	0.28056D+03	0.0	0.0	0.10528D+01	0.35180D+03
22	0.15961D+07	0.39669D+03	0.41686D+03	0.58588D+03	0.34556D+03	0.11317D+00	0.0	0.10308D+01	0.45902D+01
23	0.15971D+07	0.45902D+01	0.32174D+03	0.72400D+03	0.30167D+03	0.0	0.0	0.86197D+00	0.12807D+03
24	0.15989D+07	0.12807D+03	0.28906D+03	0.77264D+03	0.27556D+03	0.0	0.0	0.60747D+00	0.14863D+03
25	0.16052D+07	0.14863D+03	0.28908D+03	0.77273D+03	0.27556D+03	0.0	0.0	0.10321D+00	0.33014D+01
26	0.16046D+07	0.33014D+01	0.26198D+03	0.80916D+03	0.25222D+03	0.0	0.0	0.20239D+00	0.43012D+01
27	0.15961D+07	0.43012D+01	0.34660D+03	0.67543D+03	0.32111D+03	0.0	0.0	0.28712D+01	0.59944D+05
28	0.10408D+05	0.59953D+05	0.71061D+02	0.57203D+03	0.71000D+02	0.14959D-03	0.0		

********** HEAT SLAB QUANTITIES **********

SLAB NO.	R VOL	R HT MODE	R HT FLUX (KCL/S/M2)	DNB FLUX (KCL/S/M2)	R HT COEF (KCL/S/M2/C)	CENT TEMP (C)	FUEL TEMP (C)	SURF TEMP (C)	R POWR H2O (KCL/S)	POWR GEN. (MW)
	L VOL	L HT MODE	L HT FLUX (KCL/S/M2)		L HT COEF (KCL/S/M2/C)				L POWR H2O (KCL/S)	
1	11	0	0.0		0.67815D-02			0.28167D+03	0.0	
	0	0	0.0		0.67815D-02			0.28167D+03	0.0	

********** JUNCTION QUANTITIES **********

JUN NO.	IN. VOL	OUT. VOL	CHOKE	JUN FLOW (KG/SEC)	JUN ENTH (KCAL/KG)	JUN SPVL (M3/KG)	PRESSURE DIFFERENTIAL NODE (KG/M2)	ELEV (KG/M2)	FRIC (KG/M2)	ACCL (KG/M2)	PUMP (KG/M2)
1	1	2	0	0.26585D+03	0.29648D+03	0.13116D-02	0.49226D+03	0.0	-0.48920D+03	-0.30611D+01	0.0
2	2	3	0	0.26585D+03	0.29716D+03	0.13136D-02	0.49227D+03	-0.38055D+02	-0.45419D+03	-0.22198D-01	0.0
3	3	4	0	0.26585D+03	0.29716D+03	0.13136D-02	0.64698D+04	-0.13402D+04	-0.60999D+04	0.97037D+03	0.0
4	4	5	0	0.26585D+03	0.29685D+03	0.13129D-02	0.13361D+05	0.36884D+00	-0.13362D+05	0.16098D+00	0.0
5	5	6	0	0.26585D+03	0.29650D+03	0.13124D-02	0.45007D+04	0.18135D+04	-0.53478D+04	-0.96644D+03	0.0
6	6	7	0	0.13295D+03	0.29583D+03	0.13108D-02	-0.17792D+05	0.64184D+02	-0.18774D+04	0.17613D+04	0.17844D+05
7	6	8	0	0.13291D+03	0.29583D+03	0.13108D-02	-0.17792D+05	0.64184D+02	-0.18606D+04	0.17617D+04	0.17846D+05
8	7	9	0	0.13295D+03	0.29717D+03	0.13137D-02	-0.14205D+05	-0.49639D+03	-0.13760D+04	-0.17659D+04	0.17844D+05
9	8	9	0	0.13291D+03	0.29717D+03	0.13137D-02	-0.14205D+05	-0.49639D+03	-0.13784D+04	-0.17663D+04	0.17846D+05
10	9	10	0	0.26555D+03	0.29715D+03	0.13134D-02	0.35162D+03	0.0	-0.35160D+03	-0.15809D-01	0.0
11	10	11	0	0.26585D+03	0.29715D+03	0.13134D-02	-0.56259D+03	0.12731D+04	-0.17460D+04	0.10355D+04	0.0
12	11	12	0	0.26555D+03	0.29648D+03	0.13117D-02	-0.91420D+03	0.22160D+04	-0.14363D+04	0.13449D+03	0.0
13	12	13	0	0.26585D+03	0.29560D+03	0.13100D-02	0.23910D+04	-0.16607D+04	-0.66747D+03	-0.62848D+02	0.0
14	13	14	0	0.26585D+03	0.29648D+03	0.13117D-02	0.24613D+04	-0.19296D+04	-0.51308D+03	-0.18627D+02	0.0
15	14	1	0	0.26585D+03	0.29716D+03	0.13135D-02	0.29536D+04	0.10187D+03	-0.19698D+04	-0.10857D+04	0.0
16	14	15	0	0.0	0.29716D+03	0.13135D-02	0.29536D+04	0.10187D+03	0.0	0.0	0.0
17	24	15	0	0.0	0.26908D+03	0.12543D-02	0.63291D+03	0.24714D+03	0.0	0.0	0.0
18	15	16	0	0.0	0.29378D+03	0.13053D-02	0.10549D+04	-0.25662D+03	0.0	0.0	0.0
19	16	17	0	0.0	0.29640D+03	0.12976D-02	0.10549D+04	-0.14229D+04	0.0	0.0	0.0
20	17	18	0	0.0	0.26382D+03	0.12819D-02	0.0	0.0	0.0	0.0	0.0
21	18	19	0	0.0	0.26382D+03	0.12819D-02	-0.21097D+04	0.19529D+04	0.0	0.0	0.0
22	19	20	0	0.0	0.27086D+03	0.12538D-02	0.0	0.23647D+03	0.0	0.0	0.0
23	20	23	0	0.0	0.25507D+03	0.12230D-02	0.15878D+07	0.88582D+03	0.0	0.0	0.0
24	11	21	0	0.0	0.29648D+03	0.13117D-02	0.56259D+03	-0.12731D+04	0.0	0.0	0.0
25	25	21	0	0.0	0.26908D+03	0.12941D-02	0.63291D+03	0.34326D+03	0.0	0.0	0.0
26	21	26	0	0.0	0.29512D+03	0.13084D-02	0.0	-0.73969D-01	0.0	0.0	0.0
27	22	27	0	0.0	0.39098D+03	0.25915D-02	0.0	0.34158D+03	0.0	0.0	0.0
28	23	2	0	0.0	0.32174D+03	0.13812D-02	-0.63291D+03	0.48129D+03	0.0	0.0	0.0
29	26	28	0	0.0	0.26196D+03	0.12359D-02	0.15942D+07	0.14028D+04	0.0	0.0	0.0
30	27	23	0	0.0	0.34860D+03	0.14740D-02	-0.98453D+03	0.41169D+03	0.0	0.0	0.0

********** NO. OF RESTART TAPE DUMP COUNT = 1

********** NO. OF PLOT QUANTITIES TAPE DUMP COUNT = 1

ALARM-P (MOD1(VERSION 01) DATE 77.06.30) PWR LOSS OF COOLANT ANALYSIS PROGRAM
LOFT(L1-2) ANALYSIS BY ALARM-P1

ELAPSED TIME 0.50000D+02 SEC TIME STEP NUMBER 70000

********** TOTAL SYSTEM BALANCE **********

NORM POWER	POWER (MW)	HEAT REMOV. (KCAL/SEC)	ENERGY LEAK (KCAL)	MASS LEAK (KG)	ENERGY BAL. (KCAL)	MASS BAL. (KG)	TOTAL REAC. (*)	PERIOD (SEC)
0.10000D+01	0.0	0.0	0.0	0.0	0.87143D+07	0.65645D+05	0.0	0.0

********** VOLUME QUANTITIES **********

VOL NO.	AVG. PRES (KG/M2)	TOT. MASS (KG)	AVG. ENTH (KCAL/KG)	AVG. DENS (KG/M3)	AVG. TEMP (DEG C)	AVG. QUAL	BUBL MASS (KG)	MIX. LEVEL (M)	LIQ. MASS (KG)
1	0.42879D+05	0.31445D+00	0.65529D+03	0.22569D+01	0.14711D+03	0.10000D+01	0.0	0.0	0.0
2	0.42941D+05	0.14855D+00	0.66338D+03	0.21677D+01	0.16255D+03	0.10000D+01	0.0	0.0	0.0
3	0.42816D+05	0.47841D+00	0.54443D+03	0.28877D+01	0.14538D+03	0.78361D+00	0.37489D+00	0.38405D+00	0.10352D+00
4	0.42789D+05	0.23845D+02	0.17905D+03	0.33814D+02	0.14536D+03	0.64630D-01	0.68491D-01	0.26492D+00	0.22304D+02
5	0.42726D+05	0.18954D+01	0.57325D+03	0.26879D+01	0.14530D+03	0.84039D+00	0.15929D+01	0.34290D+01	0.30254D+00
6	0.42677D+05	0.48705D+00	0.55749D+03	0.27874D+01	0.14526D+03	0.80942D+00	0.39423D+00	0.16855D+01	0.92823D-01
7	0.42644D+05	0.59158D+00	0.52201D+03	0.30473D+01	0.14523D+03	0.73964D+00	0.43755D+00	0.15200D+01	0.15403D+00
8	0.42644D+05	0.70625D+00	0.51516D+03	0.31037D+01	0.14523D+03	0.72617D+00	0.51285D+00	0.15200D+01	0.19339D+00
9	0.42591D+05	0.35805D+00	0.50985D+03	0.31450D+01	0.14519D+03	0.71576D+00	0.25628D+00	0.28407D+00	0.10177D+00
10	0.42568D+05	0.48548D+00	0.49905D+03	0.32406D+01	0.14519D+03	0.69451D+00	0.33717D+00	0.28407D+00	0.14831D+00
11	0.42765D+05	0.84045D+02	0.15788D+03	0.89119D+02	0.14535D+03	0.22991D-01	0.15677D+01	0.42870D+01	0.82113D+02
12	0.43054D+05	0.99981D+01	0.21975D+03	0.15545D+02	0.14558D+03	0.14431D+00	0.14428D+01	0.82387D+00	0.85552D+01
13	0.43027D+05	0.15677D+02	0.21276D+03	0.17138D+02	0.14556D+03	0.13060D+00	0.20473D+01	0.35317D+01	0.13629D+02
14	0.42832D+05	0.61405D+02	0.15079D+03	0.19892D+03	0.14539D+03	0.89502D-02	0.13094D+00	0.61500D+00	0.60855D+02
15	0.42674D+05	0.64453D+00	0.43770D+03	0.39274D+01	0.14526D+03	0.57373D+00	0.36967D+00	0.28407D+00	0.27466D+00
16	0.41702D+05	0.48404D-01	0.43943D+03	0.38143D+01	0.14442D+03	0.57812D+00	0.27983D-01	0.76901D+00	0.20421D-01
17	0.41266D+05	0.12291D+01	0.44946D+03	0.36501D+01	0.14404D+03	0.59828D+00	0.73532D+00	0.28883D+01	0.49373D+00
18	0.40351D+05	0.11767D+01	0.45595D+03	0.34946D+01	0.14323D+03	0.61195D+00	0.72007D+00	0.28883D+01	0.45662D+00
19	0.39439D+05	0.17011D+00	0.45690D+03	0.34050D+01	0.14241D+03	0.61474D+00	0.10458D+00	0.20726D+01	0.65537D-01
20	0.24070D+05	0.32825D-01	0.45619D+03	0.20841D+01	0.12555D+03	0.63238D+00	0.20758D-01	0.12643D+01	0.12067D-01
21	0.42469D+05	0.75844D+00	0.35391D+03	0.54733D+01	0.14508D+03	0.40913D+00	0.31030D+00	0.28407D+00	0.44814D+00
22	0.12458D+06	0.31991D+02	0.28367D+03	0.31119D+02	0.18877D+03	0.19462D+00	0.48202D-02	0.53343D-01	0.25765D+02
23	0.10679D+06	0.34133D-01	0.66305D+03	0.53838D+01	0.18190D+03	0.99911D+00	0.34103D-01	0.10308D+01	0.30351D-04
24	0.42683D+05	0.15658D+01	0.26664D+03	0.94461D+01	0.14527D+03	0.23715D+00	0.37132D+00	0.86197D+00	0.11945D+01
25	0.42584D+05	0.18126D+01	0.26660D+03	0.94237D+01	0.14518D+03	0.23720D+00	0.42996D+00	0.60747D+00	0.13827D+01
26	0.36364D+05	0.19017D-01	0.35312D+03	0.46611D+01	0.13953D+03	0.41548D+00	0.79013D-02	0.10321D+00	0.11116D-01
27	0.12115D+06	0.38520D-01	0.66407D+03	0.60757D+01	0.18751D+03	0.99897D+00	0.38480D-01	0.20239D+00	0.39683D-04
28	0.16396D+05	0.65375D+05	0.91709D+02	0.62375D+03	0.91530D+02	0.25317D-03	0.0	0.31728D+01	0.65358D+05

********** HEAT SLAB QUANTITIES **********

SLAB NO.	R VOL	R HT MODE	R HT FLUX (KCL/S/M2)	DNB FLUX (KCL/S/M2)	R HT COEF (KCL/S/M2/C)	CENT TEMP (C)	FUEL TEMP (C)	SURF TEMP (C)	R POWR H2O (KCL/S)	POWR GEN. (MW)
	L VOL	L HT MODE	L HT FLUX (KCL/S/M2)		L HT COEF (KCL/S/M2/C)				L POWR H2O (KCL/S)	
1	11	3	0.74190D+00		0.19249D-01			0.18390D+03	0.56537D+02	
	0	0	0.0		0.67815D-02			0.28167D+03	0.0	

********** JUNCTION QUANTITIES **********

JUN NO.	IN, VOL	OUT, VOL	CHOKE	JUN FLOW (KG/SEC)	JUN ENTH (KCAL/KG)	JUN SPVL (M3/KG)	PRESSURE DIFFERENTIAL NODE (KG/M2)	ELEV (KG/M2)	FRIC (KG/M2)	ACCL (KG/M2)	PUMP (KG/M2)
1	1	2	0	-0.19863D+00	0.66336D+03	0.46201D+00	0.30621D+02	0.0	0.36057D+02	0.37600D-02	0.0
2	2	3	0	0.36693D+00	0.66338D+03	0.46201D+00	0.33141D+02	-0.14440D+00	-0.98607D+02	-0.12604D+01	0.0
3	3	4	0	0.53367D+00	0.54443D+03	0.34617D+00	0.27713D+02	-0.18227D+02	-0.92482D+01	0.60415D+00	0.0
4	4	5	0	0.71187D+00	0.65438D+03	0.29573D-01	0.63905D+02	-0.12081D+02	-0.51139D+02	-0.98526D+00	0.0
5	5	6	0	0.10121D+01	0.57325D+03	0.37198D+00	0.48842D+02	0.64793D+01	-0.51918D+02	-0.50754D+01	0.0
6	6	7	0	0.54911D+00	0.55749D+03	0.35869D+00	0.33013D+02	0.70053D-01	-0.12547D+02	0.70859D+01	-0.29077D+02
7	6	8	0	0.54291D+00	0.55749D+03	0.35869D+00	0.32597D+02	0.35213D-01	-0.12356D+02	0.71076D+01	-0.29035D+02
8	7	9	0	0.65030D+00	0.52201D+03	0.32810D+00	0.53102D+02	-0.19876D+01	-0.12102D+02	-0.11586D+02	-0.29077D+02
9	8	9	0	0.66319D+00	0.51516D+03	0.32214D+00	0.53517D+02	-0.20243D+01	-0.12439D+02	-0.11608D+02	-0.29035D+02
10	9	10	0	0.13743D+01	0.50985D+03	0.31791D+00	0.28528D+01	0.0	-0.43677D+01	-0.11160D+01	0.0
11	10	11	0	0.14567D-01	0.49905D+03	0.30853D+00	-0.19665D+03	0.20306D+03	-0.17153D+02	0.82965D+01	0.0
12	11	12	0	-0.14734D+01	0.21975D+03	0.64319D-01	-0.26957D+03	0.25996D+03	0.22117D+01	-0.11184D+00	0.0
13	12	13	0	-0.16192D+00	0.21276D+03	0.58343D-01	0.27045D+02	-0.36671D+02	0.69679D-02	-0.60311D-01	0.0
14	13	14	0	0.18959D+01	0.21276D+03	0.58343D-01	0.19484D+03	-0.19963D+03	-0.13213D+01	0.83399D-01	0.0
15	14	1	0	-0.24422D+00	0.65229D+03	0.44303D+00	-0.48850D+02	-0.13344D+03	0.18059D+03	-0.27922D+00	0.0
16	14	15	0	0.16776D+01	0.43330D+03	0.50272D-02	0.15848D+03	-0.13344D+03	-0.16046D+01	-0.22006D+02	0.0
17	24	15	0	0.22663D+00	0.26664D+03	0.10585D+00	0.10483D+02	0.30218D+01	-0.16620D+01	-0.22222D+02	0.0
18	15	16	0	0.18022D+01	0.43770D+03	0.25466D+00	0.97144D+03	-0.12700D+01	-0.35003D+03	-0.61964D+03	0.0
19	16	17	0	0.17959D+01	0.43943D+03	0.26220D+00	0.43656D+03	-0.67379D+01	-0.10516D+04	0.62151D+03	0.0
20	17	18	0	0.18468D+01	0.44946D+03	0.27396D+00	0.91537D+03	-0.19602D+00	-0.91494D+03	-0.88860D+00	0.0
21	18	19	0	0.19063D+01	0.45595D+03	0.28615D+00	0.91160D+03	0.85747D+01	-0.84038D+03	-0.80741D+02	0.0
22	19	20	0	0.19148D+01	0.45690D+03	0.29367D+00	0.15371D+05	0.18350D+01	-0.13681D+05	-0.16944D+04	0.0
23	20	28	1	0.19157D+01	0.45619D+03	0.47981D+00	0.76762D+04	0.0	0.0	0.0	0.0
24	11	21	0	0.46608D+01	0.36877D+03	0.11221D-01	0.31532D+03	-0.20306D+03	-0.61392D+01	-0.10728D+03	0.0
25	25	21	0	0.19763D+00	0.26660D+03	0.10610D+00	0.11525D+03	0.36403D+01	-0.52144D+01	-0.11011D+03	0.0
26	21	26	0	0.51420D+01	0.35391D+03	0.18264D+00	0.61067D+04	-0.42636D-03	-0.15674D+04	-0.45467D+04	0.0
27	22	27	0	0.57077D+00	0.66477D+03	0.32134D-01	0.34199D+04	0.89874D+00	-0.10434D+04	-0.23807D+04	0.0
28	23	2	0	0.78681D+00	0.66305D+03	0.18460D+00	0.64965D+05	0.30995D+01	-0.11266D+04	0.12162D+04	0.0
29	26	28	0	0.51486D+01	0.35312D+03	0.21447D+00	0.19971D+05	0.15293D+04	-0.43337D+04	0.43703D+04	0.0
30	27	23	0	0.57571D+00	0.66407D+03	0.16457D+00	0.13351D+05	0.31599D+01	-0.13307D+05	0.80396D+03	0.0

********** NO. OF RESTART TAPE DUMP COUNT = 150

********** NO. OF PLOT QUANTITIES TAPE DUMP COUNT = 5005